MSc Thesis

APPLICATION OF AUTOMOTIVE ALTERNATORS IN SMALL WIND TURBINES

O.A. Ajayi
4122089

Supervisors
Dr. ir. H. Polinder
ir. S.O. Ani

July 2012

Thesis submitted to the faculty of Electrical Engineering, Mathematics and Computer Science (EEMCS): Electrical Power Processing (EPP) group in partial fulfillment of the requirements for the degree of Master of Science in Electrical Power Engineering

MSc Thesis Committee:

Prof. dr. J.A. Ferreira
Dr.ir. H. Polinder
Prof. ir. L. van der Sluis
ir. S.O. Ani

Acknowledgement

I am grateful to God for blessing me with a lovely wife, a supportive family, great supervisors, gladsome friends and the opportunity to be here.

I thank my wife for her endurance and encouragement for these two years. I thank my parents, brothers & sisters for the psychological and financial support. I am grateful to my supervisors for their untiring tutoring. And to my course mates, colleagues, and friends - you have positively impacted my life in various ways, thank you all. God bless you all.

Abstract

Small wind turbines have been in existence for several years but it seems they are not used where they are needed the most-distant off grid communities in developing countries. Cost and maintenance have been attributed to be reasons for this. One of its expensive constituents is its generator. The automotive alternator is considered as a cheaper alternative for generators in small wind turbines.

In this project work, an off-the-shelf recycled automotive alternator is experimentally parameterized and modeled with an assumed small wind turbine. The wind turbine's characteristics have been designed to match the power requirements of the alternator. The dynamic response of the alternator to wind speed variations is modeled in Matlab simulink and the effect of turbine blades' inertia on the generator speed and by extension on the wind turbine's performance coefficient indicates the need for a speed control mechanism to attain turbine optimal power operation. The speed control serves the purpose of tracking the turbine's maximum power characteristics. Other requirements for adaptation of the alternator are investigated and discussed in this report.

A speed transformation method for up scaling wind speed to generator speed, field winding control for automating the field excitation, and a maximum power point tracking (MPPT) scheme for improving energy yield are found to be requirements that go along with the alternator. A chain drive is proposed for up scaling wind speed while a centrifugal switch is proposed for field winding control. An MPPT scheme based on microcontroller and dc chopper technology is proposed for tracking the turbine's maximum power characteristics.

The dynamic responses of the wind turbine system to wind speed variations with and without the MPPT are simulated and compared and the advantage of the MPPT scheme is justified for a wind energy conversion system that can automatically adapt to various battery capacities. This report also comprises of measurements (No-load and load tests) carried out on the recycled alternator.

Table of contents

Chapter 1
Introduction

1.1 Background

In a world driven by business and trade, the necessity of energy can not be over-emphasized. For developing countries, availability of affordable clean energy is required as a driving force for development. The cost of transporting energy to some regions is quite expensive and it may be cheaper to locally produce the energy to be consumed in the region. Examples of such regions are distant farm settlements or remote villages. The use of small scale energy ranges from domestic purposes such as home entertainment, cooking, computing, lighting to commercial applications such as telecommunication equipment in Base stations. The availability of this energy can give better quality of life to residents of remote locations. More remote villages can be integrated to the telecommunication network because of reduced capital cost of installing equipment. Specifically considering the telecommunication service providers, the periodic cost of fuelling internal combustion engines at remote base stations can be saved while zero pollution is also achieved with small scale wind turbines.

Many small wind turbines have been developed but market penetration has been slow or even non existent in developing countries because of lack of local maintenance and high cost of the product. One of the goals of this project work is to explore more affordable small wind turbines with easily accessible spare parts and maintenance.

The possibility of using automotive alternators (also known as claw-pole alternators or Lundell alternators) for wind turbines has been indicated [1]. Typical passenger vehicle and light truck alternators use Lundell or claw-pole field construction, where the field north and south poles are all energized by a single winding, with the poles looking like fingers of two hands interlocked with each other. The Lundell alternators have been in existence for more than 50 years and are currently being manufactured at cost effective price. They are easily available in auto spare part shops and are quite affordable. The application of Lundell alternators in small wind turbines could make the construction and availability of such turbines feasible in developing societies where stable grid power is still unavailable. This forms the basis for considering it for small wind turbines in developing regions of the world.

However the possibility is faced with some challenges as follows:

- The required rotational speed to generate energy from the Lundell alternator is in a much higher range than what is obtainable from the wind.
- Rotor field excitation is required for Lundell alternators to produce voltage.

The Lundell alternator is a synchronous generator which uses a diode bridge rectifier at the output to convert ac to dc and to regulate output voltage via field control. Without this rectifier, ac voltage is obtainable.

1.2 Objectives

The aim of this research is to evaluate the possibility of applying Lundell alternators in small wind turbines. One of the challenges to the use of Lundell alternators for wind turbines is insufficient speed directly obtainable from the wind. This means that direct drive approach can not be used for this alternator and it is subject to the extra cost, reliability and complexity of a mechanical transmission system. The design and construction of a simplified mechanical transmission system will be investigated. The transmission system is to matchup the wind speed to the required speed for the Lundell alternator to generate energy. Some possibilities considered for the gear box design are as follows:

- Contact gears
- Transmission belts

- Chain drive

Another challenge is the provision of rotor field excitation in the Lundell alternators required for output voltage induction in its stator coils. Most automotive alternators use a rotor field winding, which allows control of the generated voltage by varying the current in the rotor field winding.

Some possible directions to be investigated are:

- External excitation
- Mechanically controlled self excitation

Another challenge is the low efficiency of the alternator. Methods of achieving lesser losses and running the turbine in an optimal manner are considered. These methods will mainly be centered on power electronics modification of the basic alternator used in the automobiles.

Overall, the integration of the alternator into the wind turbine with all that is required for its adaption at an affordable cost and with ease of maintenance is considered.

1.3 Master project work

In the course of the research, experimental measurements were carried out on a typical recycled automotive alternator. The alternator was coupled to a dc motor in the Electrical Power Processing (EPP) Laboratory and different power loss measurements and feasibility techniques were tried out. A simulation model of the Lundell alternator under the influence of low wind speed as a prime mover was developed and compared with some observations from the measurement of the alternator.

Positive results that indicate the correlation between the experiment and the simulation model will allow for predictable operation of the turbine under various wind speeds and optimization to achieve best results. A positive result could also indicate a high possibility of market penetration of small wind turbines based on this approach with less expenditure for energy consumers in distant communities.

A lot of recent effort has gone into development of the Lundell alternator for higher power applications. These developments could be quite useful for wind energy applications in the future. They are built around modifying the power electronics at the alternator's output. Some possible modifications in place of the diode rectifiers are: combined rectifier-boost converter; switched mode rectifier configuration; inverter [2].

1.4 Procedures

The procedures followed are:

1. Literature study of the proposed system and analysis of the alternator. This culminated in the development of an analytical model of a small wind turbine with the automotive alternator as generator.

2. A simulation model was developed to combine the parameters of the wind turbine and generator and observe possible power output. Simulation based on combination of alternator machine parameters and attainable wind speed integrated by gear mechanism was done using Matlab Simulink software. This way, the impact of adjusting input variables such as wind speed, and field current were evaluated for turbine optimal operation.

3. The alternator's power electronics converter was also investigated with a view of modifying it to suit wind turbine application. Different power electronics schemes were investigated to evaluate the most suitable for this application with a view of achieving improved efficiency at an affordable price.

4. Experimental measurements were carried out on an off-the-shelf recycled alternator and used to obtain machine specific constants for the computation and simulation. Variable shaft speeds were emulated using a dc generator in the EPP Laboratory. Voltmeters, ammeters, wattmeters and other workbench tools were used to measure voltage, current and power in the EPP Laboratory.

Chapter 2

Literature study

2.1 Introduction

The demand for energy is constantly rising while availability of fossil fuels is constantly declining. The environmental impact of most high energy density systems is also quite a subject of concern. It is important that energy should be harnessed from the environment in a sustainable manner that preserves the earth for future generations. In the automotive industry, electrical energy consumption in vehicles has been on the rise in recent years. Development of the electrical generator in the automobile is constantly being investigated to meet up with the demand without adversely affecting the environment and within reasonable cost limits. The evolution of the wind turbine as a sustainable prime mover for electrical generators has become a well accepted development in recent years. The combination of these two technologies might present a possibility of satisfying a rising demand for energy in an environmentally-friendly manner and at an affordable cost.

In this review, recent developments of the small wind turbine technology and also of the alternator will be discussed. Recent development with regards to the prospects of a proposed small wind turbine using the claw-pole alternator as its electrical power generator will be discussed. The review is segmented as follows:

- Overview of small wind turbines
- Background theory of the claw-pole alternator
- Adaptation of the alternator to a small wind turbine

Physical descriptions, component parts, comparison of design options and justification for design selection are also included while the review is concluded with a proposed system design.

2.2 Overview of small wind turbines

Small wind turbines are wind energy converters which have lower energy output than large commercial wind turbines used in wide area wind farms. The U.S. Department of Energy's National Renewable Energy Laboratory (NREL) defines small wind turbines as those with power rating smaller than or equal to 100 kilowatts [3]. Small wind turbines may be used for a variety of applications including on- or off-grid residences, telecom towers, offshore platforms, rural schools and clinics, remote monitoring and other purposes that require energy where there is no electric grid, or where the grid is unstable. Small wind turbines may be as small as a 50 Watts generator for boat or caravan use. Small units often have direct drive generators, direct current output, aero-elastic blades, lifetime bearings and use a vane to point into the wind.

Small scale turbines for residential use are available; they are usually approximately 2.1–7.6 m in rotor blade diameter and produce power at a rate of 300 to 10,000 watts at their rated wind speed. Some units have been designed to be very lightweight in their construction, e.g. 16 kilograms allowing sensitivity to minor wind movements and a rapid response to wind gusts typically found in urban settings and easy mounting much like a television antenna [4].

Small wind turbines have been produced by several manufacturers howbeit the market prices of these systems are quite high. This could be attributed to cost of component parts, fabrication and also marketing overheads. In 2010, the U.S. market for small wind systems grew 26% to 25.6 megawatts (MW) of sales capacity, nearly 8,000 units, and $139 million in sales. Sales revenue grew sharply at 53%, while the number of units sold continued to decline. The average installed cost of small wind turbines installed in the U.S. in 2010 was $5.43 per installed watt [6]. Market growth for small wind turbines in the U.S. is shown in figure 2.1. Another interesting trend reflected

in the U.S. report is that the number of small wind turbines sold is going down, even as the sales measured by capacity go up. One reason is that people are buying fewer tiny wind turbines for off-grid applications, like homes or sailboats, and more are buying turbines that can provide a bit more power. About one-third of the units sold by U.S. manufacturer "Southwest Windpower" last year were to customers in foreign countries, according to the U.S. wind energy association report. An array of several small wind turbines is shown in [7] with prices, specification sheets and ratings.

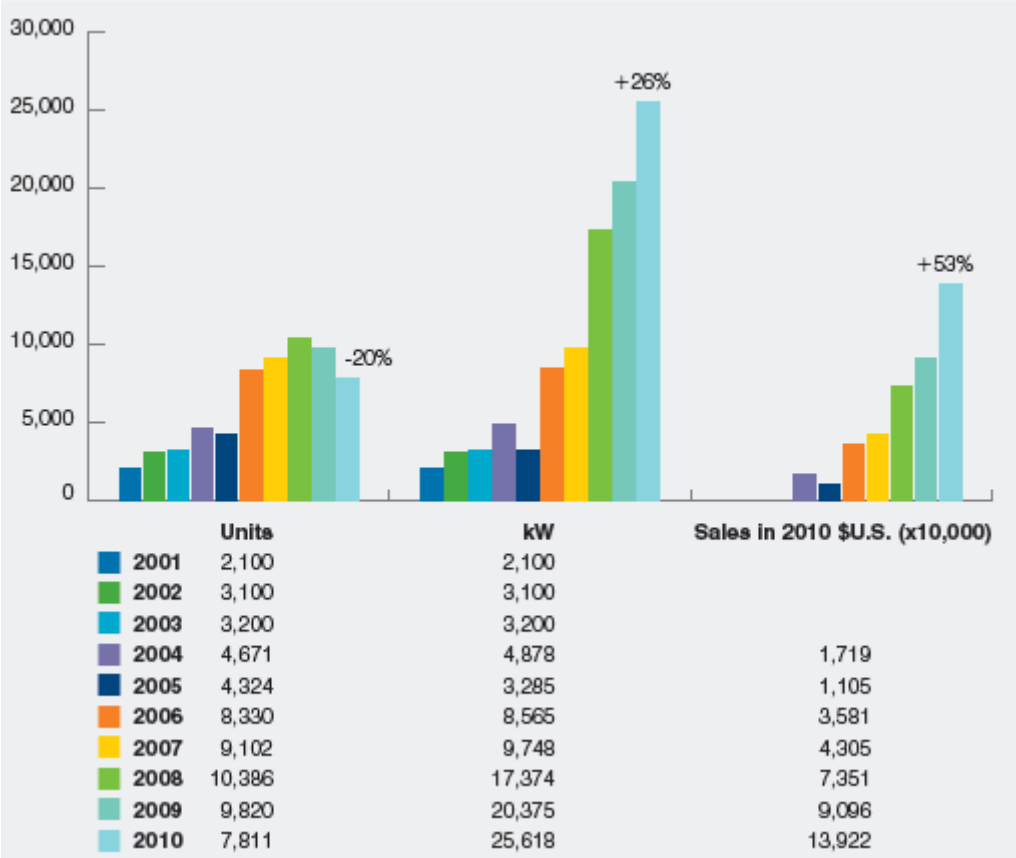

	Units	kW	Sales in 2010 $U.S. (x10,000)
2001	2,100	2,100	
2002	3,100	3,100	
2003	3,200	3,200	
2004	4,671	4,878	1,719
2005	4,324	3,285	1,105
2006	8,330	8,565	3,581
2007	9,102	9,748	4,305
2008	10,386	17,374	7,351
2009	9,820	20,375	9,096
2010	7,811	25,618	13,922

Figure 2.1: U.S. Small Wind Turbine Market Growth [6]

The electrical power generator used in the wind turbines is one of the expensive components of the wind turbine. Types of generators typically used for small wind turbines are dc generators, permanent magnet alternators and induction generators. A permanent magnet alternator from Windblue® cost $300 as at June 2012 [8].

In order to obtain certain quantity of wind power from a wind turbine's blade, the prevailing wind speed of the region where the turbine is to be situated must be known. This data is normally represented with the Weibull distribution diagram indicating the probability of different wind speeds. For wind speeds slightly higher than the more probable wind speeds in the region, the tip speed ratio and an optimal turbine rotor diameter can be used to derive the torque that will supply sufficient power to the generator. In this way, the wind energy of the region is properly harnessed.

Some different designs of horizontal and vertical axis wind turbines culled from [9] are shown in figure 2.2 and figure 2.3 respectively.

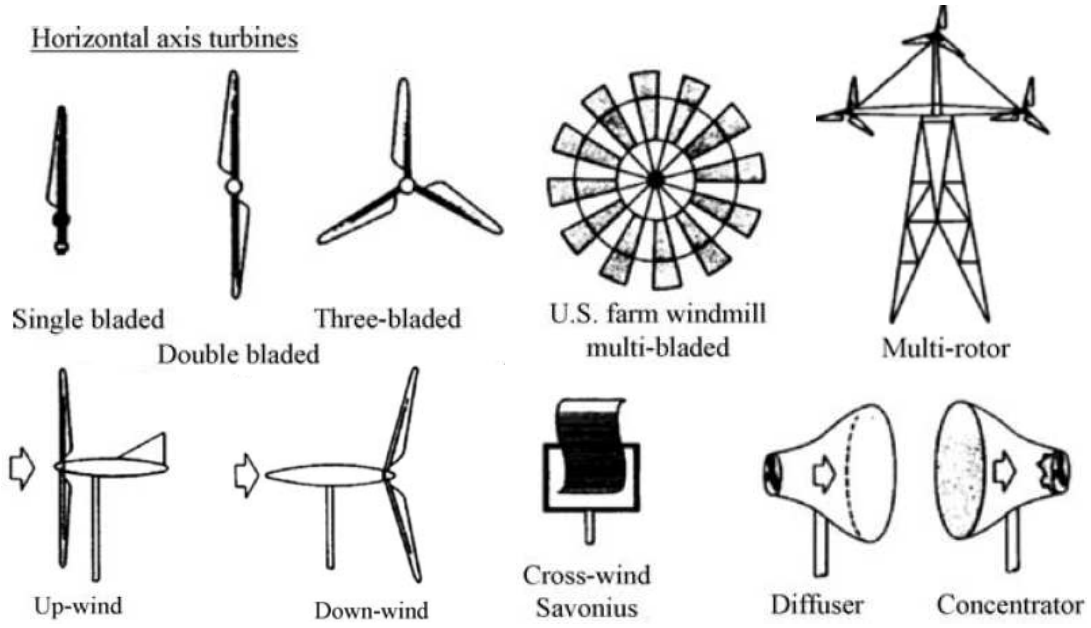

Figure 2.2: Some horizontal axis wind turbine concepts.

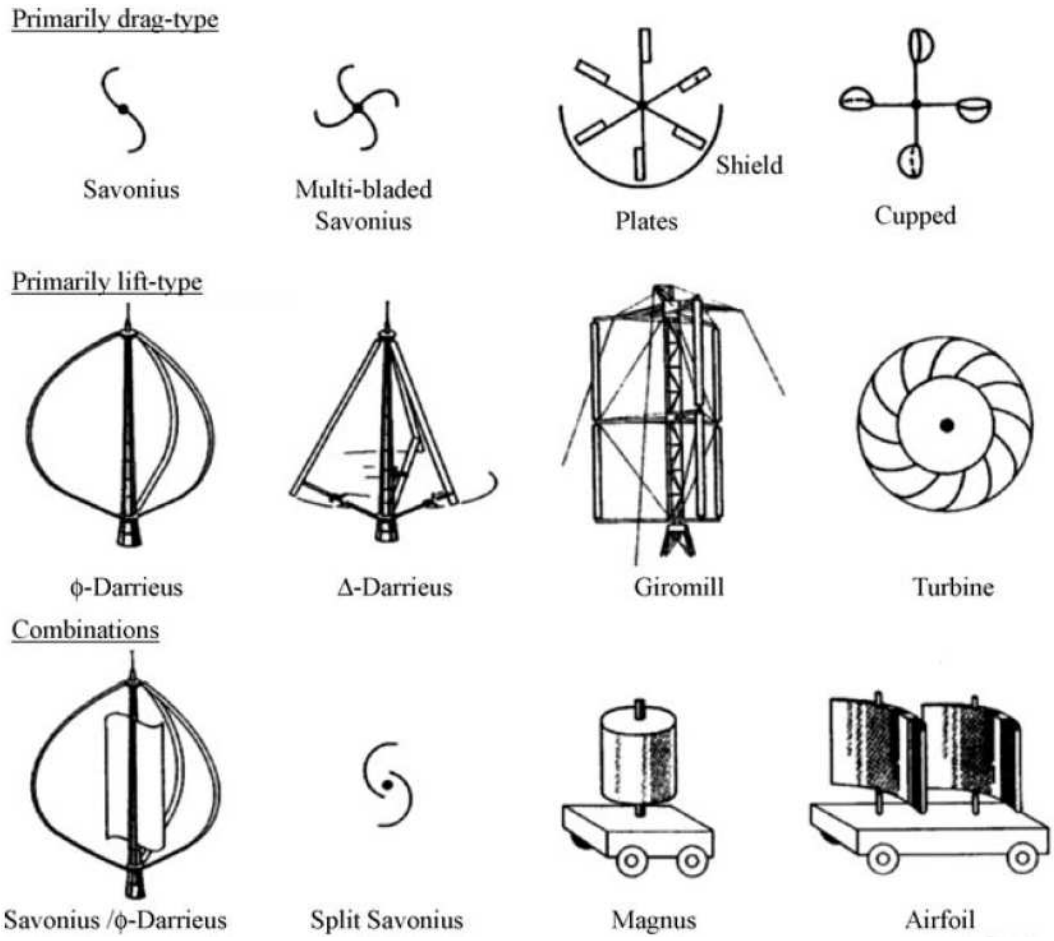

Figure 2.3: Some vertical axis turbine concepts

An expression generally used to describe the power harnessed by a 3-bladed horizontal axis wind turbine from the wind is:

$$P_w = \frac{1}{2} C_p(\lambda,\theta)\pi.r^2 v^3 \rho \qquad (2.1)$$

Where

P_w = Wind mechanical power

$C_p(\lambda,\theta)$ = coefficient of performance: function of λ and θ

λ = tip speed ratio

θ = pitch angle of rotor blades

$\pi.r^2$ = rotor blade swept area where r is rotor radius

v = wind velocity

ρ = air density

$$\lambda = \frac{r\omega_G}{vG} \qquad (2.2)$$

G = Gearbox ratio,

ω_G = Generator rotor speed

Wind turbine coefficient of performance (C_p) is dependent on the ratio of the turbine's blade tip speed to the wind velocity (λ or TSR). It is also dependent on the turbine's blade pitch angle (θ). An illustration of the relationship between C_p and TSR for different wind turbines types is shown in figure 2.4 [10]. The 3-bladed turbine is seen to have the highest coefficient of performance at an optimal tip speed ratio.

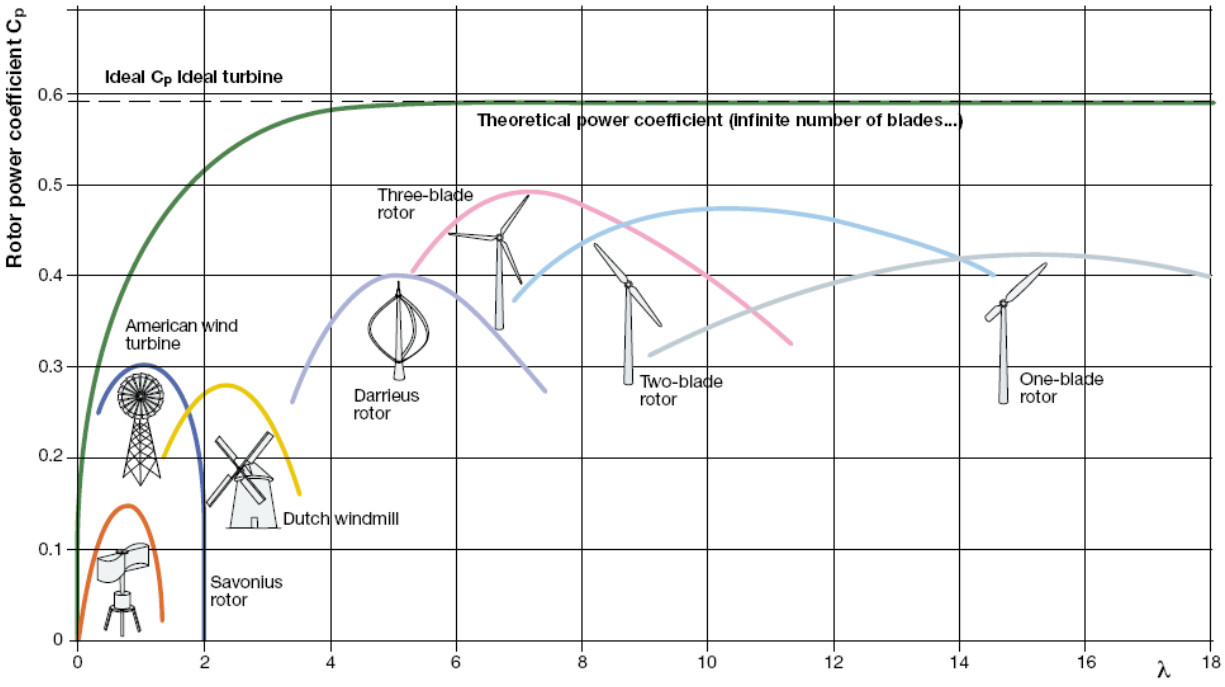

Figure 2.4: C_p - λ characteristics of different wind turbine blade designs.

The majority of small wind turbines are traditional horizontal axis wind turbines but vertical axis wind turbines are growing in the small-wind market. These turbines, by being able to take wind from multiple dimensions, are more applicable for use at low

heights, on rooftops, and in generally urbanized areas. Their ability to function well at low heights is particularly important when considering the cost of a high tower necessary for traditional turbines [4].

Conventional designs of vertical axis wind turbines are the Savonius and Darrieus types. Savonius turbines are used whenever cost or reliability is much more important than efficiency. Most anemometers are Savonius turbines for this reason, as efficiency is irrelevant to the application of measuring wind speed. Much larger Savonius turbines have been used to generate electric power on deep-water buoys, which need small amounts of power and get very little maintenance. Vertical-axis machines are good for high torque, low speed applications and are not usually connected to electric power grids. They can sometimes have long helical scoops to give smooth torque [11].

Some hobbyists have built wind turbines from kits, sourced components, or from scratch. Do it yourself or DIY-wind turbine construction has been made popular by websites such as www.instructables.com, www.otherpower.com and homepower.com [12]. DIY-made wind turbines are usually smaller (rooftop) turbines of approximately 1 kW rating or less. These small wind turbines usually use tilt-up or fixed/guyed towers. However, larger (freestanding) and more powerful wind turbines are sometimes built as well. In addition, people are also showing interest in DIY-construction of wind turbines with special designs as the Savonius and Panemone wind turbines to boost power generation. When compared to similar sized commercial wind turbines, these DIY turbines tend to be cheaper. Through the internet, the community is now able to share designs for constructing DIY-wind turbines and there is a growing trend toward building them for domestic requirements. The DIY-wind turbines are now being used both in developed countries and in developing countries, to help supply power to residences and small businesses. At present, organizations such as Practical Action have designed DIY wind turbines that can be easily built by communities in developing nations and are supplying design documents for constructing the turbines [13]. To assist people in the developing countries, and hobbyists alike, several projects have been open-designed such as Hugh Piggot's wind turbine [14], Chispito Wind Generator [15], and the Zoetrope Vertical-Axis Wind Turbine [16].

As a result of size, the design complexity of small wind turbines is quite limited. It is important that a control scheme be put in place for the turbine’s optimal power coefficient to be realized. Some research by Mirecki et al [17] describes methods of achieving energy efficiency in small wind turbines. Most of the methods require a sensor (wind speed, generator speed, or induced voltage) and an optimization algorithm to compute and set the electrical load to a value that converges the drive train towards the optimal wind power curve.

2.3 Background theory of the claw-pole alternator

The alternator is used in automobiles for supplying electrical power. It consists of a rotor mounted on the two end bearings of the machine frame, a stator, six diodes, and a regulator. The type of generator used in the automotive alternator is a wound-field three-phase synchronous generator.

Its rotor is made of iron pole pieces and many turns of fine wire, which are mounted over the shaft of the machine. The rotor coil leads are traced out through slip rings and brushes to the external circuit. When the rotor coils are energized, an electromagnetic field is produced. This magnetizes one set of six teeth claw poles at magnetic north and the other set at magnetic south [18].

The stator of the alternator consists of a three-phase winding usually connected in star. The output of the stator is fed to the three-phase rectifier made of six semiconductor diodes to give a DC voltage and then regulated to battery voltage. The

regulator begins to function when the alternator reaches cut-in speed, which is approximately 1000 rpm at its shaft.

The output voltage of the alternator increases linearly with speed if field current is maintained constant. Automotive alternators are designed to yield nominal voltage for charging the vehicle's battery at the vehicle's idle speed; at higher speeds, if the voltage is not regulated, it would result in a very high over-voltage for the battery. Figure 2.5 shows a conventional alternator rotor and stator.

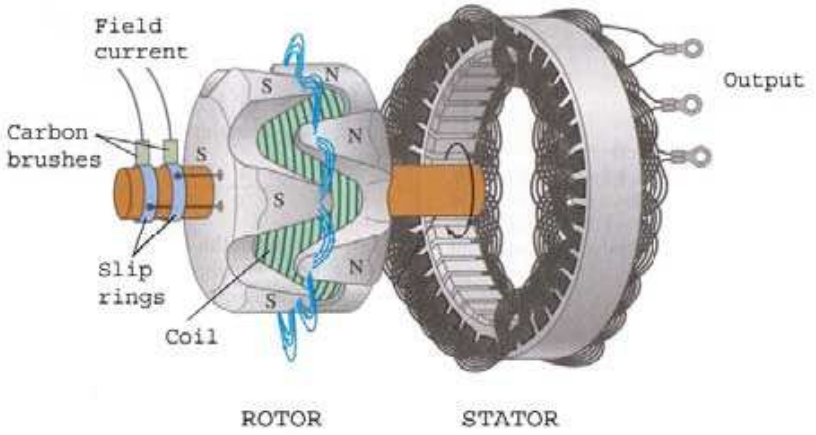

Figure 2.5: Exploded view of an automotive alternator [19], [20].

In the automobile, the voltage is controlled by an internal regulator that continuously samples the battery voltage and adjusts the field current accordingly. The field current is controlled by varying the duty-cycle of the pulse-width modulated (PWM) voltage applied to the field winding. This is illustrated in Figure 2.6. As the electrical load increases (more current is drawn from the alternator), the output voltage falls. This drop in output voltage is detected by the voltage sampler which increases the duty-cycle to increase the field current and hence raise the output voltage. Similarly if there is a decrease in electrical load (the output voltage climbs), the duty cycle decreases to reduce the output voltage.

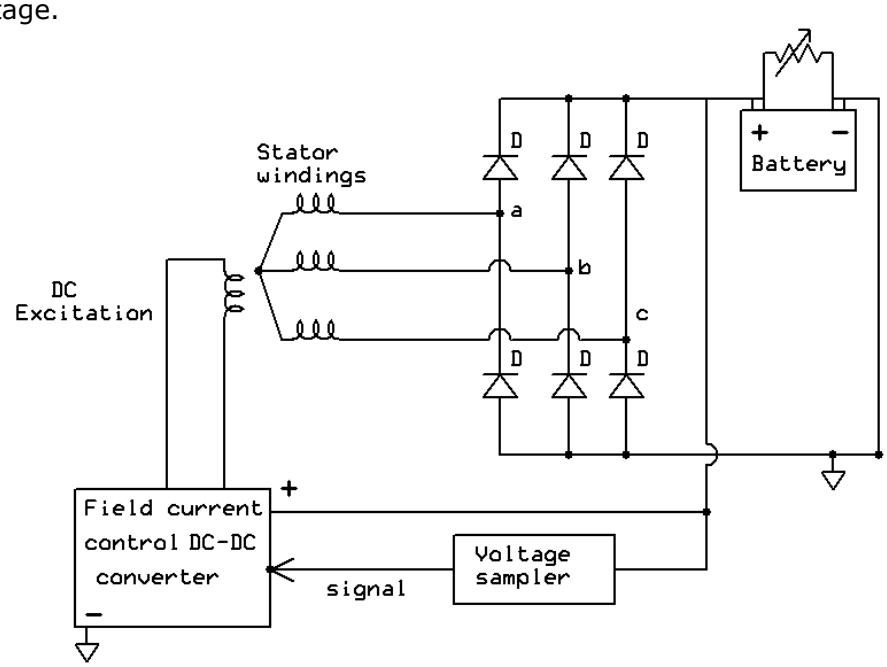

Figure 2.6: Circuit equivalent of the automotive alternator system.

Automotive alternators are classified according to the output voltage/current characteristics and the field winding adjustment whereby the optimal point of operation will be dependent on the most frequent speed of the prime mover. Currently, the voltage output of automotive alternators is 14V for small cars and 28V for trucks and bigger cars. The maximum alternator output is limited by heating of the rotor and stator windings and by magnetic saturation of the machine. Conventional alternators used in automobiles are limited to about 1.6kW maximum output power at 9000 rpm.

The peak efficiency for an alternator tends to occur at 30-40% of its maximum output which corresponds to shaft speed between 2000-2500 rpm [21]. The efficiency of a 1.5 kW rated alternator increases to 64% (at 2000 rpm) and decreases to about 40% at higher speed (8500 rpm) [22]. Since the rotor is made from iron without laminations, there is high eddy current loss at high speed. Also at higher speeds, temperature of the copper windings increase and winding resistance increases therefore copper losses increase the more with high temperature. For this reasons, alternators are built with fans to reduce machine running temperature. The claw pole structure of the alternator allows for simpler rotor construction but has the disadvantage of 3 dimensional flux linkages with air gap fringing losses. The leakage flux between the claws amounts to about 30% of the main flux at the position of the iron core at no-load condition and may increase to about 50% under full load [22].

It has been suggested in [22] and [23] that efficiency of the alternator can be improved by use of assisting permanent magnets placed between the claws to compensate for this leakage flux. A lot of research is indicating the possibility of a 42V system as a result of more electrical loads in automobiles [20], [24]-[26]. Perreault and Caliskan [26] demonstrated that higher efficiencies can be realized from the automotive alternator by using switched mode rectifiers.

Permanent magnet alternators (PMA) are used in some small wind turbines such as: WindBlue's Breeze and Lite; Mandalay Wind 500; and Mike's Mallard LW. This type of alternator has similar rotor claw pole shape as shown in figure 2.7. N40 grade Neodymium rare earth magnets are placed in the inner ring of the WindBlue PMA [8]. However, they are not used in vehicles because their rotor magnetic flux is not variable hence rotor magnetic field cannot be adjusted to control output voltage. They are used for wind turbine applications but they come at a much higher price than a recycled automotive alternator and are not as easily available in the market.

Figure 2.7: WindBlue's claw pole permanent magnet rotor [8]

Jurca et al carried out an analysis of a permanent magnet claw pole synchronous machine used in wind power application [27]. A 3-D Finite element analytical software was used in this research to compute air gap magnetic field density distribution and harmonic contents while the machine was assumed to be directly driven by the wind.

However there was no indication of current or power output computation and /or measurement. Klades et al [28] have also done some research on design considerations for claw pole alternators used in small scale wind power application. This research was focused on the development of a 3D finite element model for optimization of a 24-poles-rotor claw geometry with a combination of permanent magnets and field windings for rotor excitation. Another research carried out by Ani et al demonstrated the possibility of using the automotive alternators in small wind turbines as a substitute for permanent magnet generators used in most small wind turbines [1]. This research indicated that the automotive alternator used in a small wind turbine could achieve a reduced cost of energy obtainable per rotor blade swept area.

2.4 Adaptation of the automotive alternator to small wind turbines

In order to use the alternator effectively in a small wind turbine, three basic requirements are considered:

a. Mechanical transmission system: The alternator generates power at much higher mechanical speed than directly obtainable from the wind. A mechanical transmission system is needed to matchup the wind speed to the required speed for the alternator to yield energy.
b. Field winding current: Rotor field excitation is required for automotive alternators to generate voltage at the stator windings.
c. Power converter modification: In order to maximize power output, the possibility of modifying power converters of the alternator is also considered as part of the adaptation.

These three will be considered in more details in the following pages.

2.4.1 Mechanical transmission System

Some methods that could be used for matching low wind speed to the required mechanical speed for the alternator are as follows:

i. Contact Gears are used for transmitting torque and speed at different complementing ratios. A complex design is required for gear systems which make them more expensive to manufacture while they also require expensive lubrication [29]. For these reasons, contact gears will not be considered for this application.

ii. The transmission belt is a loop of flexible material used to link two or more rotating shafts mechanically. Belts may be used as a source of motion, to transmit power efficiently, or to track relative movement. Belts are looped over pulleys. In a two pulley system, the belt can either drive the pulleys in the same direction, or the belt may be crossed, so that the direction of the shafts is opposite. They run smoothly and with little noise, and cushion motor and bearings against load changes, albeit with less strength than gears or chains. They need no lubrication, minimal maintenance and are quite available as automobile spare parts in most developing countries. However some tension is required to hold it in place.

The efficiency of belts is reduced by 0.5–1% due to belt slip and stretch. Some typical belt types are Vee belts, Timing belts, Multi-groove belts.

iii. Chain drives: Power transmission chains are commonly found in bicycles and motorcycles. An illustration is shown in figure 2.8. Some of the advantages of chain drives over belt drives are [30]:

- No slippage between chain and sprocket teeth.
- Negligible stretch, allowing chains to carry heavy loads.

- Long operating life expectancy because flexure and friction contact occur between hardened bearing surfaces separated by an oil film.
- Operates in hostile environments such as high temperatures, high humidity or oily areas.
- Long shelf life because metal chain ordinarily doesn't deteriorate with age and is unaffected by sun, reasonable ranges of heat, moisture, and oil.

Drawbacks of chain drives that might affect drive system design are:

- Noise is usually higher than with belts or gears, but silent chain drives are relatively quiet.
- Chain drives can elongate due to wearing of link and sprocket teeth contact surfaces.
- Chain flexibility is limited to a single plane whereas some belt drives are not.
- Usually limited to somewhat lower-speed applications compared to belts or gears.
- Sprockets usually should be replaced because of wear when worn chain is replaced.
- Their greater mass increases drive train inertia.

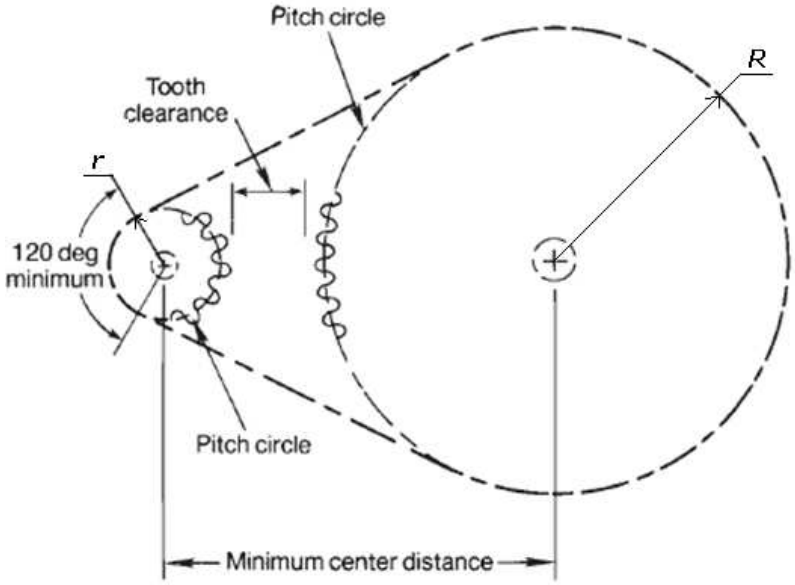

Figure 2.8: Chain drive illustration

Some videos on YouTube indicate the use of chain drives and permanent magnet alternators with vertical axis wind turbine (VAWT) blades built by Do-It-Yourself (DIY) enthusiasts [31].

2.4.2 Field winding current

The field current that flows through the rotor field winding is responsible for the flux generated in the rotor poles which subsequently links with the stator windings to produce voltage. Field current is not required to exceed 4 Amps because rotor iron core becomes magnetically saturated beyond 4 Amps of field current. Applicable options for supplying current to the field winding of the Lundell alternator are as follows:

i. Separate excitation: For large or older generators, it is usual for a separate exciter dynamo to be operated in conjunction with the main power generator. This is a small permanent-magnet or battery-excited dynamo that produces the field current for the larger generator [32]. Another method of separate excitation applicable to the

automotive alternator could be to use a capacitor to supply initial field current at alternator start up speed subsequently self excitation would be supplied during running operation while the capacitor is recharged. The possibility of providing a separate rechargeable battery for the excitation winding is also considered. These options are suitable for supplying constant field current.

ii. Self excitation: Modern generators with field coils are self-excited, where some of the power output from the rotor is used to power the field coils. The rotor iron retains a residual magnetism when the generator is turned off. The generator is started with no load connected; the initial weak field creates a weak voltage in the stator coils, which in turn increases the field current, until the machine "builds up" to full voltage. Self-excited generators must be started without any external load attached. An external load will continuously drain off the buildup voltage and prevent the generator from reaching its proper operating voltage. If the machine does not have enough residual magnetism to build up to full voltage, usually provision is made to inject current into the rotor from another source. This may be a battery or rectified current from a source of alternating current power. Since this initial current is required for a very short time, it is called "field flashing". Small portable internal combustion engine generator sets may occasionally need field flashing to restart [32].

In vehicle applications, the alternator's field winding is energized when the ignition key is switched 'on' so that its battery source is not depreciated. For application in a small wind turbine, a mechanical switch could be used to fulfill this purpose. Such a mechanical switch as the centrifugal switch or speed switch installed on the shaft would be necessary for switching 'on' the field winding when sufficient wind speed is attained and 'off' when there is insufficient or excessive wind speed.

2.4.3 Power converter modification

Recently there has been a considerable amount of effort directed towards developing automotive alternators with improved efficiency. These techniques basically involve replacing the diodes in the rectifier with controlled switches which make it possible to adjust the magnitude and phase of the different harmonic components that constitute the phase currents in order to enhance the average power delivered to the output [24]. Most of this work has focused on using inverter driven machines, surface permanent magnet (PM), and interior PM machines [25]. The main issue with inverter driven machines is that the system cost is several times the cost of the conventional alternator, due to the cost of the power electronics, control circuitry, and permanent magnets.

Perreault and Caliskan [26] proposed a method of improving the output power of the automotive alternator without using an expensive inverter. This is based on a switched-mode rectifier (SMR) which allows the alternator to operate at its maximum output power point over a wide range of speeds. A simplified version is described in Figure 2.9.

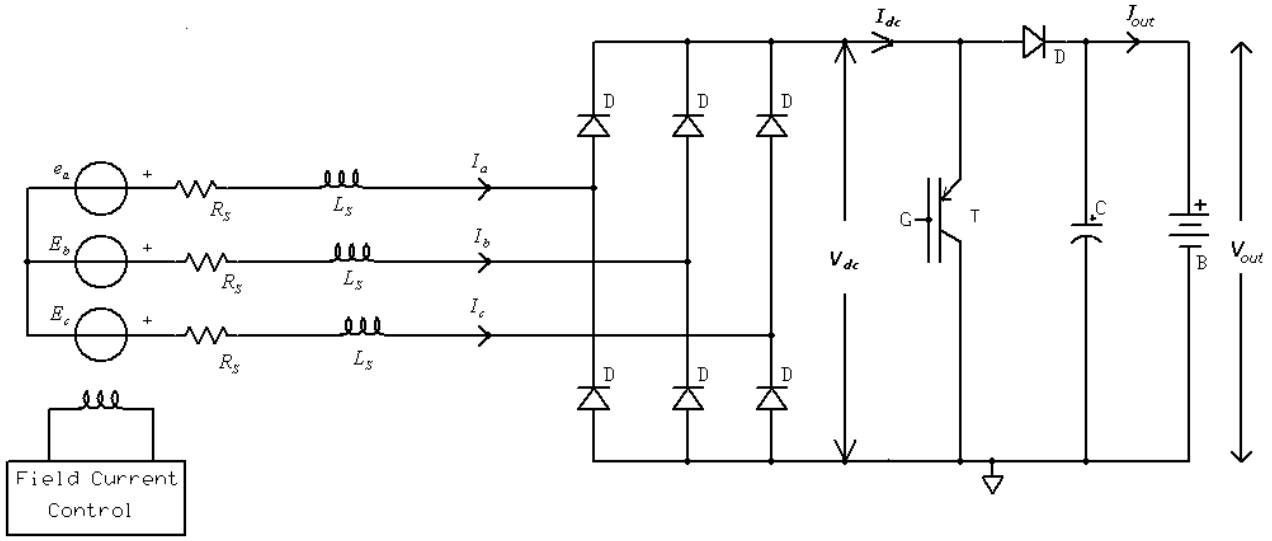

Figure 2.9: SMR automotive alternator system [26].

The increase in power is not solely due to a higher output voltage, as rewinding the stator would raise the output voltage, but would lower the output current, thus not improving the output power. For example if a 14V stator was rewound to obtain 42V output, the output current rating would be only one third of the 14V stator's output current rating; thus rewinding cannot improve the output power of an alternator. Instead, higher output power is obtained with a SMR as it allows the alternator's DC output voltage at the input of the SMR to be varied to maximize output power at any speed, while maintaining a constant DC output voltage to the battery. The new concept as suggested in [25] shows that with the use of a switched mode rectifier, additional control can be used to extract more power from the alternator. By adjusting the duty ratio, the alternator can generate up to its maximum power as speed varies, while supplying a constant output voltage, (of 50 V, for example). The switched-mode rectifier provides the necessary controlled voltage transformation to match the constant-voltage load to the alternator. The output power can be efficiently regulated to any value below the achievable maximum with field control.

Koutroulis and Kalaitzakis [33] demonstrated the use of switched mode converters in maximum power tracking systems used in wind turbines. Their research indicated the use of a buck converter with a microcontroller serving as output voltage sensor and duty ratio regulator for the transistor switches in the circuit. They also verified the possibility of using other dc-dc converters (boost converter, buck-boost converter, Cuk converter and flyback converter) for similar application.

Mirecki et al [17] described some methods of maximum power point tracking for a vertical axis, permanent magnet synchronous machine wind generator. An interesting extract from their research is the use of a DC chopper at the output of the 3 phase rectifier to achieve optimal load conditions. An illustration of the concept is shown in fig. 2.10. The gate control of the IGBT is from a microcontroller which simultaneously samples the machine speed from its output voltage computes an optimal load current and tunes the output current accordingly.

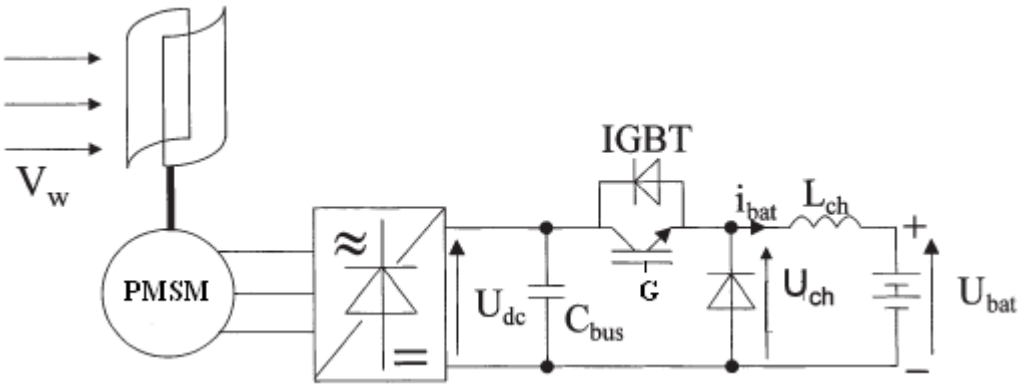

Figure 2.10: Diode bridge chopper structure [17]

2.5 Conclusion

In the course of this review, some details about the design options and components of a proposed wind turbine are discussed. The horizontal axis wind turbine is preferred for this application because of its higher performance coefficient. The gear system to be used is the chain drive system because of its preferred characteristics. The field current control will consist of constant current supply from a battery at start up while the alternator will supply its own field current during running. A centrifugal switch would also be used to automate the field winding at suitable wind speeds. The dc chopper is proposed as method of maintaining maximum point operation of the turbine. The system parts can be integrated together to yield an overall proposed system as described in figure 2.11.

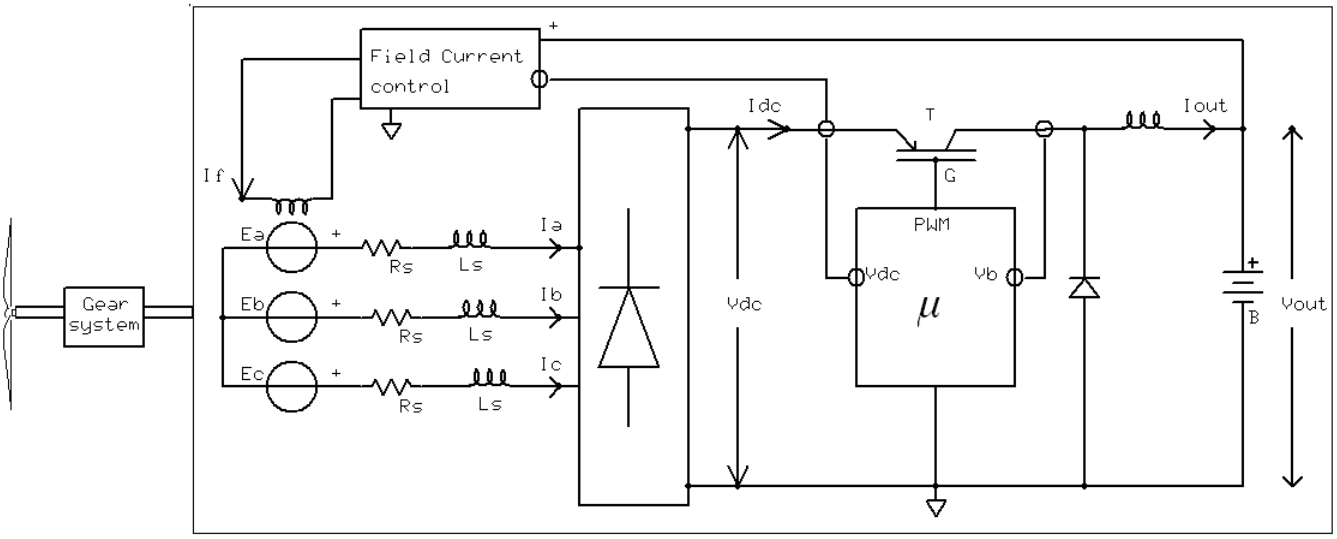

Figure 2.11: Proposed system design

The duty ratio of the dc chopper transistor is obtainable from a microcontroller that simultaneously samples the machine speed via the dc voltage, computes the optimal load current, samples battery voltage and regulates the load current to achieve optimal power point operation.

Chapter 3

An analytical model of the proposed small wind turbine system

3.1 Introduction

An analytical model is developed to compute the electrical power realized from the wind power that is extracted by the turbine blades. The model combines the mathematical representations of the segments of the complete wind turbine system. This model is developed based on the block diagram illustration shown in Figure 3.1. This indicates the energy flow from the wind turbine blades to the energy storage.

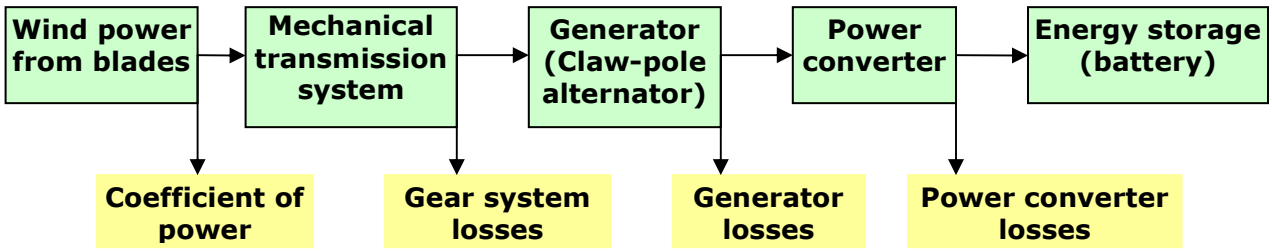

Figure 3.1: Model block diagram

3.2 Wind power model

The wind turbine is assumed to be a 3-bladed horizontal axis wind turbine. It is also assumed to be controlled such that at wind speeds lower than 8m/s, the rotor speed is adjusted so that the turbine operates at maximum aerodynamic efficiency (maximum C_p value). At higher wind speeds of 8m/s and above, the C_p value is reduced by turning the turbine away from wind using its tail vane such that the blade pitch angle changes and the turbine rotates at lower speeds as shown in Figure 3.2. The behavior of the wind turbine after rated wind speed is assumed to be based on the response of its yaw system (tail vane) to wind velocity. At cut out speed of 25m/s, the generator is shut down by disconnecting field winding or parking the wind turbine as shown in figure 3.2. The plot of figure 3.2 is based on an assumed wind turbine described by parameters in table 3.1.

The equation used for a conventional horizontal axis wind turbine design is as follows:

$$P_w = \frac{1}{2} C_p(\lambda,\theta)\pi.r^2 v^3 \rho \qquad (3.1)$$

Where

P_w = wind mechanical power

$C_p(\lambda,\theta)$ = coefficient of performance which is a function of λ and θ

λ = tip speed ratio

πr^2 = rotor blade swept area where r is rotor radius

v = wind velocity

ρ = air density

θ = pitch angle of rotor blades

$$\lambda = \frac{r\omega_G}{vG} \qquad (3.2)$$

G = gearbox ratio,

ω_G = generator rotor speed

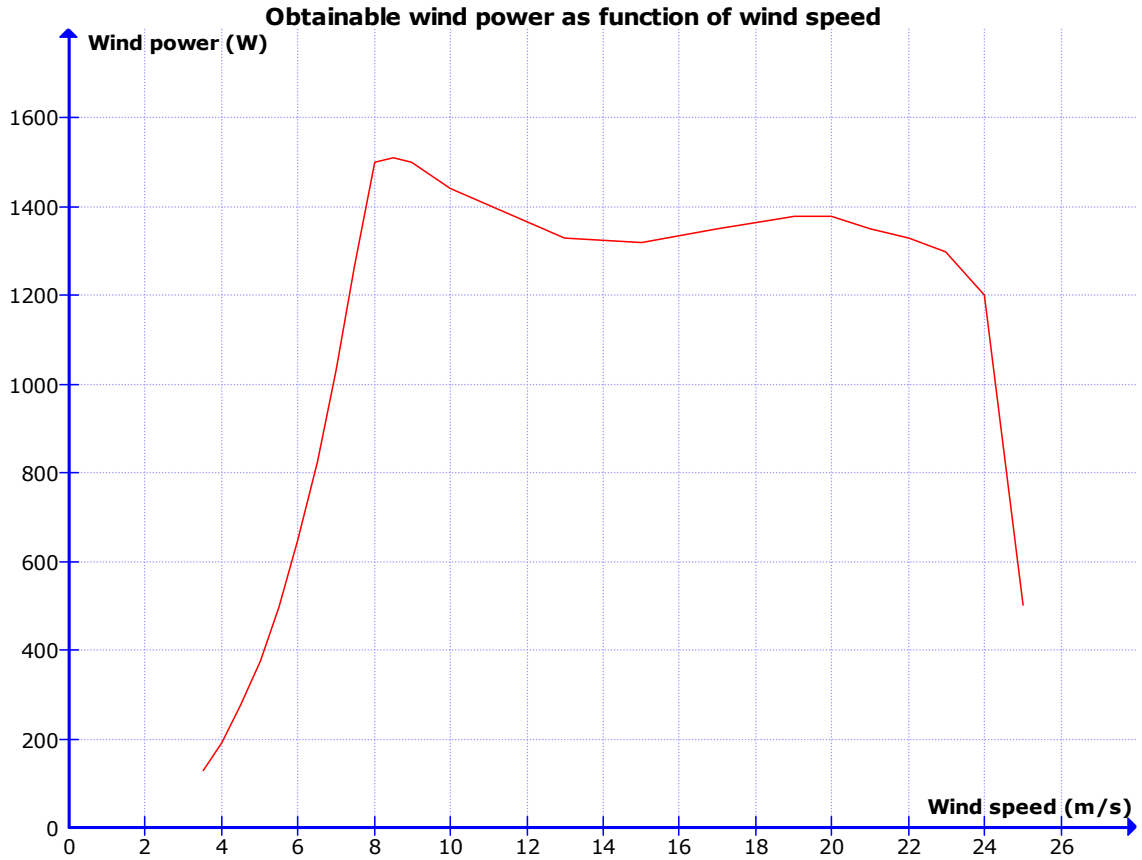

Figure 3.2: Wind power as a function of wind velocity.

For the purpose of this design, a cut-in wind speed of 3.5m/s is used with a gear ratio of 10:1. This corresponds to a cut in shaft speed of 1080 rpm at the alternator. The cut out wind speed is set at 25 m/s. The alternator has the inherent quality of running at very high speeds (as high as 8000 rpm) without disintegrating. Other assumed parameters of the wind turbine are indicated in table 3.1. For the optimal tip speed ratio and power coefficient, a suitable turbine diameter that harnesses rated wind power (shaft input power) for the generator is computed in an excel worksheet.

Table 3.1: Assumed wind turbine parameters

Rotor blade diameter (*2r*)	4 m
Rated wind speed (v_r)	8 m/s
Rated alternator speed ($\omega_{G,r}$)	260 rad/s (~2500rpm)
Rated shaft input power to alternator	1.5 kW
Rated alternator output power	0.6 kW
Optimum tip speed ratio or blade tip speed divided by wind speed (λ_{opt})	6.5
Maximum aerodynamic coefficient ($C_{p,\max}$)	39%
Air density (ρ)	1.225 kg/m^3

3.3 Mechanical transmission system model

The chain drive system was selected for this application. Chain length can be computed using the following expression [30]:

$$L_C = 2C + \frac{N+n}{2} + \frac{(N-n)^2}{4\pi^2 C} \qquad (3.3)$$

Where: L_C = Chain length, pitches

C = Shaft centers, pitches

N = Number of teeth in large sprocket

n = Number of teeth in small sprocket

The speed of each sprocket is inversely related to number of teeth on each sprocket.

$$\frac{1}{G} = \frac{\varpi_N}{\varpi_n} = \frac{n}{N} \qquad (3.4)$$

Where: ϖ_N = Speed of large sprocket

ϖ_n = Speed of small sprocket

With sufficient tension maintained between the sprockets, the transmission efficiency can be as high as 98.6% [35].

3.3.1 Chain drive design

One of the best known chains is the roller chain and it is the first to be standardized by ANSI (American National Standards Institute). One of the design guidelines for chain transmission is that the arc of roller chain engagement should not be less than 120 deg as illustrated in Figure 3.3 so as to ensure sufficient grip.

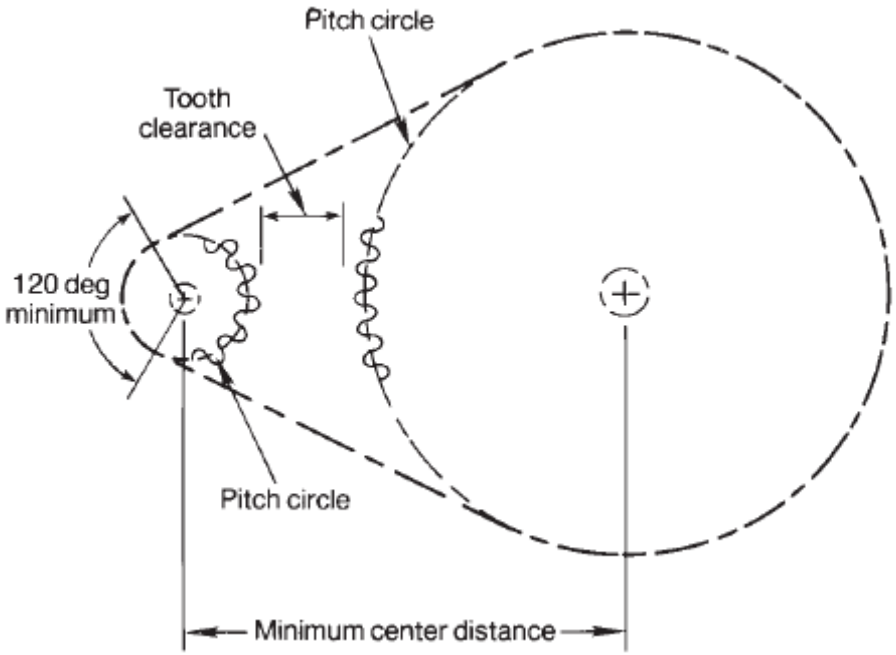

Figure 3.3: Arc of roller chain engagement should not be less than 120 deg [30]

The required speed transformation is ratio 10:1. An initial computation was made which resulted in a bigger sprocket of diameter 424.8 mm. Due to the unavailability of

the bigger sprocket in the open-market; a 2-stage chain drive can be constructed with ratio 3.2:1 for each stage.

The design of the roller chain for this research starts with the power rating of the high speed (smaller) sprocket. This is similar to an average input power to the alternator at 1.5kW (~2 horsepower) and optimal wind speed of 8m/s which corresponds to a generator shaft speed of 2500 rpm. From the chain selection chart in figure 3.4, using 'Number of strands'=1 on the vertical axis, it can be inferred that chain number 40 can be used satisfactorily to transmit 2 horsepower within shaft speed limits of 200 rpm to 5000 rpm.

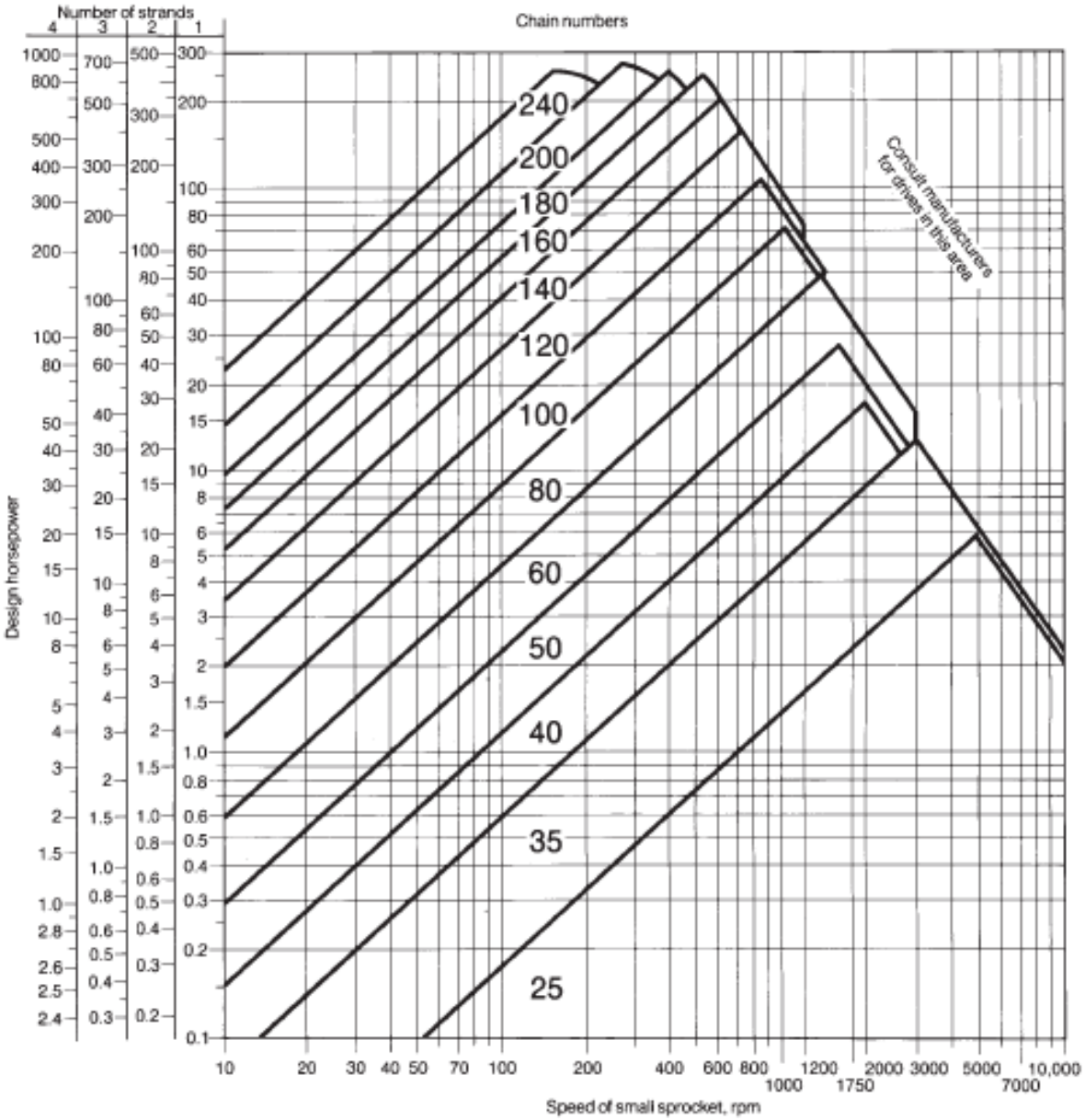

Figure 3.4: Roller chain pitch selection standard chart [30].

From the metric chain dimensions as shown table 3.2, the tentative chain number 40 corresponds to 4/8 in.(12.7mm) pitch(P) roller chain with roller diameter (D)=7.95mm and roller width (W) = 7.85mm. An indication of these dimensions is shown in Figure 3.5.

Table 3.2: Metric Chain Dimensions [36]

Standard name	Chain pitch	Roller diameter (D)	Roller width	Exterior width	Exterior height
#25	6.35 mm	3.3 mm	3.18 mm	7.9 mm	6 mm
#35	9.52 mm	5.08 mm	4.77 mm	12.4 mm	9 mm
#40	12.7 mm	7.95 mm	7.85 mm	16.6 mm	12 mm
8mm 05T	8 mm	4.71 mm	4.61 mm	11.48 mm	7.6 mm
8mm 05B	8 mm	5 mm	3 mm	8.2 mm	7.1 mm
420	12.7 mm	7.77 mm	6.25 mm	14.7 mm	12 mm
428	12.7 mm	8.51 mm	7.75 mm	16.7 mm	11.8 mm

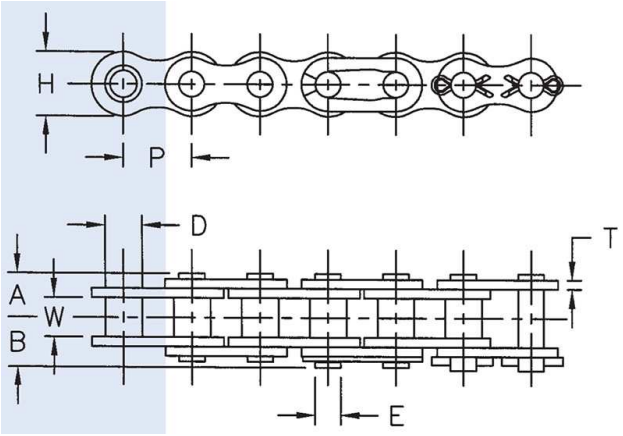

Figure 3.5: Chain size dimensions [37]

For each transformation stage, the speed ratio is 3.2:1; the large sprocket should have 3.2 times the teeth of the small sprocket. Some available small sprockets in the open-market are 11T, 12T, 13T, 14T all 420 (where T is number of teeth and 420 is similar pitch size with 40). Sprocket 13T 420 is selected for optimal strength and size, hence for the larger sprocket required size is 42T 420 which is available in the open market. The sprockets can be purchased from a scooter spare parts shop. The circumference of the larger sprocket is ~42 pitches, so the radius of the larger sprocket can be determined as:

$$R = \frac{42\,pitches}{2\pi} = 6.69 \text{ pitches (85mm)}$$

While for the smaller sprocket, radius is:

$$r = \frac{13\,pitches}{2\pi} = 2.07 \text{ pitches (26.3mm)}$$

Also considering suitable clearance between the 2 sprockets, shaft center distance is initially selected as 32 pitches. The chain length can be computed using the expression of (3.3):

$$L_C = 2C + \frac{N+n}{2} + \frac{(N-n)^2}{4\pi^2 C} \qquad (3.3)$$

Where:

L_c = Chain length, pitches
C = Shaft centers, pitches
N = Number of teeth in large sprocket

n = Number of teeth in small sprocket

For shaft center of 32 pitches, this yields L_c = 90.2 pitches

Whenever possible, chain length should be an even number of pitches. An odd number of pitches requires the use of an offset section which weakens the chain and increases cost [38]. In order to couple chain at an even number of pitches, 90 pitches (1.143m) will be used and the center distance will be re-computed back using (3.6):

$$C = \frac{L_C - \frac{N+n}{2} + \sqrt{(L_C - (\frac{N+n}{2}) - \frac{8(N-n)^2}{4\pi^2}}}{4} \qquad (3.6)$$

This yields a value for shaft center as 31.92 pitches (392.5mm). Pictures of the suitable chain sprockets are shown in Figure 3.6 [39].

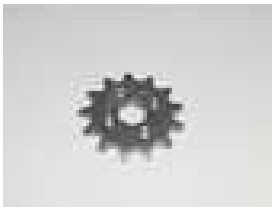

Figure 3.6: (a) Small sprocket 13T 420 **(b)** Big sprocket 42T 420

3.4 Automotive alternator model

The alternator is a 12-pole synchronous generator with salient poles. In a salient pole synchronous machine, if the excitation is varied over the normal operating range, the effect of the saliency on the power or torque developed is not significant. Only at low excitation does the power or torque due to saliency become important. Cylindrical-rotor theory can also be used for salient pole machines except at low excitation or when high accuracy is required [40].

The main parameters that describe the characteristics of the Lundell alternator are described in table 3.3.

Table 3.3: Lundell alternator parameters

Constants (based on machine dimension)		**Variables** (function of operating point)	
p	number of poles	ω_S	electrical frequency (rad/sec)
N_S	number of turns/stator phase	ω_G	mechanical speed (rad/sec)
N_f	number of field winding turns	I_f	excitation or field current (A)
τ_p	pole pitch (mm)	f	frequency (Hz)
α_p	average pole width to pole pitch ratio	ϕ_f	flux per pole due to excitation current, (Wb)
k_W	winding factor	n	rotor speed (rpm)
l_g	length of air gap (mm) (shown in Figure 3.7a)	k_S	saturation level (function of field current)
b_{P1}	rotor claw pole breadth at base (mm) (shown in Figure 3.7b)	E_f	rms excitation voltage/ no load voltage (V)
b_{P2}	rotor claw pole breadth at tip (mm)	B_g	fundamental of airgap flux density (T)

r_s	radius of stator		
μ_o	air gap permeability		
k_C	carter factor		
l_s	stator stack length (mm)		

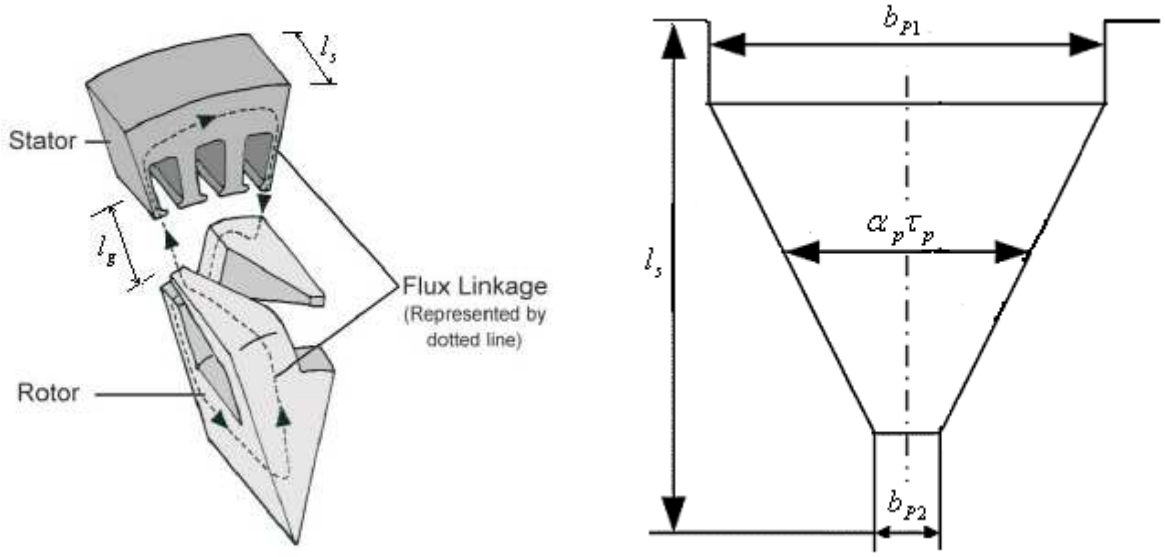

Figure 3.7: (a) Rotor-stator geometry [21] (b) Claw pole geometry

These predefined parameters can be mathematically related by equations (3.7) to (3.11) [40]. Frequency is defined in terms of mechanical speed as:

$$f = \frac{n \cdot p}{120} = \frac{\omega_S}{2\pi} = \frac{p \cdot \omega_G}{4\pi} \qquad (3.7)$$

while average rotor claw pole breadth as shown in Fig. 3.7(b) can be described as:

$$\frac{b_{P1} + b_{P2}}{2} = \alpha_p \tau_p \qquad (3.8)$$

No-load rms voltage per phase can be expressed as:

$$E_f = \frac{2\pi}{\sqrt{2}} k_W N_S f \phi_f \qquad (3.9)$$

Substituting (3.7) into (3.9) yields

$$E_f = \frac{2\pi}{\sqrt{2}} k_W N_S \frac{p\omega_G}{4\pi} \phi_f = k_W N_S \frac{p\omega_G}{2\sqrt{2}} \phi_f \qquad (3.10)$$

According to [23], the flux per pole is described as:

$$\phi_f = B_g \frac{2}{\pi} \tau_p l_s \qquad (3.11)$$

Where fundamental of airgap flux density can be described as:

$$B_g = \frac{4}{\pi} \frac{N_f I_f}{2} \frac{\mu_o}{l_g k_S k_C} \sin\left(\alpha_p \frac{\pi}{2}\right) \qquad (3.12)$$

Substituting (3.12) and (3.11) into (3.10), the no-load rms voltage per phase can be rewritten as:

$$E_f = \left(\frac{\sqrt{2}}{\pi^2} p N_S k_W \tau_p l_s \sin(\alpha_p . \frac{\pi}{2}) \frac{N_f \mu_o}{l_g k_S k_C} \right) I_f \omega_G \qquad (3.13)$$

It could be established that almost all the parameters except for I_f and ω_G are functions of machine dimensions and could be considered as machine parameters.
So effectively,

$$E_f = K_M I_f \omega_G \qquad (3.14)$$

where K_M is the machine constant in (V-s/rad-A) and it could be expressed as:

$$K_M = \frac{\sqrt{2}}{\pi^2} p N_S k_W \tau_p l_s \sin(\alpha_p . \frac{\pi}{2}) \frac{N_f \mu_o}{l_g k_S k_C} \qquad (3.15)$$

The machine constant could also be determined from experimental observation. For the assumed parameters of the alternator as shown in table 3.4, a machine constant estimate of K_M =0.016 (V-s/rad-A) can be obtained.

Table 3.4: Machine dimensions and parameters

Parameters	**Values**
N_S (stator copper turns)	36
k_W winding factor	0.8
τ_p pole pitch (m)	0.025
l_S stator stack length (m)	0.04
$\alpha_p \pi/2$ (degrees)	59.4
N_f (field copper turns)	400
l_g air-gap length (m)	0.00035
$k_S k_c$ Saturation factor & Carter factor	1.3
μ_o air permeability (H/m)	1.26E-06

3.5 Power electronics converter model

This analysis of a conventional automotive alternator's rectifier is based on the assumptions that the rectifier receives continuous ac-side conduction and yields a constant voltage output at the battery. A three-phase rectifier with a constant-voltage load V_0 is shown in figure 3.8. Also included are line inductances L_s in series with a balanced three-phase set of sinusoidal voltages: e_a, e_b and e_c with amplitude E and angular frequency ω.

$$e_a = E\sin(\omega t) \tag{3.16}$$

$$e_b = E\sin(\omega t - \frac{2\pi}{3}) \tag{3.17}$$

$$e_c = E\sin(\omega t - \frac{4\pi}{3}) \tag{3.18}$$

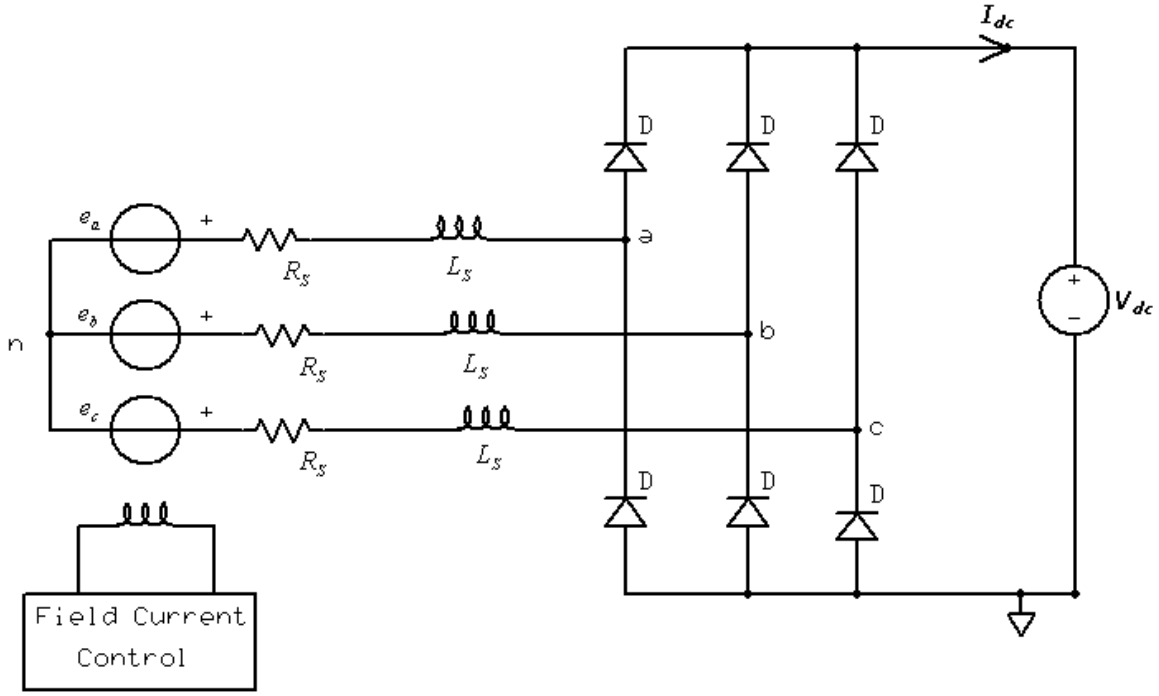

Figure 3.8: Lundell alternator equivalent circuit

There is a phase difference between back emf and current as a result of the line inductance. Phase currents i_a, i_b, and i_c can be approximated by their fundamental components i_{a1}, i_{b1} and i_{c1}, respectively because the phase currents' fundamental can be assumed to be responsible for power transfer. This assumption is also used in [22],[23] and [41]. The phase currents can be expressed as:

$$i_a \approx i_{a1} = I_{s1}\sin(\omega t - \phi) \tag{3.19}$$

$$i_b \approx i_{b1} = I_{s1}\sin(\omega t - \phi - 2\pi/3) \tag{3.20}$$

$$i_c \approx i_{c1} = I_{s1}\sin(\omega t - \phi - 4\pi/3) \tag{3.21}$$

where I_{s1} and Φ are the magnitude and phase, respectively, of the fundamental component of the phase currents

The phase current fundamental is considered essentially sinusoidal (star connection), as shown in figure 3.9 though, at low speeds, it tends to be rectangular — discontinuous [23].

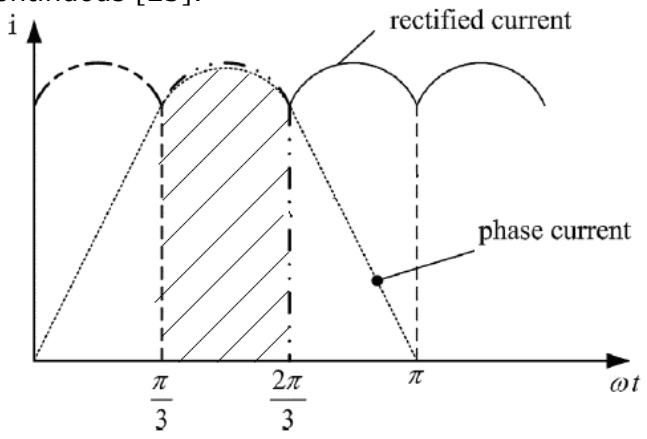

Figure 3.9: Waveforms of alternator currents (star connection) [23]

Let rms phase voltage and current fundamental be:

$$E_s = \frac{E}{\sqrt{2}} \quad \text{and} \quad I_s = \frac{I_{s1}}{\sqrt{2}} \quad \text{respectively} \tag{3.22}$$

Considering the current waveforms in fig 3.10 with emphasis on the shaded portion

$$i_{dc} = \sqrt{2} I_s \sin \omega t : \qquad \frac{\pi}{3} < \omega t < \frac{2\pi}{3} \tag{3.23}$$

Integrating i_{dc}, the ampere-second area A can be obtained as:

$$A = \int_{\pi/3}^{2\pi/3} \sqrt{2} I_s \sin \omega t . d(\omega t) \;=\; \sqrt{2} I_s \tag{3.24}$$

To obtain the average dc current I_{dc}, area A can be divided by the $(\pi/3)$ interval:

$$I_{dc} = \frac{\sqrt{2} I_s}{\pi/3} \;=\; \frac{3\sqrt{2} I_s}{\pi} \tag{3.25}$$

Taking the power balance across the rectifier into consideration,

$$3 I_s E_s \cos\phi - P_{\mathrm{Re}ct+cu,S} = V_{dc} I_{dc} \tag{3.26}$$

where $P_{Rect+cu,s}$ is rectifier and stator phase power loss expressed as:

$$P_{\mathrm{Re}ct+cu,S} = 3 V_d I_s + 3 I_s{}^2 R_s \tag{3.27}$$

where R_s is the stator phase resistance
V_d is the rectifier diode voltage drop

Therefore, substituting (3.27) and (3.25) into (3.26) and making V_{dc} the subject of equation (3.26):

$$V_{dc} = \frac{3I_s E_s \cos\phi - P_{rect+cu,S}}{I_{dc}} = \frac{3I_s\left(E_s \cos\phi - V_d - I_s R_s\right)}{\frac{3\sqrt{2}}{\pi} I_s} \quad (3.28)$$

This can be rewritten as:

$$V_{dc} = \frac{\pi}{\sqrt{2}}\left(E_s \cos\phi - V_d - I_s R_s\right) \quad (3.29)$$

3.6 System integration

In order to obtain a model that can be used to determine power output of the small wind turbine, sub-systems can be combined based on power balance as follows:

Mechanical power realized from wind – mechanical transmission losses in gear system - generator losses – power converter losses = power output

Mechanical power realized from wind can be obtained from equation (1) with wind power (P_w) as input power,

$$P_w - P_{Mech.loss} - P_{Gen,loss} - P_{Conv,loss} = P_{out} \quad (3.30)$$

$$\frac{1}{2} C_p(\lambda,\theta)\pi r^2 v^3 \rho - P_{total,losses} = P_{out} \quad (3.31)$$

The generator mechanical losses are categorized together with the mechanical transmission losses while the converter losses are categorized with the generator electrical losses and described in table 3.5. Prior to the rectifier stage, power balance in steady state holds as follows:

$$P_w - P_{loss} = P_{R,out} \quad (3.32)$$

$$T_m \omega_G - P_{loss} = 3E_s I_s \cos\phi \quad (3.33)$$

where P_{loss} represents the losses prior to the rectifier stage. From (3.14), substituting for $E_s = E_f$ in (3.33)

$$T_m \omega_G - P_{loss} = 3K_M I_f \omega_G I_s \cos\phi \quad (3.34)$$

Dividing all through by ω_G

$$T_m - \frac{P_{loss}}{\omega_G} = 3K_M I_f I_s \cos\phi \quad (3.35)$$

Table 3.5: Power loss components

Electrical	
Stator winding loss	$P_{cu,S} = 3{I_S}^2 R_S$
Rotor winding loss	$P_{cu,R} = {I_f}^2 R_f$

Rectifier diode voltage drop loss	$P_{Rect} = 3V_d I_s$
Power converter device (IGBT) loss	$P_{Conv} = {I_{dc}}^2 R_{on} D + 0.5 V_{dc} I_{dc} f_S (t_{c(on)} + t_{c(off)})$
Brush loss	$P_{Brush} = {I_f}^2 R_{Brush}$
Magnetic	
Eddy current	$P_{Eddy} = K_{Ed} t^2 {\omega_G}^2 B^2$
Hysteresis	$P_{Hyst} = K_{Hyst} \omega_G B^2$
Mechanical	
Bearing friction	$P_{Be} = K_{Be} \omega_G$
Windage	$P_{Win} = K_{Win} {\omega_G}^3$
Chain drive transmission	$P_{Mech,loss} = 0.03 P_w$

Where K_{Ed} = eddy current loss constant coefficient
t = thickness or length of magnetic path in iron
ω_G = alternator rotational speed (rad/s)
B = flux density of the iron cross section
K_{Hyst} = hysteresis loss constant coefficient
K_{Be} = bearing loss constant coefficient
K_{Win} = windage loss constant coefficient
V_d = rectifier diode finite on-voltage
I_S = stator phase current
f_S = switching frequency
$t_{c(on)} + t_{c(off)}$ = hard switching conduction ON & OFF time

The iron losses comprise of stator and rotor iron losses. Experiments by Kuppers and Henneberger [22] indicate that a good approximation for rotor iron loss = 2 x stator iron loss. The magnetic and mechanical loss constants were obtained from simultaneous equations extrapolated from the measurements carried out in the EPP laboratory. The measurements are discussed in Chapter 5. The equations are shown in table 3.6. For the iron loss measurements, flux density is assumed constant since constant field current is supplied during measurement. Magnetic path length is also assumed constant.

Table 3.6: Alternator shaft speed and corresponding loss equations

Speed, ω_G (rpm)	**Iron losses (W)**
1011	$K_{Ed}(1011^2) + K_{Hsyt}(1011) = 21.5$
2612	$K_{Ed}(2612^2) + K_{Hsyt}(2612) = 83$
Speed, ω_G (rpm)	**Mechanical losses (W)**
1011	$K_{Be}(1011) + K_{Win}(1011^3) = 15.12$
2706	$K_{Be}(2706) + K_{Win}(2706^3) = 52.41$

The loss constant values obtained are shown in table 3.7.

Table 3.7: Loss constants

K_{Ed}	6.565e-06 W/rpm^2
K_{Hyst}	1.463e-02 W/rpm
K_{Be}	1.424e-02 W/rpm
K_{Win}	7.002e-10 W/rpm^3

For the purpose of evaluating the shaft torque and the dynamic effect of wind speed changes and system inertia on machine rotor, the equation (3.1) can be used in obtaining the expression for the generator torque that will satisfy optimal wind turbine operation as shown in equation (3.36). The optimizing generator torque counterbalances the mechanical torque from the wind turbine to regulate the generator speed.

$$T_e = \frac{P_W}{\omega_G} = \frac{\rho\pi.r^5 C_p(\lambda,\theta)\omega_G^{\ 2}}{2\lambda^3 G^3} \qquad (3.36)$$

$$\lambda = \frac{r\omega_G}{vG} \quad \text{From (3.2)} \qquad \omega_T = \frac{\omega_G}{G} \qquad (3.37)$$

$$T_w = \frac{T_T}{G} \qquad (3.38) \qquad T_w - T_e - T_{loss} = J\frac{d\omega_G}{dt} \qquad (3.39)$$

Where: r = turbine radius
v = wind speed
G = Gearbox ratio
ω_G = Generator speed
ω_T =Wind turbine mechanical (low) speed
T_T = Torque on low speed shaft
T_w = Torque on high speed shaft
T_e= Generator Torque
T_{loss} = Loss torque
J = Total inertia of system referred to the high speed shaft

The system inertia is estimated for turbine blades, hub and alternator rotor. Shaft and chain drive inertia are assumed negligible. The inertia J of a body can be expressed as:

$$J = \sum m_i r_i^{\ 2} \qquad (3.40)$$

A rough estimation of inertia of turbine blades is done assuming each blade has its mass middle point at about 1/3 of the radius [43]. Hence for 1 blade,

$$J_b = M\left(\frac{r_b}{3}\right)^2 \qquad (3.41)$$

where M =mass of 1 blade
r_b = length of 1 blade ~ 2m

Assuming density of wood used to build turbine blades = 650 kg/m^3
Dimension of a blade ~ 2m X 0.0381m X 0.1524m = 0.011613m^3 per blade

Mass of 1 blade = density X volume = 650 kg/m^3 X 0.011613m^3 = ~7.55kg.
For three blades

$$3J_b = 3M\left(\frac{r_b}{3}\right)^2 = \frac{7.55}{3}(2)^2 = 10.1 kgm^2$$

For the hub with diameter of 0.4m and thickness of 0.05m, volume can be expressed as:

$$Vol = \pi(r^2)h = 0.006283\text{m}^3 \qquad (3.42)$$

Assuming wood with similar density is used for hub also = 650 kg/m^3
Mass of hub = 0.006283m^3 x 650 kg/m^3 = ~4.1kg
Inertia of hub can be obtained using the expression:

$$J_h = \frac{1}{2}mr^2 \qquad (3.43)$$

where m =mass of hub and r = radius of hub

$$J_h = \frac{1}{2}mr^2 = \frac{1}{2}(4.1)(0.2)^2 = 0.082\ kgm^2$$

From [44], Inertia of alternator rotor can be computed as 0.0022 *kgm^2* assuming average mass density of a rotating copper wound field bobbin claw pole Lundell alternator is 5500 kg/m^3, rotor thickness is ~0.04m and diameter is ~0.1m.
Hence total significant inertia J:

$$J = \left(\frac{3J_b + J_h}{G^2}\right) + J_a = 0.10149+0.0022 = 0.1037\ kgm^2$$

where G is the gear system ratio=10 chosen so that cut in wind speed at 3.5m/s would correspond to alternator cut-in shaft speed at 1050rpm (~110 rad/s) at an optimal tip speed ratio (TSR) of 6.5 and wind turbine blade radius of 2m.

3.7 MPPT Model

The proposed power converter (rectifier & dc chopper) topology is shown in Figure 3.10. It consists of an MPPT scheme which is based on equation (3.36). This can also be written as:

$$P_e = \left(\frac{\rho\pi.r^5 C_p{}^{opt}}{2\lambda_{opt}{}^3 G^3}\right)\omega_G{}^3 \qquad (3.44)$$

Let $$K_{opt} = \left(\frac{\rho\pi.r^5 C_p{}^{opt}}{2\lambda_{opt}{}^3 G^3}\right) \qquad (3.45)$$

Considering the expression in the bracket to be a constant of proportionality-K_{opt}, equations (3.36) and (3.44) become:

$$T_e = (K_{opt})\omega_G{}^2 \qquad (3.46)$$

$$P_e = \left(K_{opt}\right)\omega_G{}^3 \qquad (3.47)$$

The power losses in the drive train are also taken into consideration and deducted from P_e thereby leaving the electrical power load required to balance the wind torque and regulate the generator speed. Therefore output electrical power can be adjusted to a value described in (3.48)

$$P_{opt} = P_e - P_{loss} = \left(K_{opt}\right)\omega_G{}^3 - P_{loss} \qquad (3.48)$$

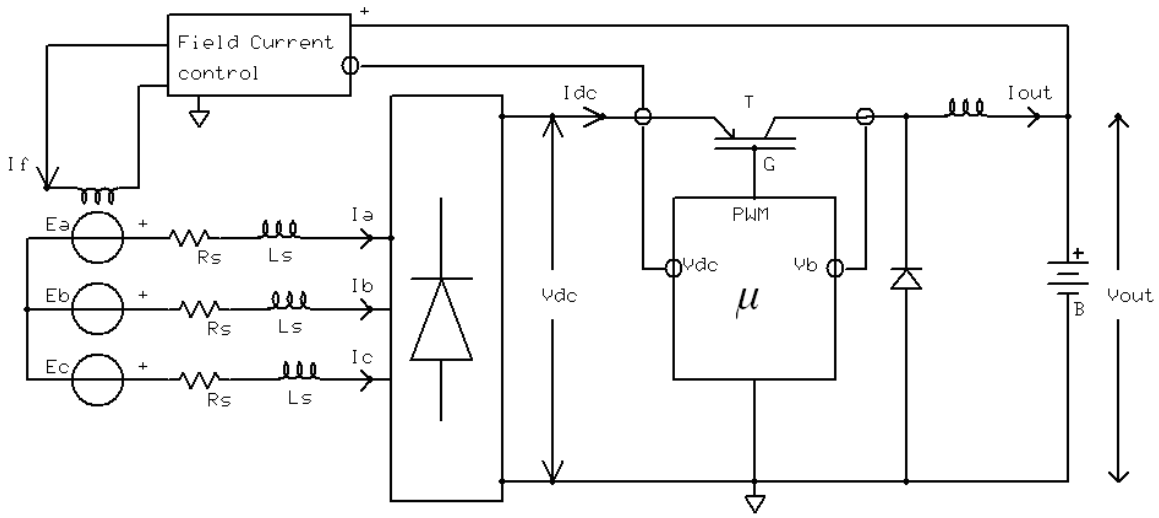

Figure 3.10: Modified alternator system 1

The required value of the optimal output power (P_{opt}) that balances the wind mechanical torque is computed in a microcontroller which simultaneously samples the generator speed (ω_G) and the battery voltage (V_b). The generator speed can be sampled via optical sensors or phase voltage frequency. The microcontroller computes the optimal power (P_{opt}) based on sampled generator speed (ω_G). It also computes the required output current that must be supplied to the battery to maintain optimal turbine operation.

$$P_{opt} = I_{out}V_{out} \qquad (3.49)$$

Based on the values of the V_{dc}; V_b; and battery internal resistance, R_{int} the microcontroller computes the reference battery current, $I_{b,ref}$.

$$I_{b,ref} = \frac{V_{out} - V_b}{R_{\text{int}}} \qquad (3.50)$$

$$V_{out} = V_b + I_{out}R_{\text{int}} \qquad (3.51)$$

Substituting (3.51) into (3.49),

$$\begin{aligned} P_{opt} &= I_{out}\left(V_b + I_{out}R_{\text{int}}\right) \\ &= I_{out}V_b + \left(I_{out}\right)^2 R_{\text{int}} \end{aligned} \qquad (3.52)$$

The microcontroller solves the quadratic equation and takes the positive value of I_{out}.

$$I_{out} = \frac{-V_b \pm \sqrt{V_b{}^2 + 4R_{\text{int}} P_{opt}}}{2R_{\text{int}}} \qquad (3.53)$$

The microcontroller now computes and sets the duty ratio, D of a pulse width modulated switch (IGBT) that can supply the optimal current I_{out} to the battery.

$$D = \frac{I_{out}}{I_{b,ref}}\left(1 - \frac{V_b}{V_{out}}\right) + \frac{V_b}{V_{out}} \qquad (3.54)$$

Another method for maximum power point tracking could be to control the field winding via the microcontroller as shown in figure 3.11. This method will require that the in-built regulator of the alternator be removed completely.

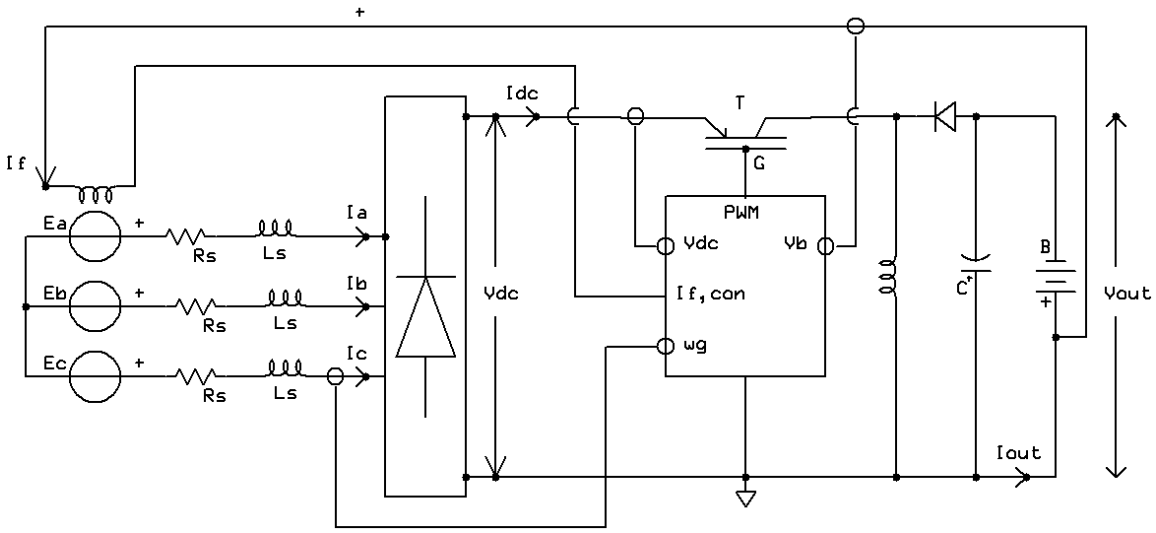

Figure 3.11: Modified alternator system 2

The required value of the optimal output power (P_{opt}) that balances the wind mechanical torque is computed in a microcontroller which simultaneously samples the generator speed (ω_G) - via the alternator's ac-side frequency, and the battery voltage (V_b). The microcontroller computes the optimal power (P_{opt}) based on sampled generator speed (ω_G). It also computes the required output dc voltage that must be supplied to the battery to maintain optimal turbine operation

$$P_{opt} = \frac{(V_{dc,ref} - V_b)^2}{R_{\text{int}}} \qquad (3.55)$$

Based on the values of V_b; and battery internal resistance, R_{int} the microcontroller also computes the reference battery output voltage, the $V_{dc,ref}$.

$$V_{dc,ref} = \left(\sqrt{R_{\text{int}} P_{opt}}\right) + V_b \qquad (3.56)$$

The microcontroller now computes and sets the field current I_f to achieve $V_{dc,ref}$.

$$I_f = \frac{V_{dc,ref}}{K_{M,dc}\omega_G} \qquad (3.57)$$

where $K_{M,dc}$ is the proportionality constant between rectified dc voltage and field current, generator speed.

The output dc voltage is now set at a value that might be unsuitable for battery charging. It may range randomly above and below 14.5V, so a buck boost converter is required to be placed at the output to maintain dc voltage at a constant value while varying current. The duty ratio can be computed from the expression in (3.58).

$$D = \frac{V_{out}}{V_{out} + V_{dc}} = \frac{I_{dc}}{I_{out} + I_{dc}} \qquad (3.58)$$

Chapter 4

Simulation of the automotive alternator used in a small wind turbine

4.1 Model parameters

The simulation was developed in Simulink®. An initialization file (.m-file) was written which contained relevant parameters (shown in table 4.1) for the simulink computation. Two scenarios are simulated as follows:

a. The alternator (with its in-built regulator) integrated in a wind turbine with parameters assumed in table 3.1 of the analytical model (Chapter 3). This will be subsequently known as system structure 1.
b. The alternator integrated in the assumed wind turbine with a maximum power point control scheme. This will be subsequently known as system structure 2.

Table 4.1: Simulink parameters

Parameters	**Connotation**	**Value**
Gear ratio	G	10
Total inertia referred to alternator side	J	0.1037 kgm^2
Turbine blade radius	r	2 m
Air density	den	1.225 kg/m^3
Field current maximum	Ifield	3.8 A
Field + Brush resistance	Rf + Rbrush	3.8 Ω
Stator resistance	Rs	0.1 Ω
Battery charging voltage limit	Vbc	14.5 V
Internal battery voltage	Vo	12.5 V
Diode voltage drop	Vd	0.8 V
Rectifier diode bulk resistance	Rb	0.005 Ω
Flux density	B	1 (for constant field)
Hysteresis loss constant	Khyst	1.463e-02 (W/rpm)
Eddy current loss constant	Ked	6.565e-06 (W/rpm^2)
Bearing loss constant	Kbe	1.424e-02 (W/rpm)
Windage loss constant	Kwin	7.002e-10 (W/rpm^3)
Machine constant	Km	0.01683 (V-s/rad-A)
Additional parameters used for system structure 2		
Transistor ON resistance	Ron	0.02 Ω
Switching frequency	fs	100 kHz
Hard-switching On & OFF time	tsw	50 ns
Optimal power coefficient	Cpo	0.39
Optimal tip speed ratio	lambdo	6.5

4.2 Simulations

For the purpose of this simulation, the wind speed is varied according to gusty wind speed profiles for 30-seconds duration. The random wind velocity oscillations are based on the sinusoidal functions described in (4.1). The frequency of oscillation is in multiples of (1/60) Hz.

$$v_w = 4 + 2\sin\left(\frac{\pi t}{30}\right) + 2\sin\left(\frac{3.5\pi t}{30}\right) + \sin\left(\frac{12.35\pi t}{30}\right) + 0.2\sin\left(\frac{35\pi t}{30}\right) \qquad (4.1)$$

4.2.1 System structure 1

The model was run for the typical 12V claw-pole alternator with its in-built regulator described by system structure 1 as shown in figure 4.1. The field excitation is supplied from the battery at start up and self supplied from the alternator during running. In order to automate this system, a centrifugal switch installed on the alternator shaft would be necessary for switching 'on' the field winding when sufficient wind speed is attained and 'off' when there is insufficient or excessive wind speed. The simulink model is shown in figure 4.2.

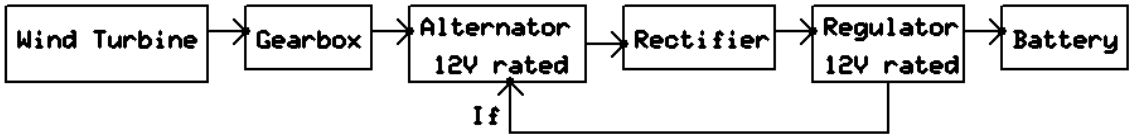

Figure 4.1: System structure 1

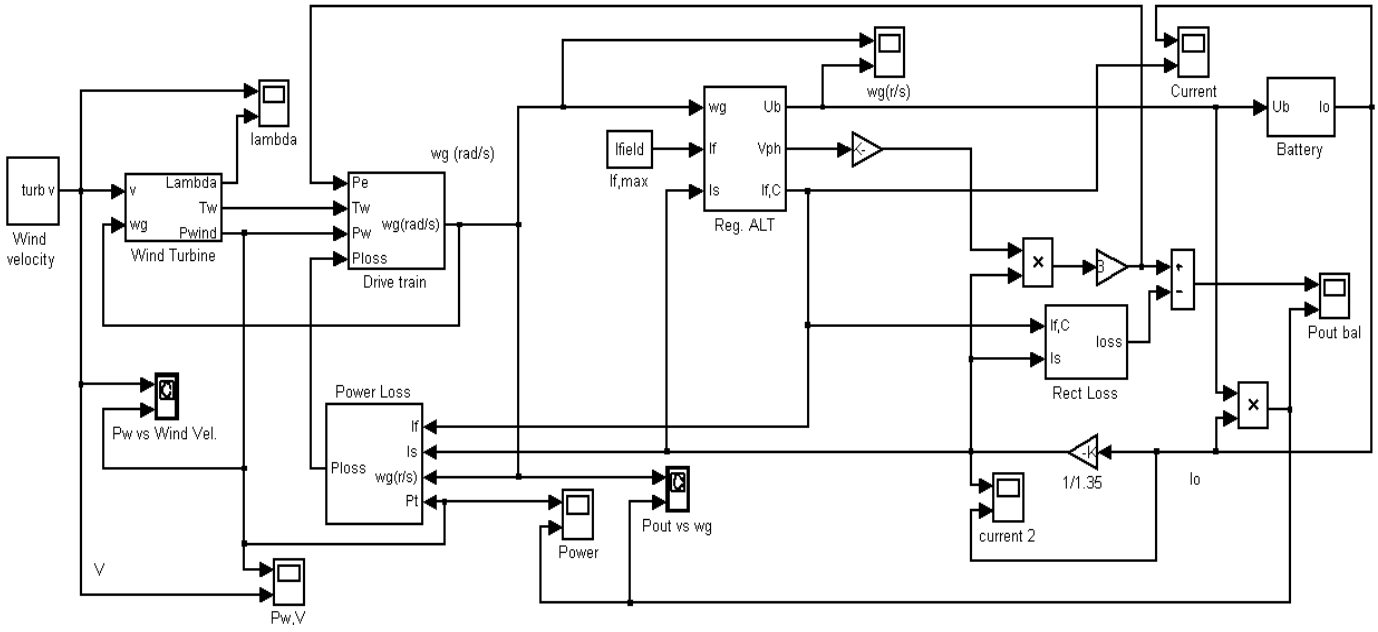

Figure 4.2: Simulink model of system structure 1.

The mathematical expressions represented by each block are discussed as follows:

1. The wind turbine converts wind velocity to mechanical power obtainable from the wind. This conversion is based on equation (4.2).

$$P_w = \frac{1}{2} C_p(\lambda, \theta) r^2 \pi v^3 \rho \qquad (4.2)$$

Numerical approximations have been developed to calculate C_p for given values of λ and θ. The following approximation is used [45]:

$$C_p(\lambda,\theta) = 0.73\left(\frac{151}{\lambda_i} - 0.58\theta - 0.002\theta^{2.14} - 13.2\right)\exp\left[-18.4/\lambda_i\right] \quad (4.3)$$

where:

$$\lambda_i = \left[\frac{1}{\lambda - 0.02\theta} - \frac{0.003}{\theta^3 + 1}\right]^{-1} \quad (4.4)$$

The constituents of the wind turbine block are shown in figure 4.3

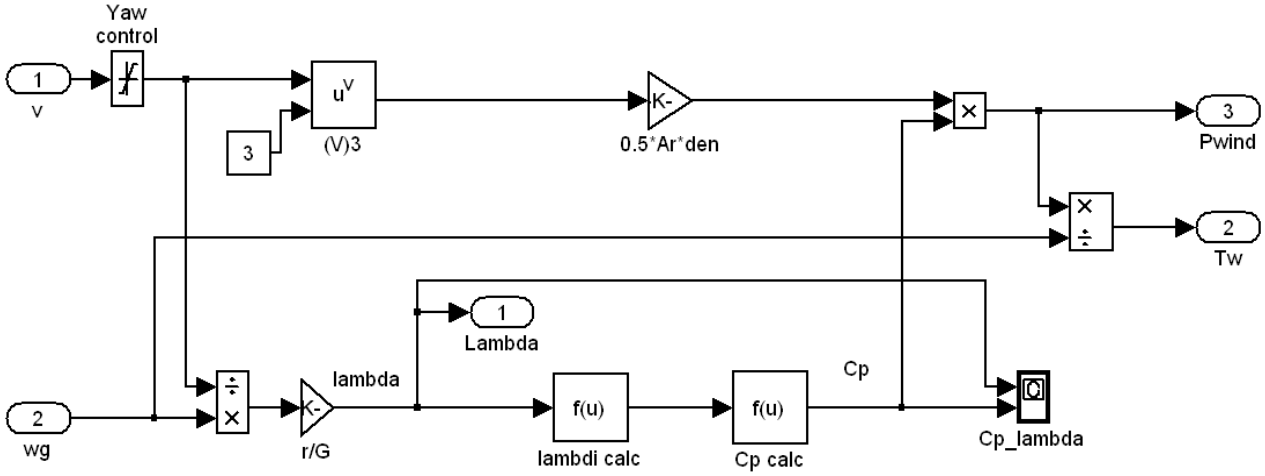

Figure 4.3: Wind turbine model

2. The drive train converts the wind speed to the generator shaft speed. In transient state when there is rapid wind speed variation, the inertia of the turbine blades has some effect on the alternator shaft speed. This is modeled based on equation (4.5).

$$T_w - T_e - T_{loss} = J\frac{d\omega_G}{dt} \quad (4.5)$$

This can be rewritten as:

$$\omega_G = \frac{1}{J}\int (T_w - T_e - T_{loss})dt \quad (4.6)$$

The constituents of the drive train are shown in figure 4.4

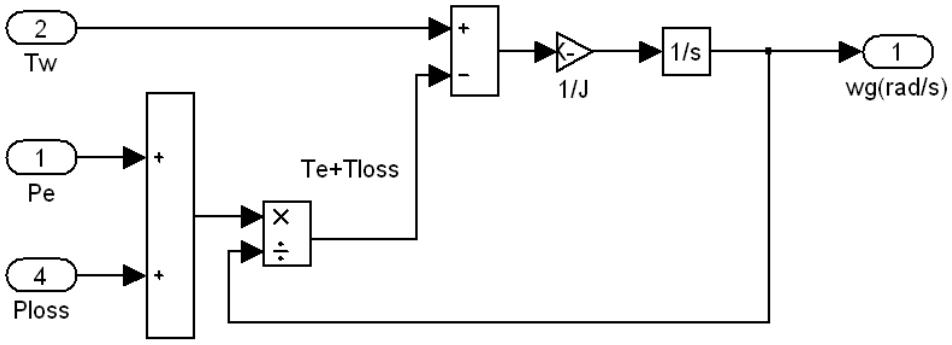

Figure 4.4: Drive train

3. The regulated alternator block (Reg. ALT) represents the specimen recycled automotive alternator (12V 50A). The contents of the block are shown in figure 4.5. It consists of the claw pole alternator, the rectifier and the in-built regulator. The alternator converts the generator shaft speed to the a.c. back emf of each phase based on equation (4.7).

$$E_f = K_M I_f \omega_G = E_s \qquad (4.7)$$

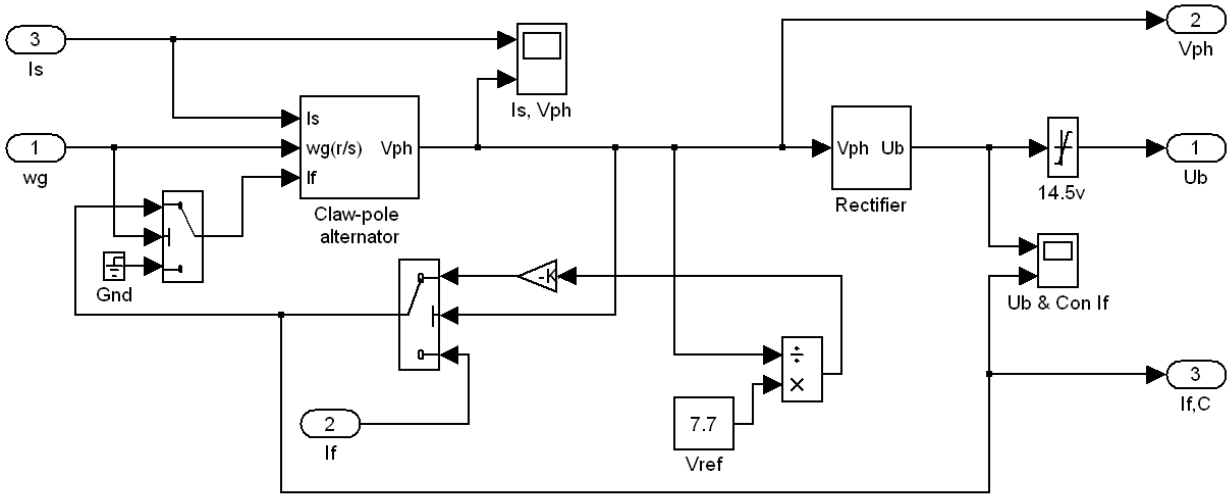

Figure 4.5: Reg. ALT model

The claw-pole alternator model is based on the proportionality constants obtained from the measurements of back emf with respect to field current and speed. The field current is varied in a manner so as to regulate the output dc voltage of the alternator to battery charging voltage. This is modeled with switches and is based on gradients obtained from the open circuit test measurements carried out on the recycled alternator (Chapter 5). For proportionality of back emf with respect to field current; and back emf with respect to speed:

$$K_1 = \frac{E_f}{I_f} \quad ; \quad K_2 = \frac{E_f}{\omega_G} \qquad (4.8)$$

Combining the constants

$$K_1 K_2 = \frac{{E_f}^2}{I_f \omega_G} \qquad (4.9)$$

This can be rewritten as:

$$E_f = \sqrt{K_1 K_2 I_f \omega_G} \qquad (4.10)$$

The rectifier converts the a.c. voltage to dc voltage based on equation (4.11).

$$V_{dc} = \frac{\pi}{\sqrt{2}}\left(E_s \cos\phi - V_d - I_s R_s\right) \qquad (4.11)$$

4. Blocks for the power losses were also developed. These took all the power losses at different stages into consideration. This way the anticipated output power could be computed. The model was based on the loss distribution in Table 3.3 of the analytical model (Chapter 3). Contents of the power loss block are shown in figure 4.6 while contents of the rectifier loss block are shown in figure 4.7. The rectifier loss block also contains a loss model of the in-built regulator.

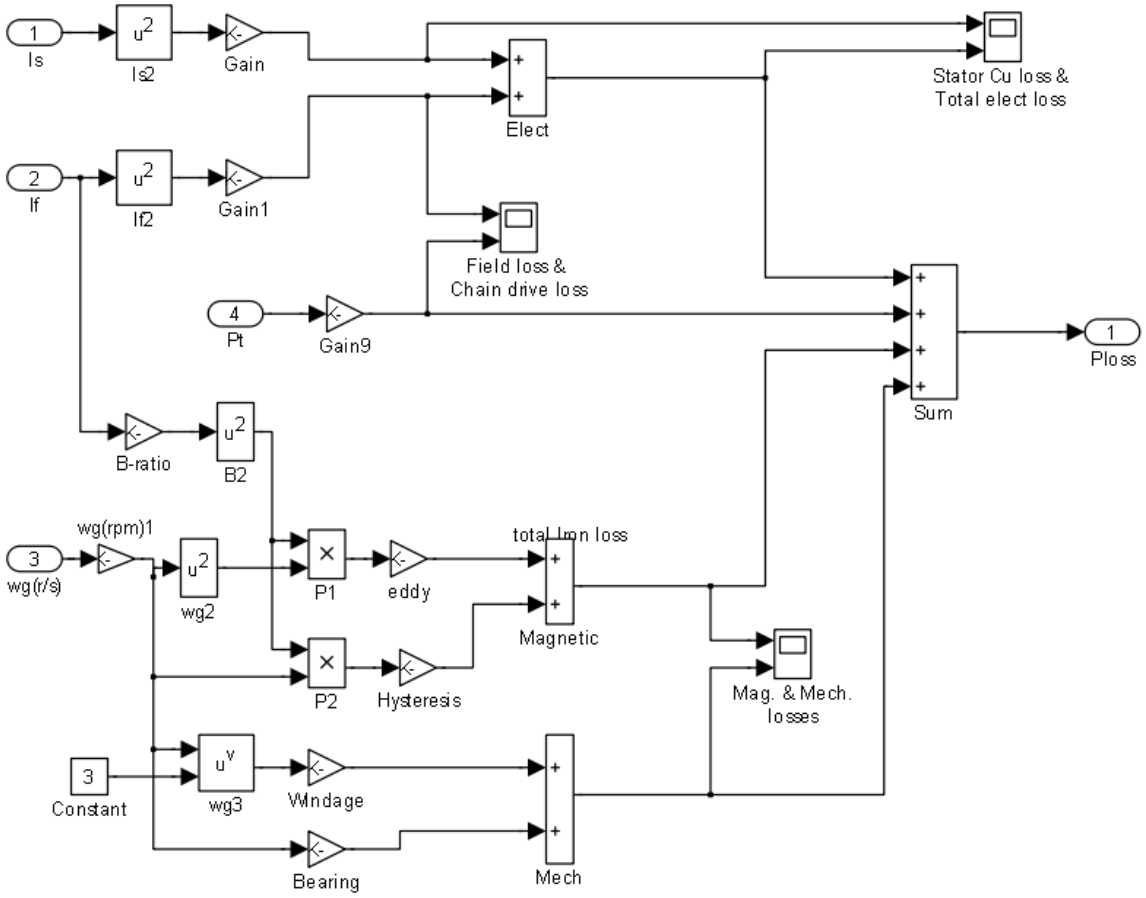

Figure 4.6: Power loss model

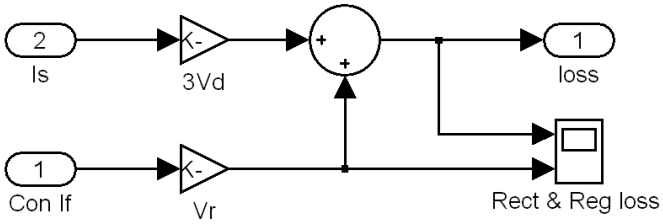

Figure 4.7: Rectifier loss model

5. The battery model was made for a 30-second-duration in which the state of charge of the battery was assumed constant. It is based on a battery internal resistance of 0.005Ω and a battery internal voltage of 12.5V. The content of the battery block is shown in figure 4.8.

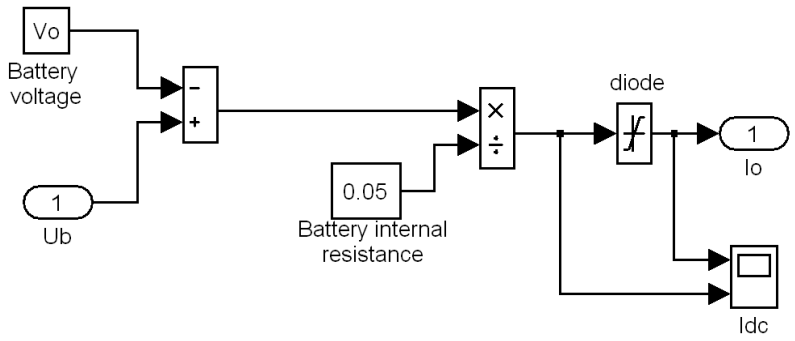

Figure 4.8: Battery model

4.2.2 System structure 1 simulation results

The simulation was run with the oscillating wind speed as described by equation (4.1) for a 30-seconds-duration. The wind profile is shown in the upper graph of figure 4.9a while the tip-speed ratio is shown in the lower plot. It can be observed from fig. 4.9a that the tip-speed ratio oscillates abruptly as wind speed changes. This is because the generator shaft acceleration is slower than wind acceleration. This is due to the effect of inertia on the shaft speed which alters the tip speed ratio of the turbine and concurrently shifts the wind turbine from operating at the optimal power coefficient. The full C_p-λ curve for the assumed wind turbine is shown in fig. 4.10a while the operating segment in the course of the simulation is shown in fig. 4.10b. Figure 4.9b shows the alternator shaft speed and the alternator's output voltage. The output voltage from the alternator rises almost instantaneously to battery charging voltage at a cut-in shaft speed of 105 rad/s. The field current as shown in fig. 4.11b remains constant for the duration of this simulation because the alternator's speed does not get to high values that could lead to over-voltage. The alternator's inbuilt regulator controls the field winding in order to keep the voltage output suitable for battery charging. The generator torque provides some damping for the alternator speed and keeps it from overshoot during wind speed changes.

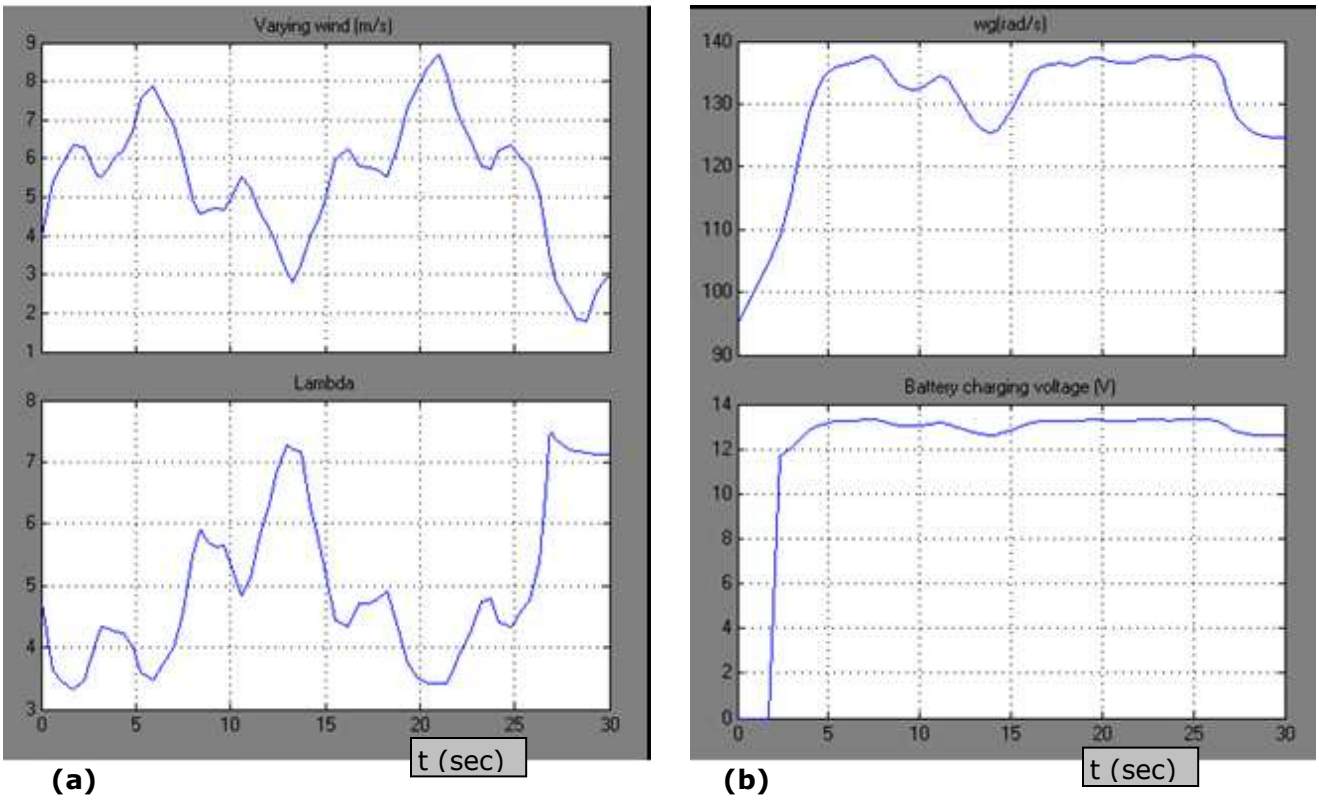

Figure 4.9: **(a)** Wind speed profile, lambda; **(b)** Alternator speed, Battery charging voltage for system structure 1

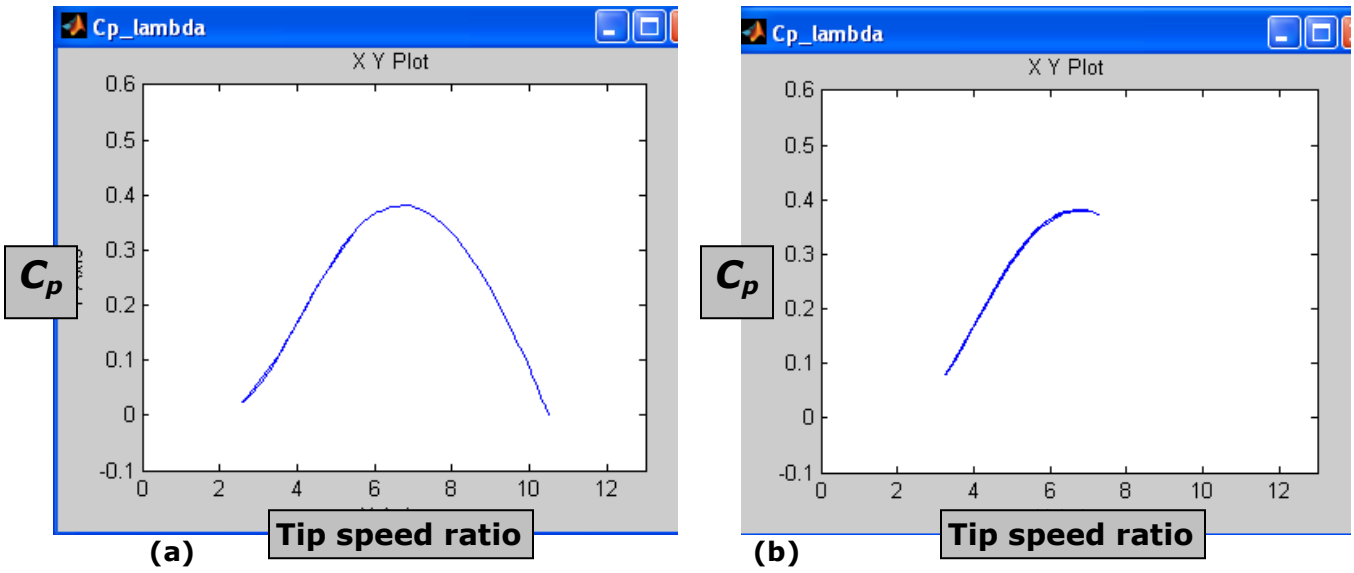

Figure 4.10: C_p - λ characteristics of wind turbine

Figure 4.11a shows the wind power and the output (electrical) power of the wind turbine simulated. It can be observed that despite the wind speed attaining rated wind speed at t=20 sec (fig. 4.9a), the wind power does not attain rated power of 1.5 kW.

The impact of inertia on the power coefficient has reduced the power obtained from the wind and thus the wind power is not following the optimal power curve of the wind turbine described in figure 3.2. The output power from the alternator is also less than its rated capacity for similar reasons as the wind power. The output current is shown in fig. 4.11b. It appears quite proportional to the output power because the voltage is almost constant.

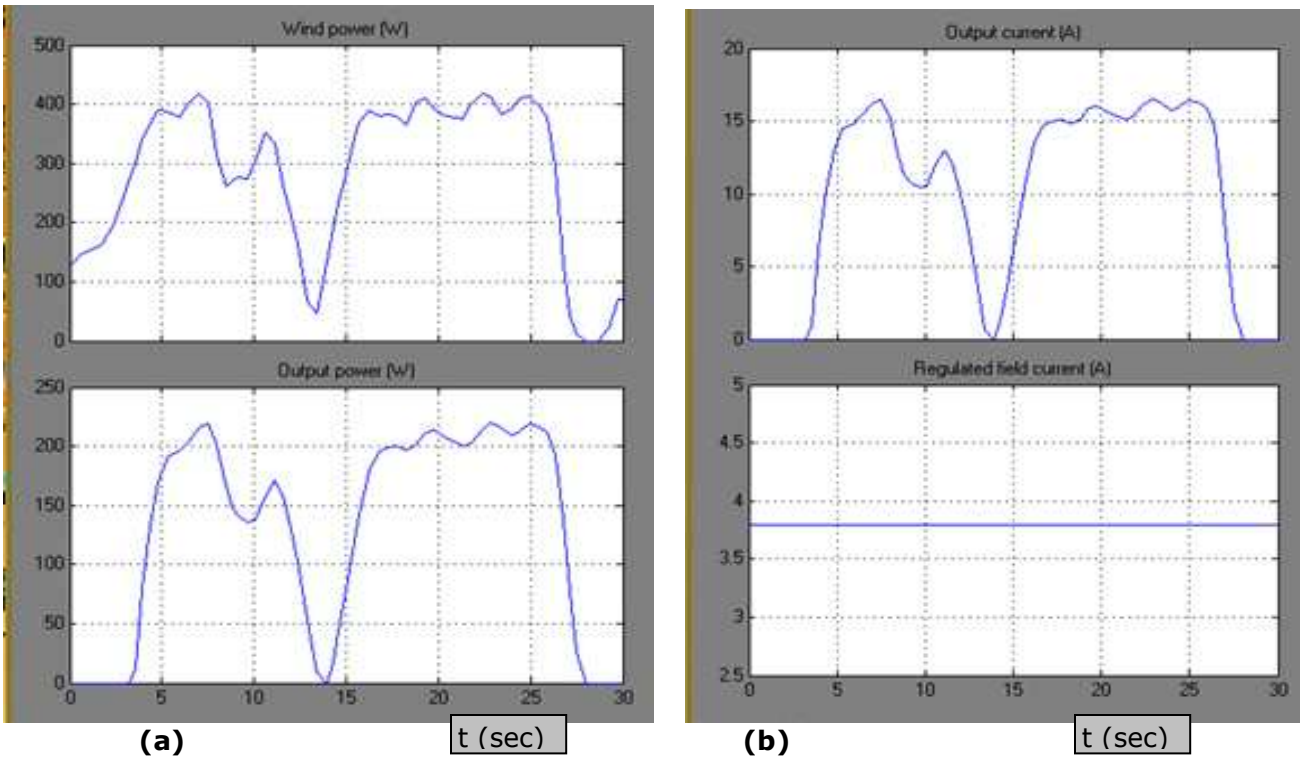

Figure 4.11: **(a)** Wind power, output power; **(b)** Output current, field current

4.2.3 System structure 2

As observed from system structure 1, the effect of turbine blades' inertia makes it impossible for the wind turbine to operate at optimal power coefficient. A speed controller is required to maintain tip speed ratio at optimum and thereby keep power coefficient optimal. For system structure 2 shown in figure 4.12, a maximum power point tracking (MPPT) microcontroller is used to maintain optimal power operation of the turbine while the alternator's inbuilt regulator keeps output voltage at a suitable level for battery charging.

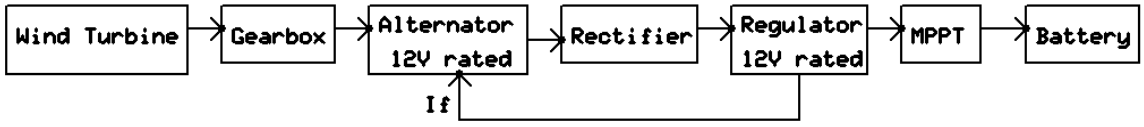

Figure 4.12: System structure 2

The difference in simulink model with system structure 1 is the inclusion of the MPPT microcontroller model and a modified drive train model. The contents of the

simulink model are shown in figure 4.13. The power consumption of the MPPT microcontroller is also taken into consideration.

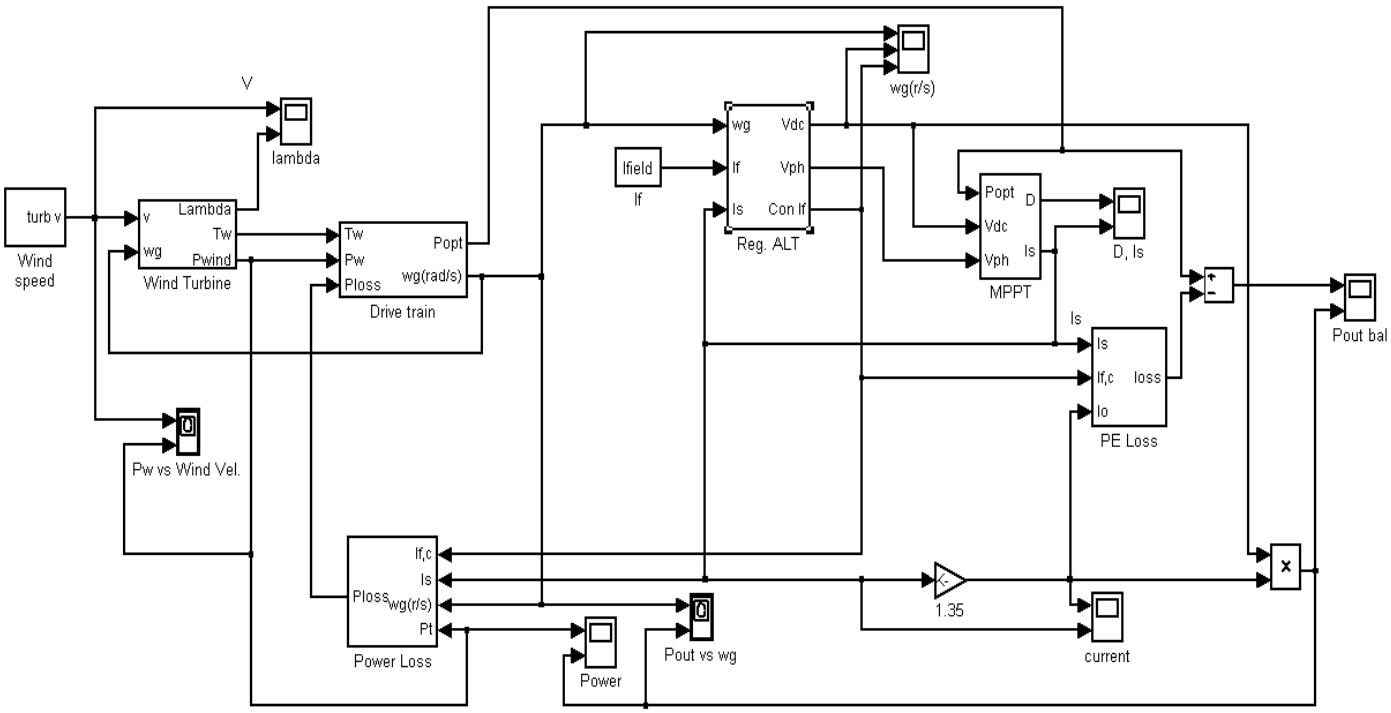

Figure 4.13: System structure 2 model

The modified drive train is shown in figure 4.14. It forms the basis of the MPPT technique used. Generator torque is used to control the generator shaft speed such that a relating algorithm between the generator speed and the generator torque is based on the optimal tip speed ratio as described with equation (4.12).

$$T_e = \left(\frac{\rho \pi . r^5 C_p^{\ opt}}{2 \lambda_{opt}^{\ 3} G^3} \right) \omega_G^{\ 2} \qquad (4.12)$$

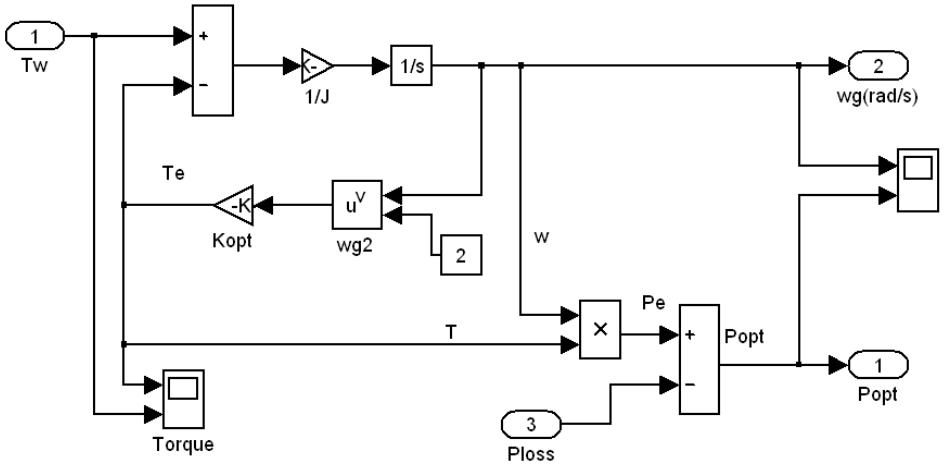

Figure 4.14: Modified drive train

Based on equations (3.44) to (3.54) of the analytical model (Chapter 3), the modified drive train and MPPT models are built. The equations are repeated here for easy readability in equations (4.13) to (4.23):

$$P_e = \left(\frac{\rho \pi . r^5 C_p{}^{opt}}{2 \lambda_{opt}{}^3 G^3} \right) \omega_G{}^3 \qquad (4.13) \qquad K_{opt} = \left(\frac{\rho \pi . r^5 C_p{}^{opt}}{2 \lambda_{opt}{}^3 G^3} \right) \quad (4.14)$$

$$T_e = \left(K_{opt} \right) \omega_G{}^2 \qquad (4.15) \qquad P_e = \left(K_{opt} \right) \omega_G{}^3 \qquad (4.16)$$

Output electrical power can be adjusted to a value described in (4.17)

$$P_{opt} = P_e - P_{loss} = \left(K_{opt} \right) \omega_G{}^3 - P_{loss} \qquad (4.17)$$

The required value of the optimal output power (P_{opt}) that balances the wind mechanical torque is computed in a microcontroller which simultaneously samples the generator speed (ω_G) and the battery voltage (V_b). The generator speed can be sampled via optical sensors or phase voltage frequency. The microcontroller computes the optimal power (P_{opt}) based on sampled generator speed (ω_G). It also computes the required output current that must be supplied to the battery to maintain optimal turbine operation.

$$P_{opt} = I_{out} V_{out} \qquad (4.18)$$

Based on the values of the V_{dc}; V_b; and battery internal resistance, R_{int} the microcontroller computes the reference battery current, $I_{b,ref}$.

$$I_{b,ref} = \frac{V_{out} - V_b}{R_{\text{int}}} \qquad (4.19)$$

$$V_{out} = V_b + I_{out} R_{\text{int}} \qquad (4.20)$$

Substituting (3.51) into (3.49),

$$\begin{aligned} P_{opt} &= I_{out} \left(V_b + I_{out} R_{\text{int}} \right) \\ &= I_{out} V_b + \left(I_{out} \right)^2 R_{\text{int}} \end{aligned} \qquad (4.21)$$

The microcontroller solves the quadratic equation and takes the positive value of I_{out}.

$$I_{out} = \frac{-V_b \pm \sqrt{V_b{}^2 + 4 R_{\text{int}} P_{opt}}}{2 R_{\text{int}}} \qquad (4.22)$$

The microcontroller now computes and sets the duty ratio, D of a pulse width modulated switch (IGBT) that can supply the optimal current I_{out} to the battery.

$$D = \frac{I_{out}}{I_{b,ref}} \left(1 - \frac{V_b}{V_{out}} \right) + \frac{V_b}{V_{out}} \qquad (4.23)$$

The MPPT microcontroller model is shown in figure 4.15. The battery model used in the MPPT model is similar to the one used in system structure 1.

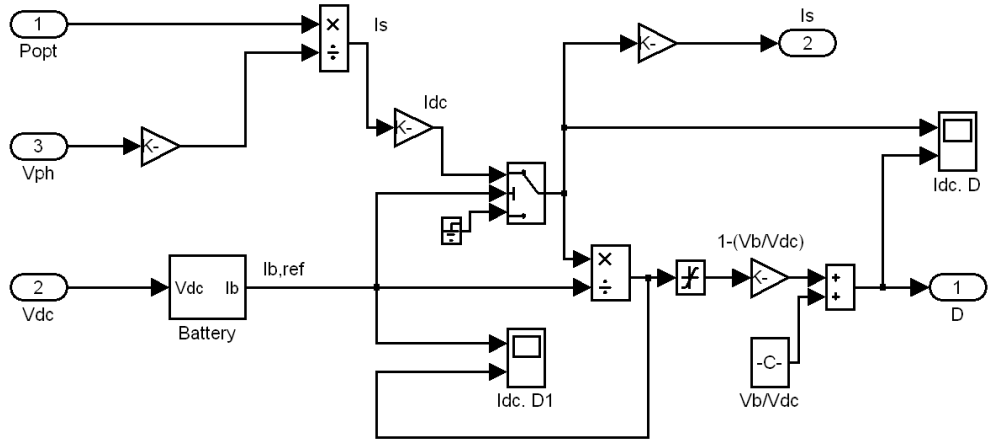

Figure 4.15: MPPT microcontroller model

4.2.4 System structure 2 simulation results

For the same input wind speed profile as used in system structure 1, the simulation shows effectively improved power levels. In figure 4.16(a), the wind speed and the tip speed ratio profile is shown. The tip speed ratio is not perfectly set to optimal value of 6.5 but is consistently trying to trace it. From fig. 4.16b, a better generator speed variation can be observed while the inbuilt regulator seeks to maintain the battery charging voltage by controlling the field current.

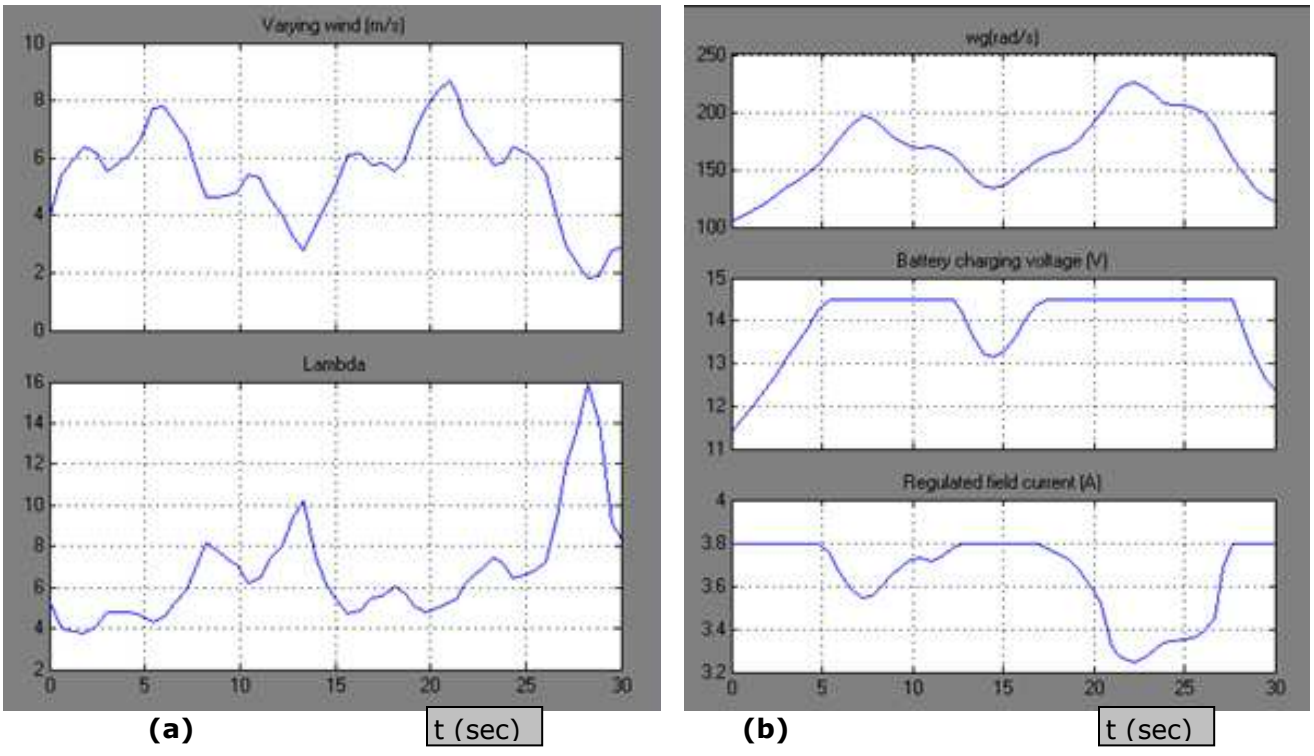

Figure 4.16: **(a)** Wind speed profile, lambda; **(b)** Alternator speed, Battery charging voltage, and field current for system structure 2

The wind power and the output power shown in fig. 4.17a represent an improvement in power harnessed from the wind as a result of tracking the optimal power point. The output current is also effectively improved as shown in fig. 4.17b. The duty ratio estimate for the PWM dc chopper that supplies current to the battery is shown in the lower plot of fig. 4.17b. This simulation was run for 30 seconds under the assumption that the battery maintains a constant state of charge within the 30-sec duration. However, under normal circumstances, battery dynamics would cause much more transients in the duty ratio.

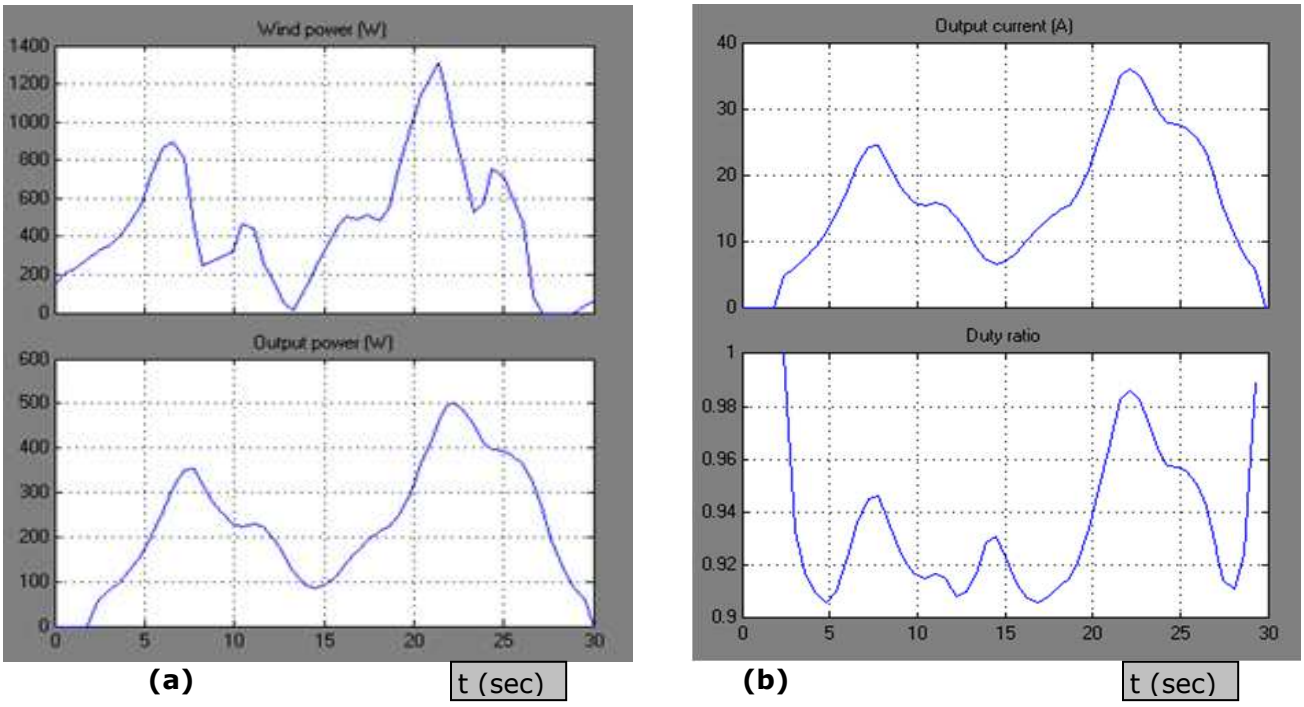

Figure 4.17: **(a)** Wind power, output power for system structure 2; **(b)** Output current and dc chopper duty ratio

A comparison of the energy harnessed over the simulation duration is obtained by integrating the power plots over time. The energy obtained with and without the MPPT scheme is shown in table 4.2.

Table 4.2: Energy comparison

System structure	Wind energy (kJ)	Output energy (kJ)
1 (Basic alternator)	8.54	3.93
2 (MPPT alternator)	13.9	6.76

Adjusting gear ratio from 10 to 8 showed that the basic alternator is able to trace optimal operation of the wind turbine without the MPPT. Figures 4.18 shows comparable wind power and output power for basic alternator and MPPT alternator. The reason for this might be that gear ratio is proportional to inverse of inertia which is a determinant of generator shaft speed according to equations (4.21) and (4.6).

$$J = \left(\frac{3J_b + J_h}{G^2} \right) + J_a \qquad (4.21)$$

$$\omega_G = \frac{1}{J}\int (T_w - T_e - T_{loss})dt \qquad (4.6)$$

$$G^2 \propto 1/J \propto \omega_G \qquad (4.22)$$

The other determinants of inertia such as mass or density of turbine blades do not cause significant change in the comparison between basic alternator and MPPT alternator energy yield.

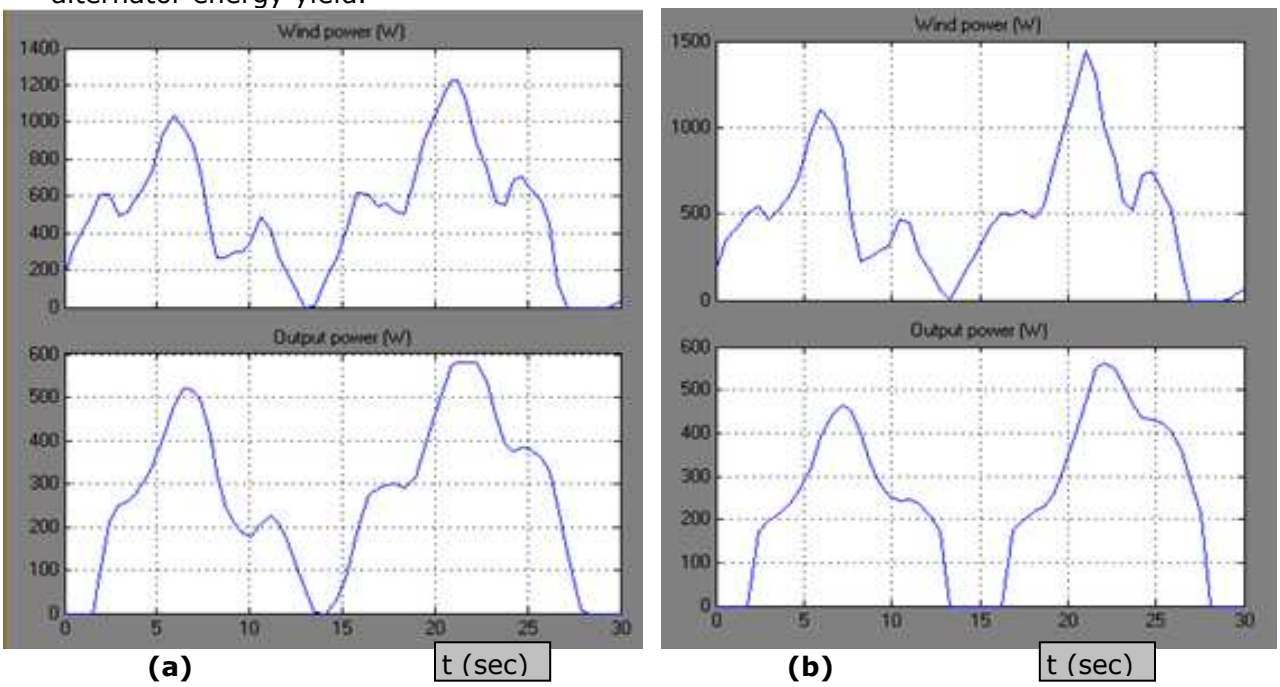

Figure 4.18: At gear ratio = 8, wind power and output power of **(a)** basic alternator **(b)** MPPT alternator

Figure 4.19 represents other parameters of modified structure 1 (with gear ratio = 8). It can be observed that the field current remains constant because there is no generator over-speed. The power inherently dissipated in the alternator in form of losses appears to provide sufficiently matching load torque to counterbalance the mechanical torque from the turbine blades and keep the generator speed regulated.

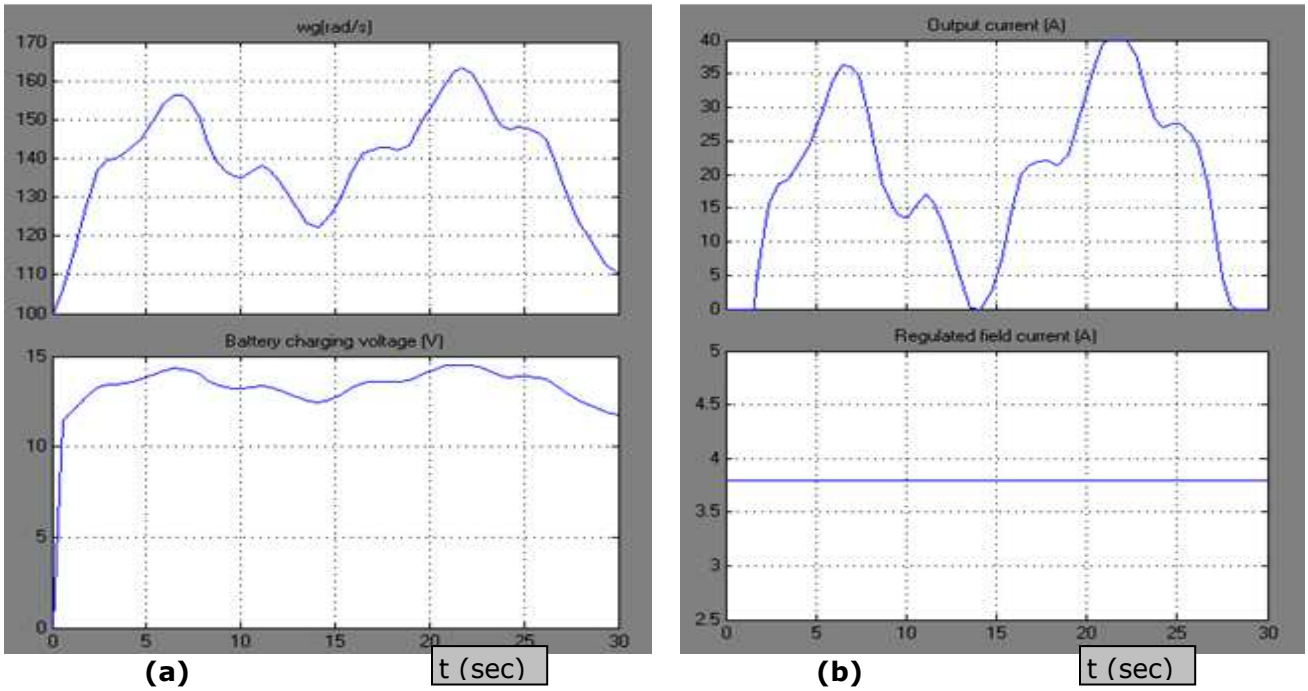

Figure 4.19: **(a)** Alternator speed, Battery charging voltage; **(b)** Output current, field current

The initial choice of gear ratio as 10 was set so that cut in wind speed at 3.5 m/s would correspond to alternator cut-in shaft speed at 1050 rpm (~110 rad/s) at an optimal tip speed ratio (TSR) of 6.5 and wind turbine blade radius of 2 m. However due to the effect of inertia (majorly dependent on gear ratio), TSR shifts its operating position because generator speed is slower in response to wind speed. In other words, generator speed slowly tracks wind speed and maintains TSR optimal point thereby maintaining optimal performance coefficient. Energy comparison based on new gear ratio = 8 is shown in table 4.3.

Table 4.3: Energy comparison (gear ratio = 8)

System structure	Wind energy (kJ)	Output energy (kJ)
1 (Basic alternator)	15.22	7.83
2 (MPPT alternator)	15.17	7.32

Replacing the battery with a higher capacity battery showed that the basic alternator ceased to operate along maximum power point because of loss of torque balance which results in loss of speed control. The power simulation results are similar to those shown in figures 4.11(a).

4.3 Conclusion

At in initially chosen gear ratio of 10, a maximum power point tracking (MPPT) scheme was simulated and shown to achieve higher energy yield. Reducing the gear ratio to 8 showed that the MPPT scheme becomes redundant. However, if the wind turbine system is to be loaded with different batteries of different capacities, the MPPT scheme is universally relevant because it automatically computes the required load torque that regulates generator speed and supplies the corresponding load power to the battery. It may not be practical to always recompute and change gear ratio for different battery loads as would be the case with the basic alternator.

Chapter 5

Measurement and testing of a recycled automotive alternator

For the purpose of experimentally evaluating the feasibility of the application of automotive alternators in small wind turbines, the following measurements were done in the EPP laboratory:

Under no load conditions,

1. Measurement of stator winding resistance
2. Measurement of rotor winding (field) resistance
3. No load voltage (back emf) variations with fixed rotor field current as shaft speed is varied.
4. No load voltage (back emf) variations with fixed shaft speed as rotor field current is varied
5. Zero field power: mechanical losses
6. Full field power: iron losses

Under load conditions,

7. Measurement of stator phase current and investigation of stator copper loss
8. Efficiency at different load ratings

This chapter will be concluded with a correction of the simulation based on loss constants obtained from measurements.

5.1 Apparatus Specifications:

The dc machine which served as a prime mover has the specifications shown in table 5.1.

Table 5.1: Prime mover specifications

DC motor type	Winkelmann GNI 112EM/4/2
Voltage rating	420 V
Current rating	20 A
Power rating	7.15 kW
Maximum shaft speed	2840 rpm
Field regulation voltage	310 V
Field regulation current	2.81 A

The DC motor's field winding was supplied with 45V at 0.5A from the Sorenson DC power supply (DCR 150-10A). The armature winding was used in controlling the shaft speed. The dc power supply to the armature winding (sourced from the HP 6483C DC power supply) ranged from 0 – 180V at 0 – 8A.

The alternator purchased was a recycled 12V, 50A rated alternator manufactured by Nippon Denso with OEM number 100211-1410. This alternator brand is used in the Suzuki Swift 1989 vehicle model. The Delta Elektronika power supply (D 050-10) was used to supply separate field excitation to the alternator.

Mechanical input power was measured with the Magtrol model 6400 torque transducer. Electrical DC voltages, currents and resistances were measured with the Fluke 289 and Tektronix TX1 multimeters. DC currents above 8A were measured with a shunt resistor (10.07mΩ, 80A) and multimeter. Electrical AC voltages and currents were measured with the Nanovip Elcontrol (SP1086) wattmeter. Inductance was measured with the Philips PM 6303 RCL meter. Surface temperature was measured with the Fluke 568 infra-red thermometer. Variable resistance load banks (5Ω, 20A) and 0.38Ω (100A) load bank was used for load tests.

The first run test was to mimic the vehicle charging circuit and observe the behavior of the alternator's in-built IC regulator. The battery used to mimic the vehicle charge system was a HGL 7.2Ah-12V Sealed Lead Acid battery. Open circuit battery

voltage is 12.5V. When connected to the alternator, it drops to 10.5V with ~4.5A flowing into the alternator. The vehicle charging circuit connection is shown in figure 5.1.

Cut in speed was observed at ~1030rpm, battery current changes gradually from 4.5A to -0.2A as prime mover speed is increased from 600rpm to 1030rpm. The negative current indicates that current begins to flow into the battery. The cut in speed (speed at which current begins flowing into the alternator is dependent on the voltage level of the battery). The regulator maintains maximum battery charging voltage at 14.5V.

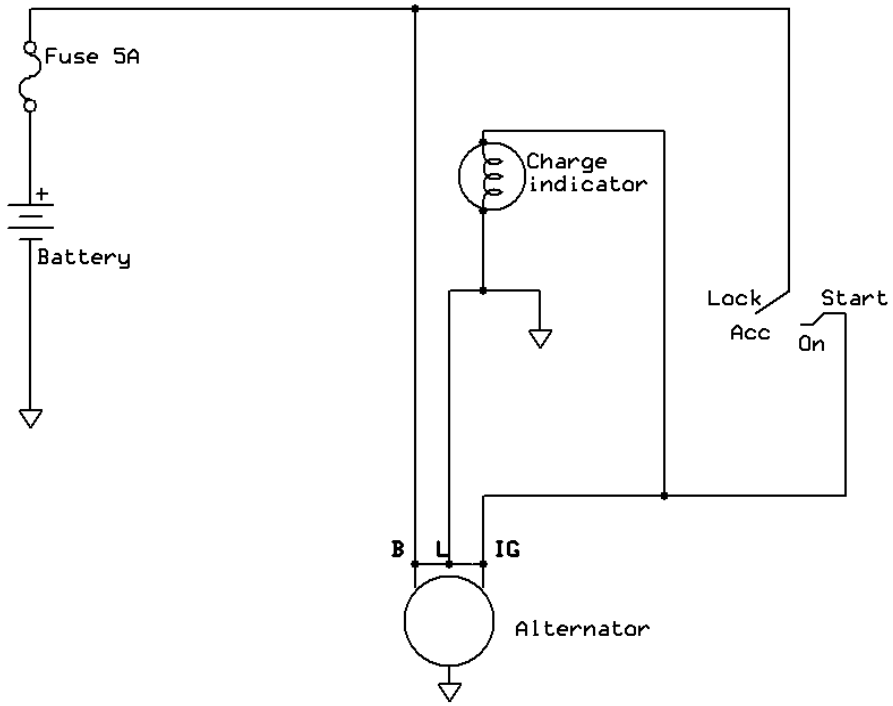

Figure 5.1: Suzuki Swift 1989 model alternator wiring diagram

5.2 No-load measurements

5.2.1 Stator winding resistance

The measurement of the stator winding resistance of each phase is useful for computing stator copper losses. This is done with the machine unloaded. The first thing that must be considered before the measurement is the type of three phase winding connection at the stator. The two types are star connection and delta connection.

a. Star connection

A basic method for doing this measurement is to use an ohmmeter (or multimeter) and measure from the winding terminal to star point (if accessible). If the star point is not accessible like in the case of the alternator of figure 5.2, the resistance can be measured across lines whereby resistance of 2 phases will be measured summed up together as illustrated in figure 5.3.

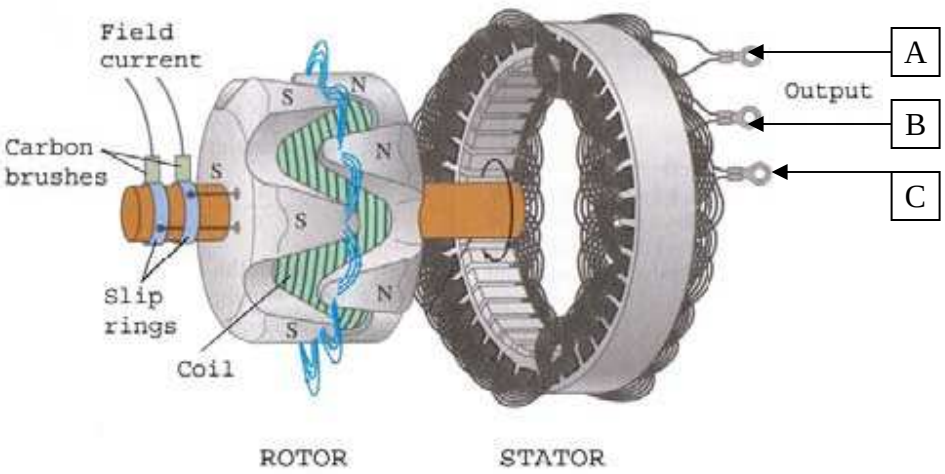

Figure 5.2: Alternator physical description

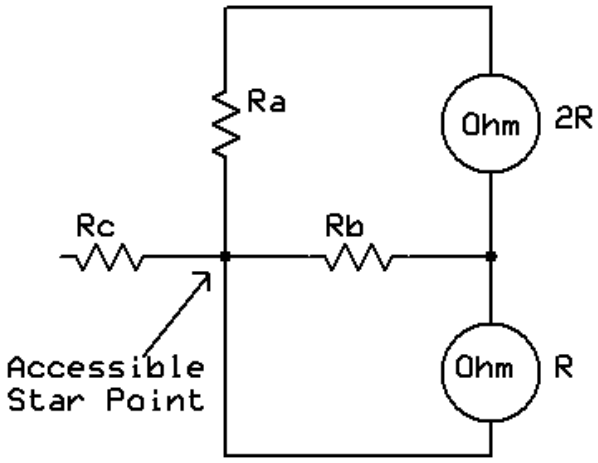

Figure 5.3: Star measurement connection

An ohmmeter (or multi-meter) used in this case can be assumed as an active measuring tool that passes a d.c. current from a d.c. voltage source across a DUT(Device Under Test). In this case, DUT is the stator copper winding.

$$R_a + R_b = \frac{V_{dc}}{I_{dc}} \qquad (5.1)$$

This measurement is carried out across the 3 terminals and if the results are different, the 3 sets of simultaneous equations based on (5.1) with 3 unknowns will be solved. It is expected that for a balanced 3-phase system, the stator winding resistances are equal and all measurements should be similar.

b. Delta connection

As described in figure 5.4, measurement can be taken across any two terminals to obtain a resistance value equivalent to $(2R/3)$ assuming the 3 phase stator windings are balanced.

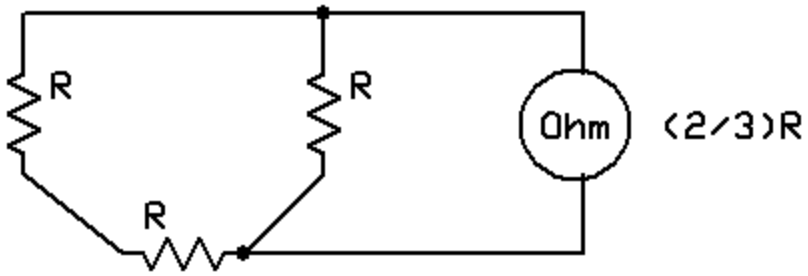

Figure 5.4: Delta measurement connection

The alternator purchased is a star-connected alternator with accessible star point. At ambient temperature (~24°C), stator resistance for each phase was measured to be 0.08Ω. After running the alternator from 100rpm to 2800rpm for 1 hour, the stator resistances for the three phases (with surface temperature of ~116°C) were measured to be 0.125Ω, 0.127Ω, and 0.122Ω. The stator inductance was also measured with the RCL meter (Philips model PM6303) to be 180.5μH, 178.3μH, and 136.4μH for the three different phases at a measuring frequency of 1kHz. The reason for the unbalanced stator inductance could be that the mutual inductance between the stator windings and eddy current field loops in the rotor iron are inconsistently distributed due to the salient poles of the rotor. The measured inductances do not represent the line inductances possibly because the measuring frequency of the RCL meter is not the synchronous frequency of the alternator. Since the alternator is a variable speed machine in which a lot of heat is produced, its line reactance value changes with frequency while its line inductance changes with temperature.

5.2.2 Rotor winding resistance and brush resistance

The resistances of the rotor winding and the brush resistance are measured to give an indication of the copper losses due to the field winding. The circuit connection is shown in figure 5.5.

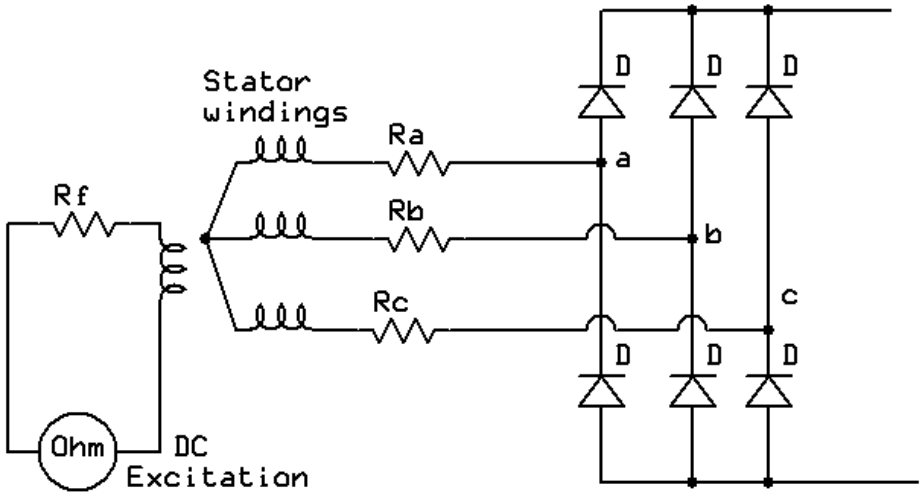

Figure 5.5: Rotor and brush resistance measurement

The resistance was computed from the ratio between battery terminal voltage and full field winding current. It is found to vary with speed because of heat accumulating in the rotor iron core while field current is flowing through it. Field winding resistance increases with temperature. The field winding and brush resistance is measured to be ~3.8Ω. The copper loss due to field winding is averagely 55W at average field current of 3.8A.

5.2.3 No-load voltage variations with regulated field current as shaft speed is varied.

The goal of this measurement is to obtain the alternator's machine constant. With field current kept constant, the speed of the claw pole generator is varied with a dc machine. The back emf is measured as shown in the circuit of figure 5.6.

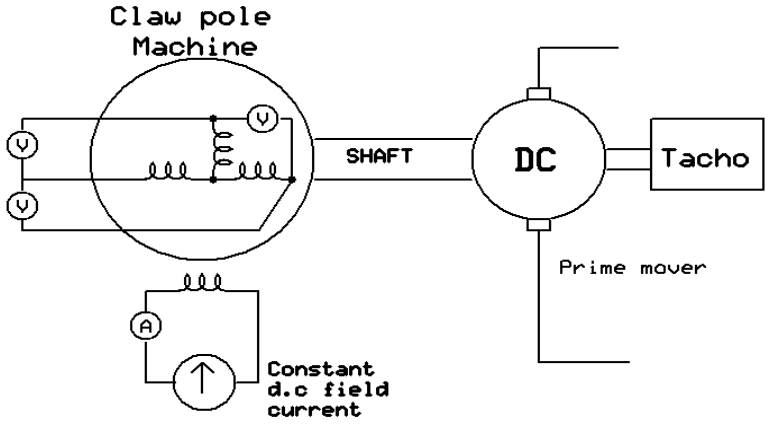

Figure 5.6: Speed variation with constant field current supplied

The back emf was measured with an external power supply energizing the rotor field winding. Even with the field current externally supplied, it was found to be slightly varying with speed change because of the changing field resistance due to temperature change in the rotor. The measurements taken are presented in table A.5.1 in the appendix while a plot is shown in figure 5.7. It can be observed that the average machine constant is approximately 0.017 (V-s/A-rad) at field current of ~3.55 A. The S.I. units are used in computing machine constant so that it can be compared to the machine's physical dimension computation as shown in table 3.4 of chapter 3.

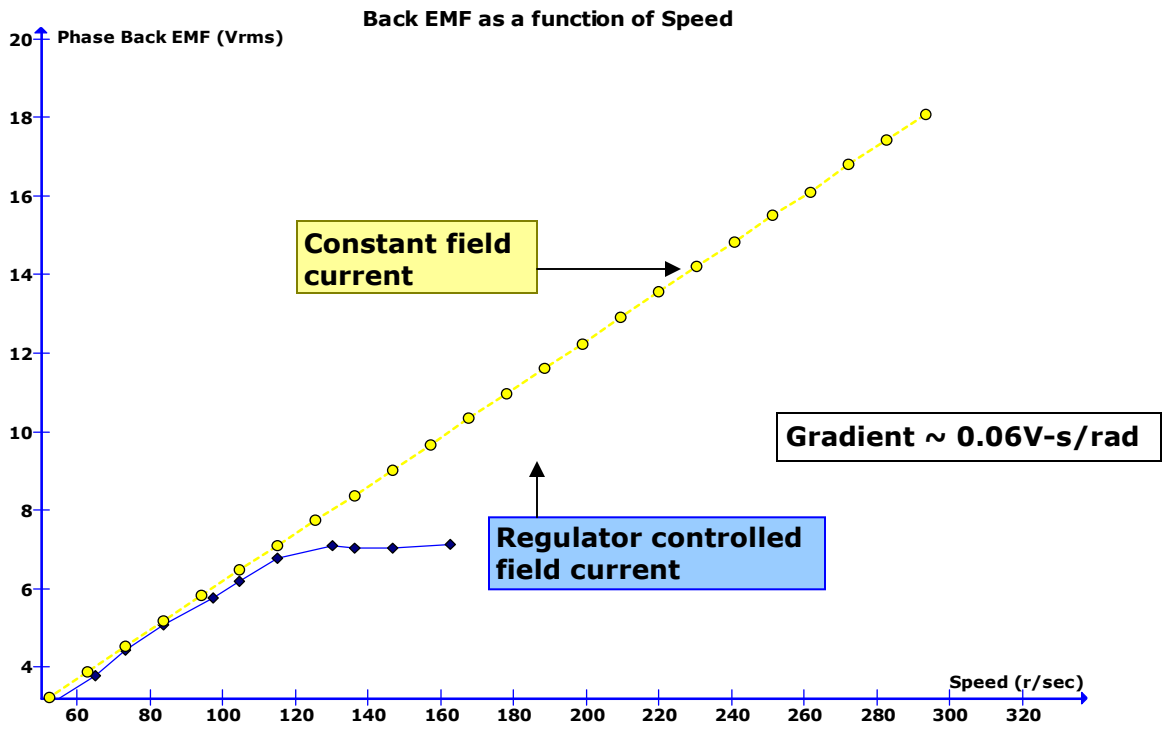

Figure 5.7: Phase back emf (rms) as function of shaft speed

The effect of speed variation on field current is depicted in figure 5.8. It can be observed that beyond 80 rad/s (760rpm), the field current is rising. This is possibly attributable to the internal fan of the alternator cooling the rotor and thereby reducing its winding resistance.

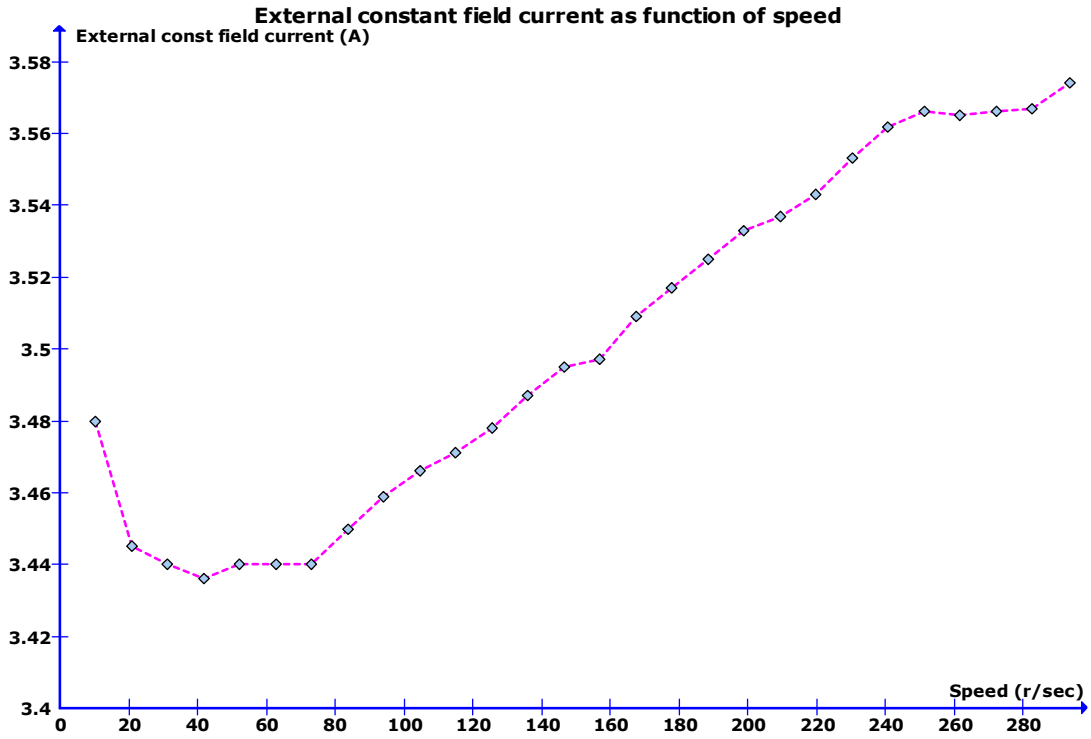

Figure 5.8: Externally supplied constant field current variation with shaft speed.

5.2.4 No-load voltage variations with fixed shaft speed as rotor field current is varied.

The goal of this measurement is to confirm the alternator's machine constant and gain some insight into the B-H characteristics of the claw pole iron. The no load voltage per phase is measured again but this time with a constant shaft speed while rotor field current is varied. The circuit is shown in figure 5.9.

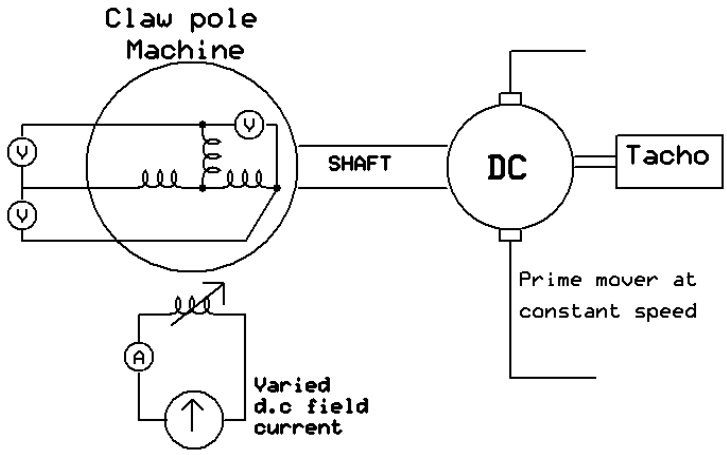

Figure 5.9: Constant speed with field current variation

A plot of the back emf with respect to field current with speed kept constant at 1000 rpm is shown in figure 5.10 with the readings shown in table A.5.2 in the appendix.

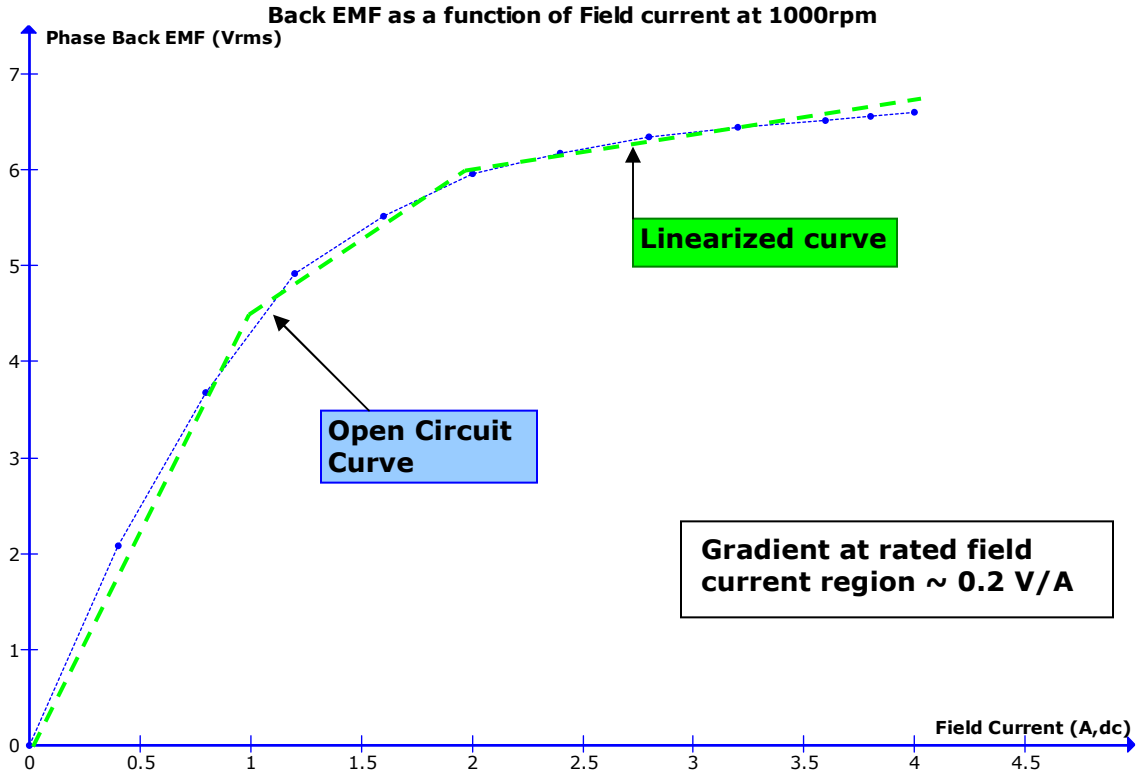

Figure 5.10: Back emf (rms) as function of field current

The open circuit curve of figure 5.10 indicates the rotor iron attains early saturation at a low field current. This may be due to the inherent characteristics of the rotor iron core material.

5.2.5 Zero field power: mechanical losses

This measurement is carried out to determine bearing friction loss and windage loss together. This type of loss is determined during a measurement where there is no field current supplied to the rotor of the machine [46]. The torque value corresponds only to friction torque. There exists for various values of mechanical speed, the corresponding mechanical losses. The set up circuit is shown in figure 5.11.

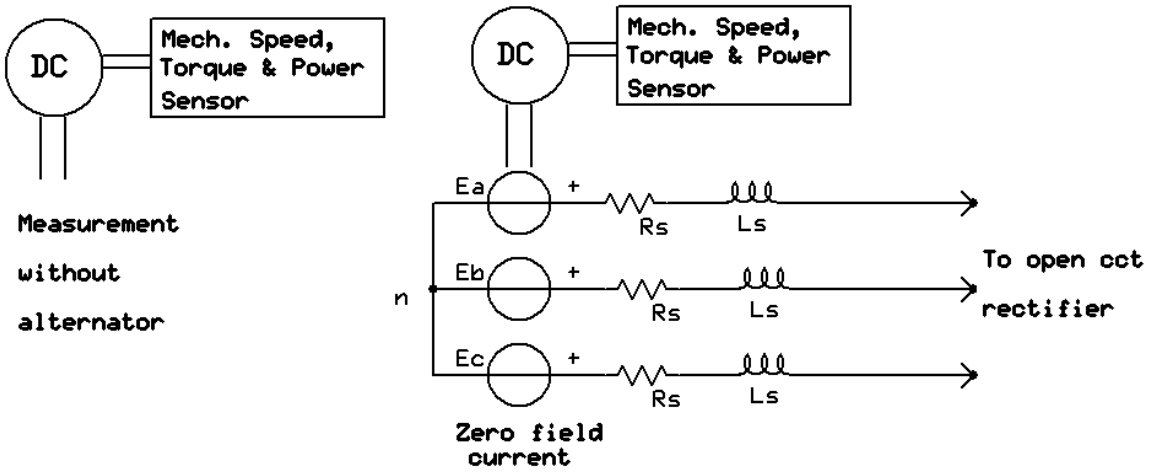

Figure 5.11: Power measured without field current

The average offset torque of the measuring equipment (torque transducer) was first measured by running the dc machine unshafted to the alternator. The mechanical loss due to this offset torque was then subtracted from the total power measurement to obtain the mechanical loss of the alternator using the expression in equation (5.2). The measurements are shown in table A.5.3 (appendix) and figure 5.12. The average offset torque, T_{shaft} during rotation was ~0.235Nm.

$$P_{Mech} = P_{in(zerofield)} - T_{shaft}\omega_G \qquad (5.2)$$

$$P_{Mech} = T_{mech,alt}\omega_{G,alt} = P_{Be} + P_{Win} = K_{Be}\omega_G + K_{Win}\omega_G^{\,3} \qquad (5.3)$$

where:

$P_{in(zerofield)}$ = Power input without field winding

K_{Be} = bearing friction loss constant coefficient

K_{Win} = windage loss constant coefficient

ω_G = alternator rotational speed

Sets of simultaneous equations based on (5.3) can be solved to obtain bearing loss coefficient and winding loss coefficient. Different alternators will have different mechanical loss constants due to their different machine designs. For instance, Delco Remy alternators have external fans while Nippon Denso alternators have in-built fans. Making use of the data from the measurements, the mechanical loss constants can be computed as K_{Be}=1.424E-2 (W/rpm) and K_{Win}=7.002E-10 (W/rpm^3) and shown in

comparison to the measurement in figure 5.12. The plot of mechanical losses using the loss constants validates the analytical expressions used.

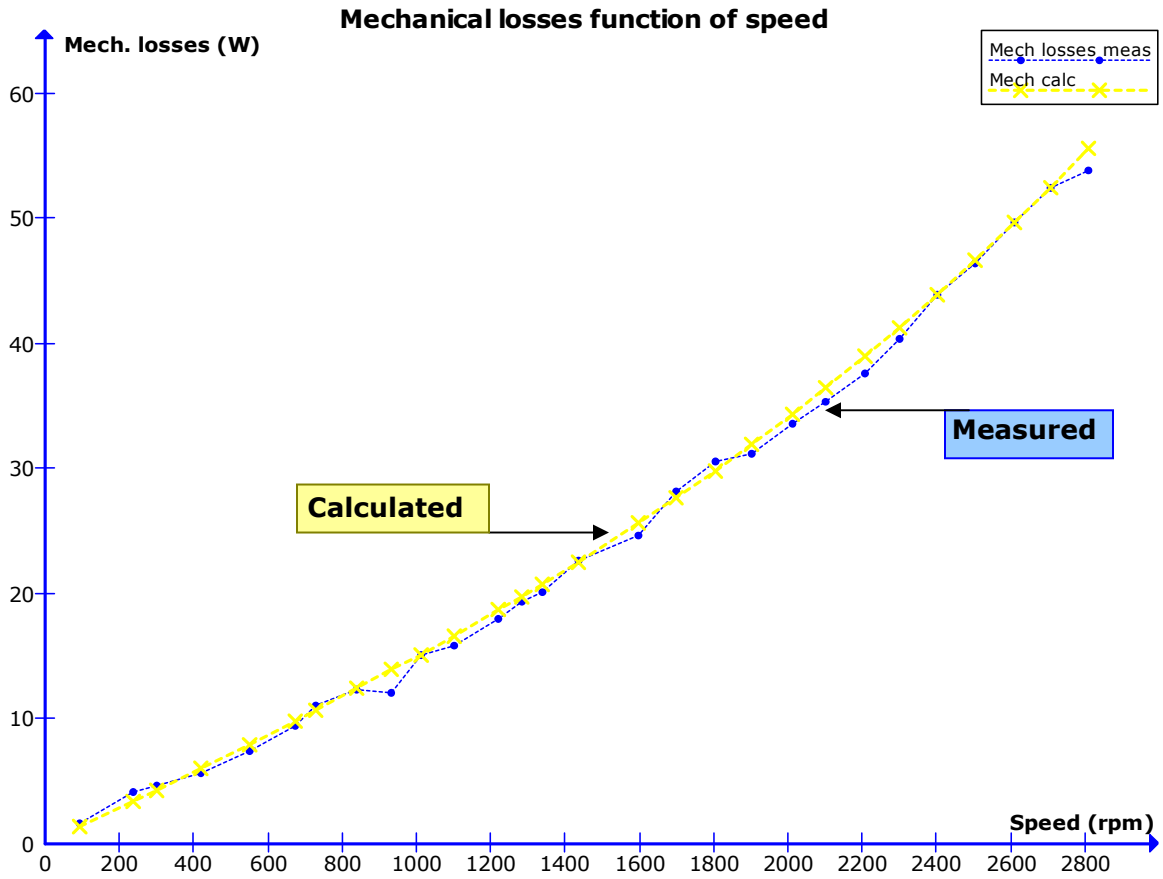

Figure 5.12: Mechanical losses vs shaft speed

5.2.6 Measurement of iron losses

The iron loss includes eddy current and hysteresis losses as a result of shaft speed variation. It was determined by measuring the power input from the dc motor used to drive the alternator at no load, with and without the field constantly excited. The difference in power measured constitutes this loss. This measurement, carried out with constant field current from an external power supply is shown in table A.5.4 (appendix) and the plot in figure 5.14. Howbeit, field current varied between 3.5A and 3.6A during the measurement due to thermal effect on the field winding's resistance. The expression of (5.4) is used at different speeds to determine iron losses.

$$P_{iron} = P_{m,\,field} - P_{m,no.\,field} \qquad (5.4)$$

where

P_{iron} = Iron losses
$P_{m,field}$ = measured power with field excited
$P_{m,no\ field}$ = measured power without field excited

Sets of simultaneous equations can also be used to obtain values for eddy current and hysteresis loss constants based on equation (5.5) with the assumption that flux density and magnetic path length are constant and incorporated in the loss

constants. A confirmed estimated ratio between rotor iron losses and stator iron losses is 2:1 [22], [46].

$$P_{iron} = P_{Eddy} + P_{Hyst} = K_{Ed} t^2 \omega_G{}^2 B^2 + K_{Hyst} \omega_G B^2 \qquad (5.5)$$

where:

K_{Ed} = eddy current loss constant coefficient

t = length of magnetic path in iron (assumed constant)

ω_G = alternator rotational speed

B = flux density (assumed constant due to constant field current)

K_{Hyst} = hysteresis loss constant coefficient

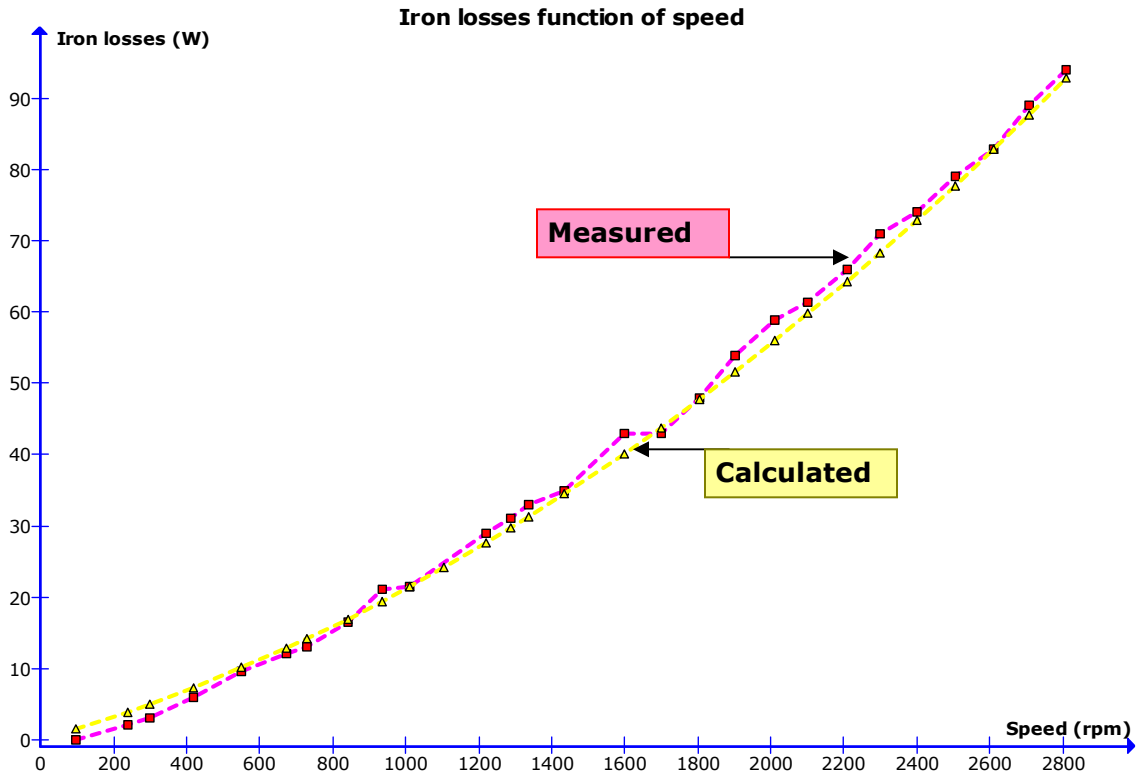

Figure 5.14: Iron loss variation with shaft speed

Figure 5.14 shows plots of the calculated iron loss compared to the measurements. Different alternators could have different iron loss constants because of differing B-H characteristic curves of their rotor irons. The calculated iron loss constants are K_{Ed}=6.565E-6 (W/rpm^2) and K_{Hyst}=0.014629 (W/rpm).

5.3 Load measurements

5.3.1 Measurement of output current and derivation of stator copper loss

For the purpose of computing stator copper loss, an average stator phase resistance of 0.11Ω is assumed. The stator copper loss function with respect to shaft speed with a 0.31Ω (42.6A rating) load resistor connected at the output is shown in figure 5.15. Stator phase current values at varying shaft speeds with the 0.31Ω load

connected are shown in appendix table A.5.5(e). The stator phase currents were obtained from the transformation equation (3.25) derived in chapter 3.

$$I_{dc} = \frac{3}{\pi}\sqrt{2}I_s \qquad (3.25)$$

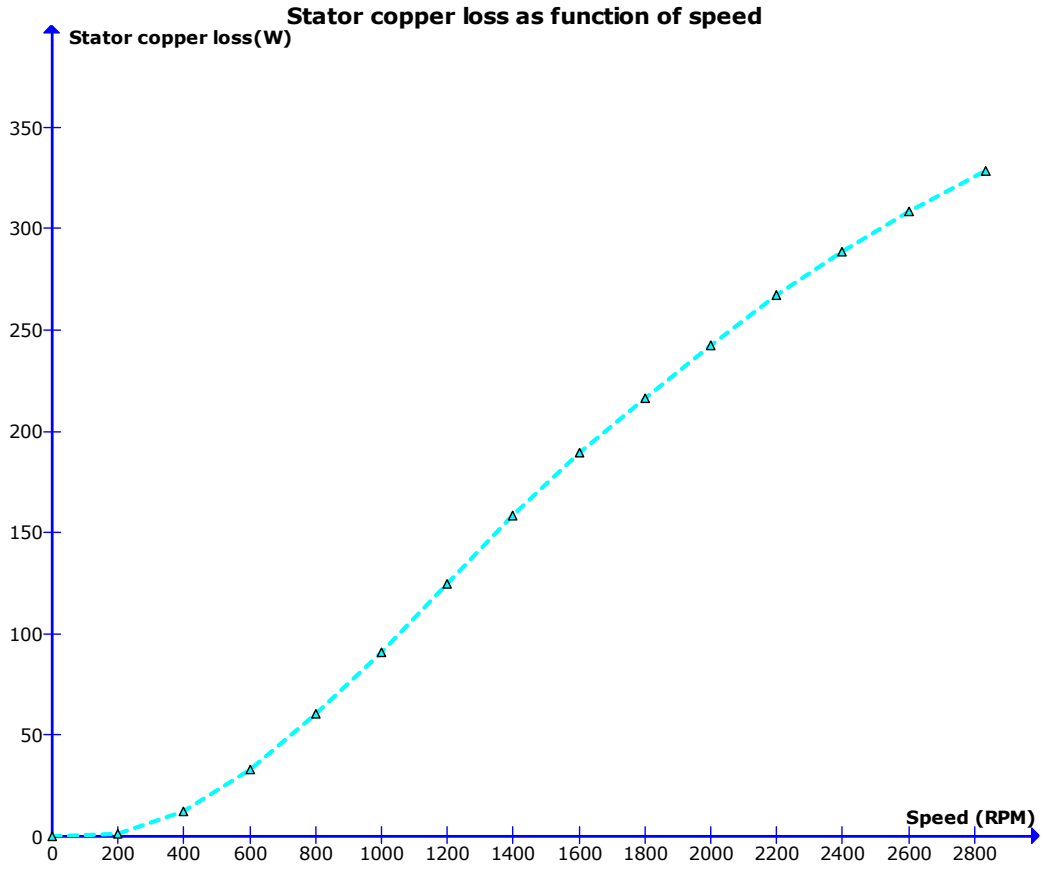

Figure 5.15: Stator copper loss as a function of shaft speed

5.3.2 Input power and output power measurements

Measurements were made of input and output power variation with shaft speed. This was done with various loads to represent 10A, 20A, 30A, 40A, 42.6A, and 42.9A rating. The measurement circuit is described in figure 5.16. The input power was measured from the Magtrol model 6400 torque transducer. A shunt resistance of 10.07mΩ with a Fluke dc voltmeter (multimeter) was used to measure the dc current at the output while voltmeters were used to measure the ac line voltage and the dc output voltage. The measurements of ac line voltages, dc output voltages, and output currents are presented in table A.5.5 (appendix). A summary of the efficiencies at different loads is graphically shown in figure 5.17. The 40A-rating measurement was taken with the in-built regulator active. Other measurements were taken with the regulator bypassed. It can be observed from figure 5.17 that power efficiency drops significantly at higher loads and speed due to the inability of the alternator to supply power beyond the rated value.

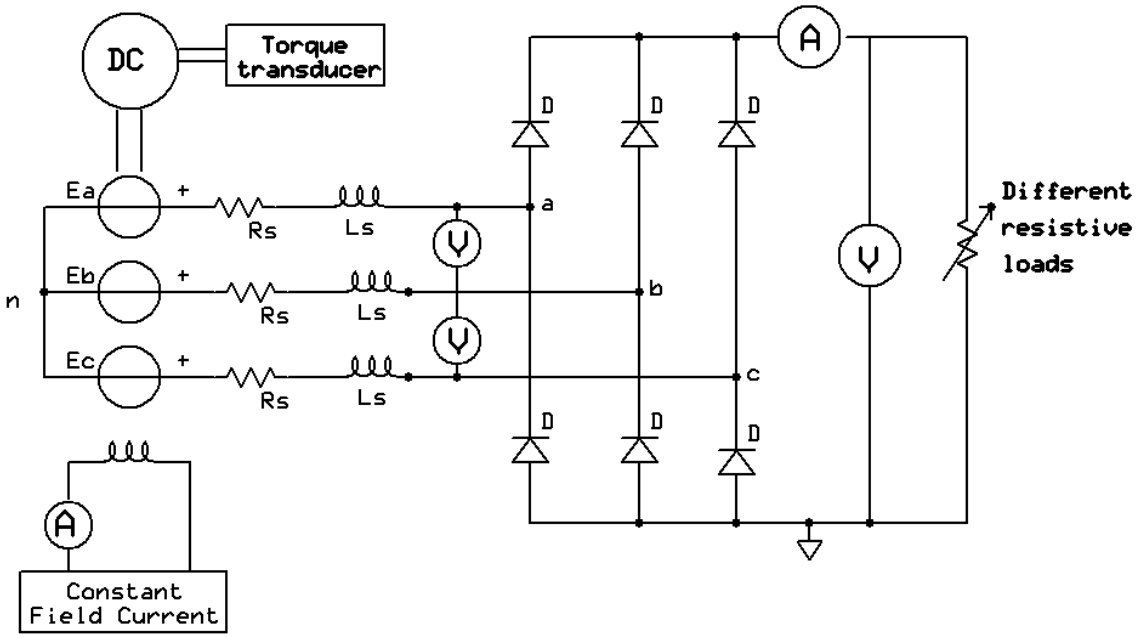

Figure 5.16: Load measurements

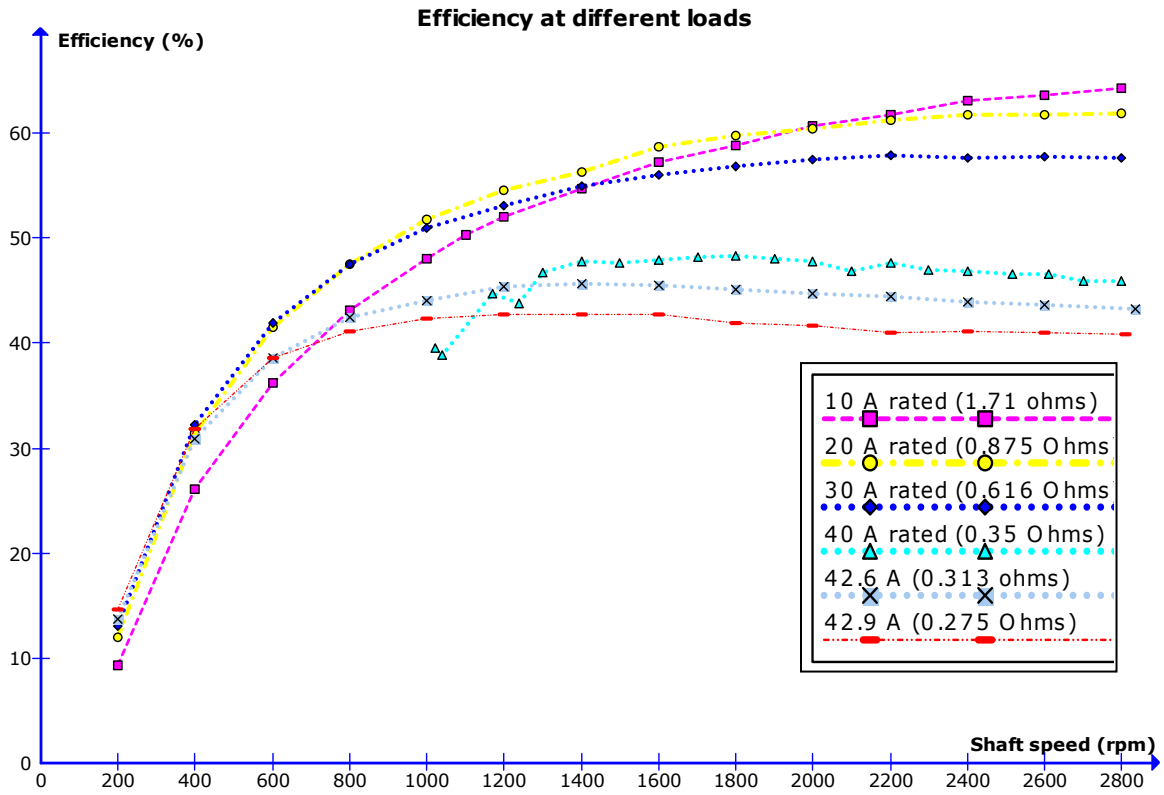

Figure 5.17: Efficiency at different load ratings

With all the losses measured taken into account and with an assumption of average stator winding resistance at 0.11Ω, a plot of the power distribution with a 0.31Ω

(42.6A rating) load resistor connected at the output is shown in figure 5.18. The field winding was externally supplied so its losses are not included in this measurement.

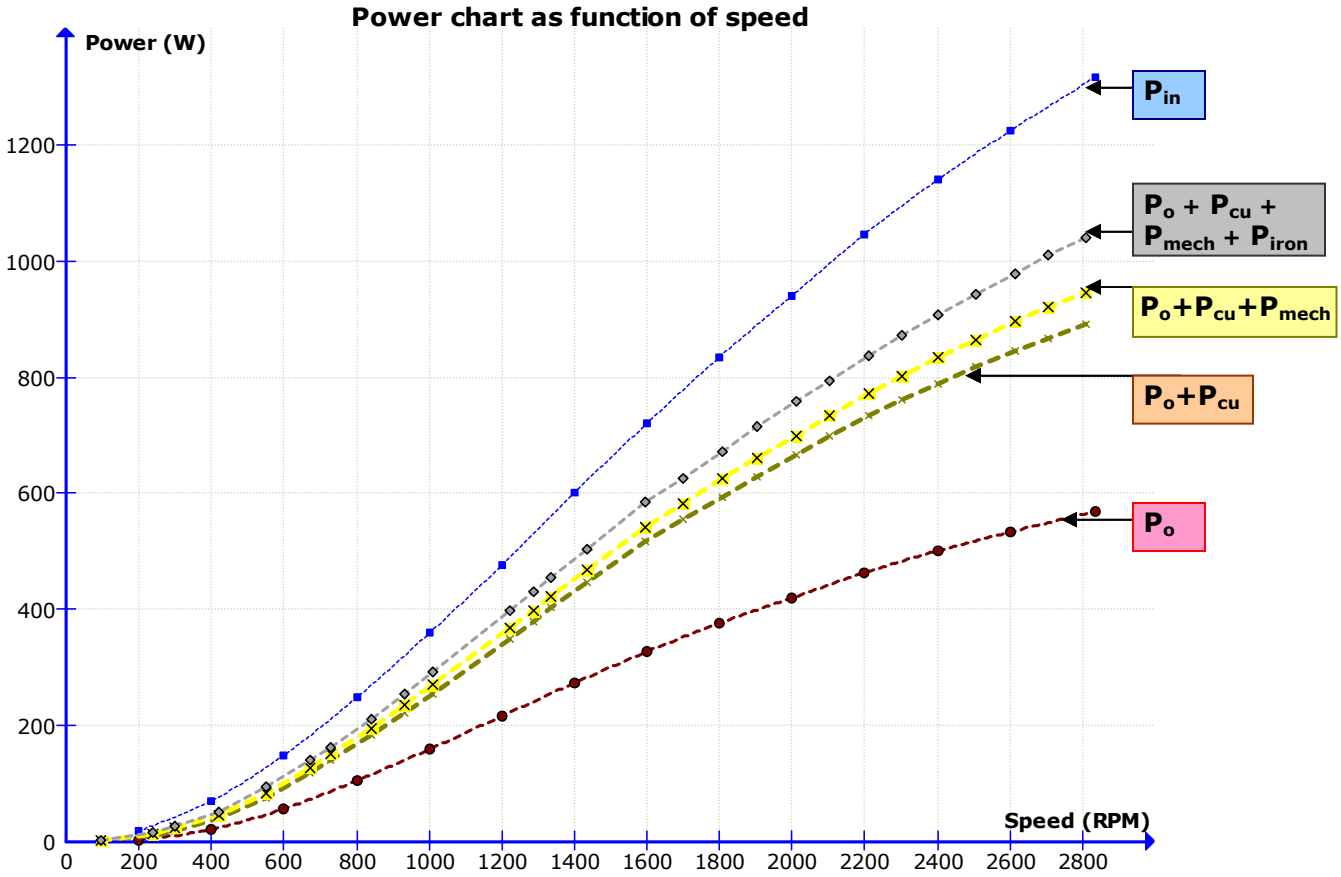

Figure 5.18: Measured power distribution in the alternator. In the graph, P_o=output power, P_{cu}=stator copper loss, P_{mech} =mechanical losses, P_{iron} =iron losses.

The remaining balance of power (P_{rect}) is assumed to be due to the rectifier. Hence,

$$P_{rect} = P_{in} - \left(P_o + P_{cu} + P_{mech} + P_{iron}\right) \qquad (5.6)$$

The major sources of power loss are the stator winding and the rectifier. The effect of temperature is significant in the stator winding copper because it contributes greatly to the losses in the stator windings. In a warm climate region, hotter stator windings would cause even more stator copper losses.

In the simulink model, thermal effect on resistance is not taken into account, whereas in the measurements, the thermal effect was well observed. At 30-40A load tests, with the Fluke IR thermometer pointed at the machine's ventilation slots, temperatures as high as 160°C were observed. The effect of such high temperature on the stator and field resistance cannot be overemphasized. A well known temperature model for resistance is described in equation (5.7).

$$R = R_{ref}\left(1 + \alpha\left(T - T_{ref}\right)\right) \qquad (5.7)$$

where

R = conductor resistance at temperature 'T'

R_{ref} = conductor resistance at reference temperature 'T_{ref}' usually 20°C

α = temperature coefficient of resistance for the conductor material (copper=0.004041)
T = conductor temperature in degrees Celsius
T_{ref} = reference temperature that α is specified at for the conductor material

This temperature model was not included in the simulations because of the unpredictable variation of temperature and the uncertainty of the temperature in the core of the windings. For temperature changes as high as 100^{o}C, the model indicates that resistance values could change by as much as 40%. The thermal effect was also responsible for the unstable field current.

After observing the practical behaviour of the recycled automotive alternator, it can be confirmed that the power rating of the alternator cannot be exceeded thus an output power limiter had to be included in the simulink model.

The measurements also showed that the alternator purchased can be used more efficiently between 10A and 30A current consumption. This is typically the charging current for batteries of capacity 100Ah to 300Ah.

Nippon Denso alternators were found to be easier to disassemble than Delco Remy alternators. This makes Nippon Denso alternators preferable for modification and adaptation to a small wind turbine.

Chapter 6

Conclusion

The feasibility of using a recycled automotive alternator in a small wind turbine has been evaluated in this report. The measurements taken from such an alternator indicate conformity with the analytical and simulation models developed. The models can give some indication of the power yield obtainable from the alternator at certain wind speeds if used in a small wind turbine. The investigated modes of using the alternator will be discussed here and recommendations will be made.

6.1 System structure 1

This structure as depicted in figure 6.1 requires the alternator be used with its original in-built regulator without any power electronics modification. The field winding is supplied from the battery at start up and self supplied from the alternator during running. In order to automate this system, a centrifugal switch or speed switch installed on the shaft would be necessary for switching 'on' the field winding when sufficient wind speed is attained and 'off' when there is insufficient or excessive wind speed.

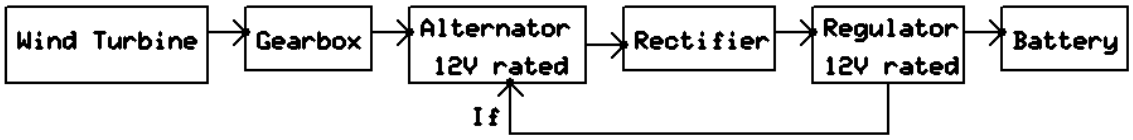

Figure 6.1: System structure 1

The dynamic model showed the effect of turbine blades' inertia on this structure causes generator speed lag and shifts the tip-speed ratio from optimal point thereby reducing the power coefficient of the turbine. This leads to lower power harnessed from the wind. The model also indicated that the machine's inherent power losses provided sufficient load torque to keep the generator speed from overshoot that may occur due to the effect of inertia of the turbine's blades.

Adapting the gear ratio to a lower value showed that optimal operation could be attained possibly because generator speed is more in phase with wind speed for optimal tip-speed ratio. However, if a different battery with a different charge capacity is to be connected at output, the wind turbine will cease to operate at optimum because the torque balance for which the gear ratio fits will be lost.

6.2 System structure 2

As depicted in figure 6.2, the modification of this system from system structure 1 is the use of a maximum power point tracker (MPPT) to achieve optimal power yield from the wind irrespective of the battery capacity at the output.

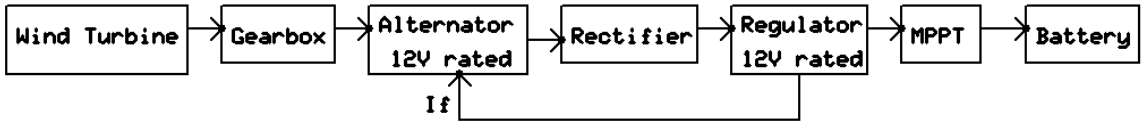

Figure 6.2: System structure 2

6.3 Recommendation

System structure 2 is recommended for application in small wind turbines because of its optimal energy yield irrespective of battery capacity. However, this comes at an increased cost compared to structure 1. For its implementation, apart from the

wind turbine, a chain drive is required for converting low wind speed to high shaft speed; a centrifugal switch is required for field winding activation and de-activation; an MPPT scheme is required for optimal operation and a battery is required for energy storage.

The effect of increased temperature on the stator and rotor winding were also shown to affect power yield. In a hot climate region, this temperature effect could substantially reduce the power output from the alternator.

The measurements also showed that the alternator purchased can be used more efficiently between 10A and 30A current consumption. This is typically the charging current for batteries of capacity 100Ah to 300Ah.

Future trends indicate that more efficient alternators will be produced because more efficient power electronics may be available in the future at a reduced price.

Bibliography

[1] S.O. Ani, H. Polinder and J.A. Ferreira, "Energy yield of two generator systems for small wind turbine application", IEMDC 2011, Niagara, Canada, May 15-18, 2011.

[2] D.M. Whaley, W.L. Soong and N. Ertugrul "Investigation of Switched-Mode Rectifier for Control of Small-Scale Wind Turbines", IEEE Industry Applications Society Annual Meeting 2005, Vol. 4, pp 2849-2856.

[3] http://www.nrel.gov/wind/smallwind/ accessed February 16 2012

[4] http://en.wikipedia.org/wiki/Small_wind_turbine accessed February 16 2012

[5] Shevory, Kristina (13 December 2007). "Homespun Electricity, From the Wind New York Times". *The New York Times*. Accessed December 4 2011.

[6] "AWEA Small Wind Global Market Study Year Ending 2010 Fact Sheet" accessed at *http://www.awea.org/learnabout/smallwind/* on March 26, 2012.

[7] http://www.allsmallwindturbines.com/ accessed 15 March 2012

[8] *http://www.windbluepower.com* accessed June 16 2012

[9] J.F. Manwell, J.G McGowan A.L. Rogers 'Wind Energy Explained: Theory, Design and Application' 2nd ed. John Wiley & sons Ltd West sussex (2009) ISBN 978-0-470-01500-1

[10] Hau, Erich, Windkraftanlagen – Grundlagen, Technik, Einsatz, Wirtschaftlichkeit (in German), Springer, 1988. Page 81.

[11] *http://en.wikipedia.org/wiki/Savonius_wind_turbine* accessed December 14, 2011.

[12] "British Wind and Energy Agency's DIY wind turbines page". *http://www.bwea.com/you/byo.html* accessed on December 14, 2011.

[13] "Basics on DIY small scale windturbines and domestic power consumption" (PDF) retrieved from *http://www.rebelwolf.com/essn/ESSN-Aug2005.pdf* on February 29 2012.

[14] *http://scoraigwind.com/* last accessed on June 20 2012

[15] *http://www.velacreations.com/makechispito.html* last accessed on June 15 2012

[16] *http://www.applied-sciences.net/library/zoetrope.php* last accessed on June 15 2012

[17] A. Mirecki, X. Roboam, F. Richardeau, *"Architecture complexity and energy efficiency of small wind turbines",* IEEE Trans. on Industrial Electronics, Vo1.54, No.1, February 2007, pp 660-670.

[18] M. Ehsani, A. Emadi , and J. M . Miller, Ed. "*Vehicular Electric Power Systems: Land, Sea, Air, and Space Vehicles"*, CRC Press 2000 Print ISBN: 978-0-8247-4751-0 eBook ISBN: 978-0-203-91346-8 DOI:10.1201/9780203913468.

[19] D.C. Giancoli, "*Physics: Principles with applications*" 5th ed., Upper Saddle River, NJ: Prentice Hall, 1998, pp 630-631.

[20] D.M. Whaley, W.L. Soong and N. Ertugrul, "Extracting More Power from the Lundell Car Alternator", Australasian *Universities Power Engineering Conference (AUPEC)*, Brisbane, Australia, 2004.

[21] M.Bradfield, "*Improving Alternator Efficiency Measurably Reduces Fuel Costs*" White paper from Delco Remy at http://www.delcoremy.com/Documents/High-Efficiency-White-Paper.aspx accessed on December 17, 2011.

[22] S. Kuppers, and G. Henneberger, "*Numerical Procedures for the Calculation and Design of Automotive Alternators*", IEEE Transactions on Magnetics, Vol. 33, No. 2, March 1997, pp 2022-2025.

[23] Ion Boldea "*Variable Speed Generators*" CRC Press 2006, Pages 6.1–6.34, Print ISBN: 978-0-8493-5715-2, eBook ISBN: 978-1-4200-3726-5.

[24] J.M. Rivas, D.J. Perreault, and T. Keim, *"Performance Improvement in Alternators with Switched Mode Rectifiers*", IEEE Trans. on Energy Conversion, Vo1.19, No.3, September 2004, pp 561-568.

[25] D.J. Perreault and V. Caliskan, "Automotive Power Generation and Control", *IEEE Trans. on Power Electronics,*. Vol.l9, No.3, May 2004, pp 618-630.

[26] D.J. Perreault and V.Caliskan, "A new design for automotive alternators". *In IEEE/SAE International Congress on Transportation Electronics (Convergence)*, SAE paper 2000-01-C084, 2000.

[27] F. Jurca, C. Martis, I. Birou and K. Biro "Analysis of a claw pole synchronous machine for wind power conversion module" Proceedings of the 2008 IEEE International conference on Electrical machines.

[28] A.G. Kladas, M.P. Papadopoulos and J.A. Tegopoulos "Design considerations for claw pole alternators for wind power applications" The International Journal for Computation and Mathematics in Electrical and Electronic Engineering, Vol. 17 No. 1/2/3, 1998, pp. 151-154.

[29] A. Ragheb and M. Ragheb, "Wind Turbine Gearbox Technologies", *Proceedings of the 1st International Nuclear and Renewable Energy Conference (INREC'10)*, ISBN: 978-1-4244-5213-2, Amman, Jordan, March 2010.

[30] http://nolu.com/eptroot/public/schools/beltchan.pdf accessed December 21, 2011

[31] *http://www.youtube.com/watch?v=d6dJVmRwtEM* accessed December 10, 2011

[32] *http://en.wikipedia.org/wiki/Excitation_%28magnetic%29* accessed December 13, 2011.

[33] E. Koutroulis, K. Kalaitzakis, "Design of a maximum power tracking system for wind-energy-conversion applications" (2006) *IEEE Transactions on Industrial Electronics*, 53 (2), pp. 486-494.

[34] S.O. Ani, H. Polinder, J.A. Ferreira, "Energy Yield of Small Wind Turbines in Low Wind Speed Areas" Presented at the *3rd IEEE International Conference on Adaptive Science and Technology (ICAST)*, 24-26 Nov. 2011, Abuja, Nigeria.

[35] J.B. Spicer, C.J.K. Richardson, M.J. Ehrlich, J.B. Bernstein, M. Fukuda, and M. Terada, "Effects of Frictional Loss on Bicycle Chain Drive Efficiency", ASME Transactions on Mechanical design, Vol. 123, December 2001, pp 598-605.

[36] *http://www.monsterscooterparts.com/chains.html* accessed February 20 2012.

[37] *http://chains.alliedlocke.com/viewitems/precision-roller-chains/rollerless-chains* accessed February 3 2012.

[38] *http://www.ramseychain.com/eng_design_tips.asp* accessed February 23 2012.

[39] *http://www.brommerhoek-ink.nl/zoek.asp?Submit11=Zoek&omschr =tandwiel&offset=100* accessed February 22 2012.

[40] P.C. Sen "*Principles of Electric machines and Power Electronics*" 2nd Ed, John Wiley & Sons, Inc 1997 ISBN 978-0-471-02295-4.

[41] V. Caliskan, D.J. Perreault, T.M. Jahns, and J.G. Kassakian, "*Analysis of Three-Phase Rectifiers with Constant-Voltage Loads*," IEEE Power Electronics Specialists Conference, pp. 715–720, Charleston, SC, USA, September, 2003.

[42] D. Stoia, M. Cernat, and R. Rabinovici "An electromagnetic model for the Lundell alternator with switched-mode rectifier", *Proceedings of IEEE 25th Convention of Electrical and Electronics Engineers*, Israel, 2008.

[43] J. Morren, J. Pierik, and S.W.H. de Haan "Inertial response of variable speed wind turbines", *Electric Power Systems Research 76 (2006) 980–987*

[44] J.M. Miller, Institution of Electrical Engineers "*Propulsion systems for hybrid vehicles*", Volume 45 of IEE power and energy series, London, 2004, ISBN: 0-86341-336-6.

[45] J. G. Slootweg,, S. W. H. de Haan, H. Polinder, and W. L. Kling, "*General Model for Representing Variable Speed Wind Turbines in Power System Dynamics Simulations*", IEEE Transactions on Power Systems, Vol. 18, No. 1, February 2003, pp 144-151.

[46] A.Gimeno, G.Friedrich, and K.El-kadri-benkara, "*Experimental and numerical evaluation of iron losses in a claw pole car generator*", Proceedings from IEEE XIX International Conference on Electrical Machines - ICEM 2010, Rome.

[47] G. Henneberger and S. Kuppers, "Field Calculation and Dynamic Simulation of a Claw-Pole Alternator", Proceedings of the 7th International Conference on Electrical Machines and Drives, Durham, England, 1995.

[48] Delco Remy Electrical Specification and Selection Guide-Starters and Alternators 2008 accessed at http://www.delcoremy.com/Alternator/ Literature.aspx on December 14, 2011.

Appendix

Table A.5.1: No load phase voltages as function of speed

Speed (rpm)	Speed (rad/s)	$E_{b,L-L}$ (V_{rms})	$E_{b,ph}$ (V_{rms})	V_{out} (V_{dc})	I_F (A_{dc})
100	10.472	1.16	0.6697263	0.82	3.48
200	20.944	2.265	1.3076984	2.26	3.445
300	31.416	3.375	1.9485572	3.73	3.44
400	41.888	4.48	2.5865292	5.23	3.436
500	52.36	5.585	3.2245013	6.74	3.44
600	62.832	6.705	3.8711336	8.215	3.44
700	73.304	7.82	4.5148791	9.724	3.44
800	83.776	8.95	5.1672849	11.223	3.45
900	94.248	10.1	5.8312377	12.74	3.459
1000	104.72	11.2	6.466323	14.225	3.466
1100	115.19	12.3	7.1014083	15.7	3.471
1200	125.66	13.4	7.7364936	17.2	3.478
1300	136.14	14.5	8.3715789	18.7	3.487
1400	146.61	15.6	9.0066642	20.24	3.495
1500	157.08	16.75	9.670617	21.72	3.497
1600	167.55	17.9	10.33457	23.3	3.509
1700	178.02	19	10.969655	24.8	3.517
1800	188.5	20.1	11.60474	26.25	3.525
1900	198.97	21.2	12.239826	27.74	3.533
2000	209.44	22.35	12.903779	29.27	3.537
2100	219.91	23.5	13.567731	30.77	3.543
2200	230.38	24.6	14.202817	32.26	3.553
2300	240.86	25.7	14.837902	33.65	3.562
2400	251.33	26.85	15.501855	33.32	3.566
2500	261.8	27.9	16.108073	36.8	3.565
2600	272.27	29.1	16.800893	38.4	3.566
2700	282.74	30.2	17.435978	39.8	3.567
2803	293.53	31.3	18.071063	41.46	3.574

Table A.5.2: Open circuit test with constant speed

I_F (A_{dc})	$E_{b,ph}$ (V_{rms}) at 500 RPM	$E_{b,ph}$ (V_{rms}) at 1000 rpm equivalent
0	0	0
0.4	1.04	2.08
0.8	1.84	3.68
1.2	2.46	4.92
1.6	2.76	5.52
2	2.979	5.958
2.4	3.09	6.18
2.8	3.175	6.35
3.2	3.219	6.438
3.6	3.256	6.512
3.8	3.279	6.558
4	3.3	6.6

Table A.5.3: Mechanical losses (P_{Mech})

Speed (rpm)	Speed (rad/s)	P_{offset} (W)	P_{IN}:I_F=0 (W)	P_{Mech} (W)
95	9.948377	2.337869	4	1.662131
239	25.02802	5.881585	10	4.118415
300	31.41593	7.382743	12	4.617257
420	43.9823	10.33584	16	5.66416
551	57.70059	13.55964	21	7.440363
673	70.4764	16.56195	26	9.438047
730	76.44542	17.96467	29	11.03533
841	88.06931	20.69629	33	12.30371
934	97.80825	22.98494	35	12.01506
1011	105.8717	24.87984	40	15.12016
1103	115.5059	27.14388	43	15.85612
1221	127.8628	30.04776	48	17.95224
1286	134.6696	31.64736	51	19.35264
1337	140.0103	32.90242	53	20.09758
1435	150.2728	35.31412	58	22.68588
1597	167.2374	39.3008	64	24.6992
1699	177.9189	41.81093	70	28.18907
1806	189.1239	44.44411	75	30.55589
1904	199.3864	46.85581	78	31.14419
2011	210.5914	49.48899	83	33.51101
2102	220.1209	51.72842	87	35.27158
2209	231.3259	54.3616	92	37.6384
2301	240.9602	56.62564	97	40.37436
2402	251.5369	59.11116	103	43.88884
2505	262.323	61.6459	108	46.3541
2612	273.528	64.27908	114	49.72092
2706	283.3717	66.59234	119	52.40766
2810	294.2625	69.15169	123	53.84831

Table A.5.4: Iron loss derivations

Speed (rpm)	P_{IN}: I_F=0 (W)	P_{IN}: I_F ~3.6A (W)	Iron loss, W
95	4	4	0
239	10	12	2
300	12	15	3
420	16	22	6
551	21	30.5	9.5
673	26	38	12
730	29	42	13
841	33	49.5	16.5
934	35	56	21
1011	40	61.5	21.5
1221	48	77	29
1286	51	82	31
1337	53	86	33
1435	58	93	35
1597	64	107	43
1699	70	113	43
1806	75	123	48
1904	78	132	54
2011	83	142	59
2102	87	148.5	61.5
2209	92	158	66
2301	97	168	71
2402	103	177	74
2505	108	187	79
2612	114	197	83
2706	119	208	89
2810	123	217	94

Table A.5.5: (a) 10 A rated (1.7 Ω), I_F =~3.5A

Speed (rpm)	P_{IN} (W)	V_{ph} (V_{rms})	V_{out} (V_{dc})	10.07mΩ shunt (V_{dc})	I_L (A_{dc})	P_{OUT} (W)	Eff
200	12	1.241303	1.47	0.0077	0.764647	1.124032	0.093669
400	35	2.419098	4.07	0.0226	2.24429	9.13426	0.260979
600	67	3.573798	6.59	0.0371	3.684211	24.27895	0.362372
800	109	4.722725	9.12	0.0519	5.153923	47.00377	0.431227
1000	160	5.888973	11.58	0.0669	6.643496	76.93168	0.480823
1100	190	6.408588	12.71	0.0758	7.527309	95.6721	0.503537
1200	218	6.985938	14	0.0815	8.093347	113.3069	0.519756
1400	284	8.082904	16.35	0.0956	9.493545	155.2195	0.546547
1600	356	9.179869	18.624	0.1102	10.9434	203.8098	0.572499
1800	437	10.27683	20.88	0.1241	12.32373	257.3196	0.588832
2000	517	11.25833	22.99	0.1373	13.63456	313.4585	0.606303
2200	608	12.3553	25.14	0.1504	14.93545	375.4773	0.617561
2400	706	13.33679	27.078	0.1656	16.44489	445.2946	0.630729
2600	809	14.26055	29.07	0.1784	17.71599	515.0038	0.636593
2800	911	15.18431	30.91	0.1906	18.92751	585.0493	0.642206

Table A.5.5: (b) 20 A rated (0.85 Ω), I_F =~3.5A

Speed (rpm)	P_{IN} (W)	V_{ph} (V_{rms})	V_{out} (V_{dc})	10.07mΩ shunt (V_{dc})	I_L (A_{dc})	P_{OUT} (W)	Eff
200	15	1.195115	1.26	0.0144	1.42999	1.801787	0.120119
400	46	2.268987	3.57	0.0408	4.051639	14.46435	0.314442
600	94	3.331311	5.85	0.0671	6.663357	38.98064	0.414688
800	155.5	4.376315	8.061	0.0922	9.155909	73.80578	0.474635
1000	228	5.398225	10.192	0.1166	11.57895	118.0126	0.517599
1200	312	6.350853	12.23	0.1402	13.92254	170.2727	0.545746
1400	405	7.332348	14.13	0.1626	16.14697	228.1567	0.56335
1600	500	8.198374	16.02	0.1846	18.33168	293.6735	0.587347
1800	604	9.064399	17.79	0.2043	20.28798	360.9232	0.597555
2000	712	9.930425	19.41	0.2232	22.16485	430.2197	0.604241
2200	827	10.62324	20.9	0.244	24.23039	506.4151	0.612352
2400	943	11.31607	22.36	0.262	26.01787	581.7597	0.616924
2600	1065	12.06662	23.78	0.2787	27.67627	658.1416	0.617973
2800	1184	12.75944	25.07	0.294	29.19563	731.9345	0.618188

Table A.5.5: (c) 30 A rated (0.62 Ω), I_F =~3.5A

Speed (rpm)	P_{IN} (W)	V_{ph} (V_{rms})	V_{out} (V_{dc})	10.07mΩ shunt (V_{dc})	I_L (A_{dc})	P_{OUT} (W)	Eff
200	16	1.143154	1.14	0.0185	1.83714	2.09434	0.130896
400	53	2.153517	3.28	0.0525	5.213505	17.1003	0.322647
600	108	3.140785	5.35	0.0853	8.470705	45.31827	0.419614
800	180	4.093413	7.33	0.1175	11.66832	85.5288	0.47516
1000	266	5.005627	9.209	0.1483	14.72691	135.6201	0.50985
1200	363	5.888973	10.97	0.1769	17.56703	192.7103	0.530882
1400	467	6.697263	12.6	0.2052	20.37736	256.7547	0.549796
1600	580	7.447818	14.15	0.2314	22.97915	325.1549	0.560612
1800	695	8.140639	15.63	0.2546	25.28302	395.1736	0.568595
2000	812	8.833459	16.95	0.2771	27.51738	466.4196	0.574408
2200	935	9.410809	18.28	0.2985	29.6425	541.8649	0.579535
2400	1056	9.959292	19.38	0.316	31.38034	608.1509	0.575901
2600	1168	10.45004	20.41	0.333	33.06852	674.9285	0.57785
2800	1281	10.91192	21.3	0.3491	34.66733	738.4141	0.576436

Table A.5.5: (d) 40 A rated (0.35 Ω)

Speed (rpm)	P_{IN} (W)	V_{out} (V_{dc})	I_L (A_{dc})	I_F (A_{dc})	P_{OUT} (W) + $I_f^2R_f$	Eff
1021	174	5.02	12.3722	1.34	68.835	0.395603
1040	181	5.09	12.4744	1.33	70.264	0.388199
1170	287	6.85	16.9018	1.81	128.176	0.446606
1240	312	7.1	17.4744	1.79	136.777	0.438388
1300	404	8.32	20.4908	2.2	188.788	0.467297
1400	465	9.03	22.2393	2.37	222.222	0.477897
1500	533	9.67	23.7219	2.52	253.759	0.476096
1600	595	10.25	25.1636	2.61	284.679	0.478452
1700	655	10.81	26.4928	2.7	315.574	0.481792
1800	716	11.3	27.863	2.75	345.927	0.483138
1900	770	11.76	28.681	2.81	370.334	0.480953
2000	834	12.21	29.7751	2.89	398.841	0.478227
2100	899	12.51	30.726	2.94	421.162	0.468478
2200	1060	13.3	34.6012	3.38	505.15	0.476557
2300	1093	13.44	34.9182	3.33	514.056	0.470317
2400	1132	13.66	35.5419	3.29	530.444	0.46859
2515	1185	13.95	36.2781	3.27	551.696	0.465566
2610	1236	14.25	37.0348	3.32	575.056	0.465256
2702	1280	14.44	37.4335	3.31	588.336	0.459638
2800	1325	14.69	38.1493	3.301	608.905	0.459551

Table A.5.5: (e) 42.6 A rated (0.31 Ω), I_F =~3.5A

Speed (rpm)	P_{IN} (W)	V_{ph} (V_{rms})	V_{out} (V_{dc})	10.07mΩ shunt (V_{dc})	I_L (A_{dc})	P_{OUT} (W)	Eff.	I_{PH} (A_{rms})
200	18	1.102739	0.9278	0.0269	2.671	2.478	0.14	1.978046
400	71	1.94567	2.66	0.0829	8.232	21.9	0.31	6.095912
600	149	2.73664	4.275	0.1356	13.47	57.57	0.39	9.971118
800	249	3.475649	5.77	0.1842	18.29	105.5	0.42	13.54484
1000	361	4.133828	7.089	0.226	22.44	159.1	0.44	16.61853
1200	476	4.693858	8.24	0.264	26.22	216	0.45	19.4128
1400	600	5.196152	9.27	0.2975	29.54	273.9	0.46	21.87616
1600	721	5.623392	10.159	0.3256	32.33	328.5	0.46	23.94245
1800	833	5.946708	10.857	0.3482	34.58	375.4	0.45	25.6043
2000	940	6.293118	11.47	0.3685	36.59	419.7	0.45	27.09703
2200	1045	6.524058	12.07	0.387	38.43	463.9	0.44	28.45739
2400	1139	6.754998	12.53	0.402	39.92	500.2	0.44	29.56039
2600	1225	6.985938	12.96	0.4155	41.26	534.7	0.44	30.55309
2834	1317	7.216878	13.36	0.429	42.6	569.2	0.43	31.54579

Table A.5.5: (f) 42.9 A rated (0.27 Ω), I_F =~3.5A

Speed (rpm)	P_{IN} (W)	V_{ph} (V_{rms})	V_{out} (V_{dc})	10.07mΩ shunt (V_{dc})	I_L (A_{dc})	P_{OUT} (W)	Eff
200	17	1.096966	0.896	0.0279	2.770606	2.482463	0.146027
400	71	1.893709	2.55	0.089	8.838133	22.53724	0.317426
600	153	2.644264	4.078	0.1456	14.45879	58.96294	0.385379
800	254	3.302444	5.41	0.1947	19.33466	104.6005	0.411813
1000	361	3.850926	6.51	0.2361	23.44588	152.6327	0.422805
1200	477	4.347448	7.515	0.2729	27.1003	203.6587	0.426958
1400	594	4.757366	8.38	0.305	30.28798	253.8133	0.427295
1600	705	5.10955	9.13	0.332	32.96922	301.0089	0.426963
1800	810	5.403999	9.67	0.354	35.15392	339.9384	0.419677
2000	910	5.66958	10.23	0.3737	37.11023	379.6376	0.417184
2200	1002	5.888973	10.64	0.3888	38.60973	410.8075	0.409988
2400	1080	6.062178	11.05	0.4044	40.15889	443.7557	0.410885
2600	1165	6.235383	11.46	0.419	41.60874	476.8361	0.409301
2808	1244	6.466323	11.84	0.4322	42.91956	508.1676	0.408495